THE EFFECTS OF INORGANIC CARBON LIMITATION IN WILD-TYPE AND CARBON SINK MUTANTS OF THE CYANOBACTERIUM *SYNECHOCYTIS* SP. PCC 6803

By

Steven Christopher Holland

Bachelor of Science in Biology
University of South Alabama
Mobile, Alabama
2006

Submitted to the Faculty of the
Graduate College of the
Oklahoma State University
in partial fulfillment of
the requirements for
the Degree of
DOCTOR OF PHILOSOPHY
May, 2016

THE EFFECTS OF INORGANIC CARBON

LIMITATION IN WILD-TYPE AND CARBON SINK

MUTANTS OF THE CYANOBACTERIUM

SYNECHOCYSTIS SP. PCC 6803

Dissertation Approved:

Dr. Robert L. Burnap

Dissertation Adviser

Dr. Rolf Prade

Dr. Wouter Hoff

Dr. Jeff Hadwiger

Dr. Ulrich Melcher

ACKNOWLEDGEMENTS

I would like to thank my advisor and mentor, Dr. Robert Burnap. His attention to scientific rigor, thirst for knowledge, and trust in his students is inspirational. He allowed me enough flexibility to follow projects that were risky, sometimes to the point of failure, but kept me grounded and clear-headed enough to know when the safer route was preferable. He has given me a great number of opportunities during my time here, and I am eternally grateful. He has proven himself a mentor both scientifically and personally.

My family has always given me encouragement and guidance when needed. If I've made them proud, then I hope they realize that most of what I am, and what I have accomplished, is due to them.

To those three rogues: Tony, Steven, and Eddie. Thank you. Those are too few words to express how instrumental you've been to me these years, but words escape me now. It's been a privilege to see you and your families grow. I hope to see you all in meatspace soon, but we've got cyberspace until then.

To my fellow Burnap Lab members, past and present: it has been great working with all of you. There were early lab meetings, writing deadlines, and failed experiments; but there were campfires and open bars as well! I feel lucky to have been able to work alongside you.

Oklahoma State University, you have given me an education, wonderful friends, and a loving wife. Thanks for the memories.

Finally, but first in my thoughts and heart, thank you to my wife. You've endured all the hardships I have, and had to endure me as well. I've got a lifetime to return the favor. I love you more today.

Name: Steven Christopher Holland

Date of Degree: May, 2016

Title of Study: THE EFFECTS OF INORGANIC CARBON LIMITATION IN WILD-TYPE AND CARBON SINK MUTANTS OF THE CYANOBACTERIUM *SYNECHOCYSTIS* SP. PCC 6803

Major Field: Microbiology and Molecular Genetics

Abstract: The efficiency of photosynthetic electron transport is an important factor in the cellular metabolism of photosynthetic organisms. The high energy molecules produced in the light reactions of photosynthesis are used to energize the reactions of the Calvin-Benson-Bassham cycle and assimilate inorganic carbon into central metabolism. Impaired electron transport can lead to photodamage and the creation of damaging oxygen radical species. The redox state of electron carrier molecules also provides regulatory feedback to a wide range of metabolic pathways and cellular functions. It is therefore important to understand the response of photosynthetic organisms to conditions where electron transport may be hindered.

Since inorganic carbon uptake and utilization is important in cellular metabolism as well as bio-engineering projects, further understanding of the interconnectedness of carbon uptake and photosynthesis is needed. This project first explores the effect of inorganic carbon limitation on the redox state of the photosynthetic electron transport chain and reductant pools. Then understanding how alterations in carbon sink availability affect photosynthetic efficiency and acclimation to low inorganic carbon availability is explored. The results provide a background for the analysis of carbon utilization and photosynthetic efficiency in future bio-engineering efforts.

TABLE OF CONTENTS

Chapter Page

Chapter Page

LIST OF TABLES

Table Page

LIST OF FIGURES

Figure Page

Figure Page

CHAPTER I

Introduction to Electron Transport

1.1 Introduction

Photosynthesis is the creation of reducing equivalents and sugar molecules performed using energy initially obtained from light. To begin, an organism absorbs a photon of light on specialized pigments. After absorption, the energy is used to separate an electron from a donor molecule. The separated electron is transferred along a series of protein complexes and intermediate molecules until it is deposited upon a carbon skeleton molecule, which serves as a storage vessel until the organism requires the energy again. During this time, the initial electron donor must be replenished or replaced with another molecule from which another electron will be extracted.

Concurrently, and also in the absence of light, electrons stored on carbon skeletons are removed and ultimately transferred back to dioxygen through different, but complementary and often intertwining, pathways. Along the pathways, energy obtained from bond rearrangements and redox reactions is stored in the form of so-called high energy molecules and electrochemical gradients. Ultimately, the electrons are delivered to their terminal electron acceptor, dioxygen, and released into the environment. The reducing equivalents and high energy molecules obtained during the anabolism and catabolism of sugar molecules are used to drive the metabolism within an organism.

This literature survey aims to review the previous and current scientific literature regarding the collection, storage, and use of energy derived from oxygenic photosynthesis. It will focus on a few key concepts regarding photosynthesis and carbon acquisition:

- Structure/function roles of important photosynthetic protein complexes and biomolecules
- Identification and analysis of electron flow pathways.
- Triggers and mechanisms regulating metabolism.
- Efficient balancing of photosynthesis due to light or nutrient stress.
- Interaction between proteins and metabolites of electron transport and anabolic/catabolic metabolism.

1.2 *Synechocystis* sp. PCC 6803 – a model for oxygenic photosynthesis

Synechocystis sp. PCC 6803 (hereafter *Synechocystis*) is a unicellular cyanobacterium capable of both photoautotrophic growth in light as well as heterotrophic growth when provided an adequate carbon source [1]. It was cataloged in the Pasteur Culture Collection in 1968 under the name Aphanocapsa N-1, after collection in a freshwater lake located in California and eventually reclassified in the *Synechocystis* genus due to its aggregate-free growth in culture [2, 3].

A number of properties make *Synechocystis* ideal for work with photosynthesis and energy related fields. First, *Synechocystis*, like most cyanobacteria, has fully functional photosynthetic apparatuses that are structurally and functionally similar to those of higher plants. It houses two functionally similar photosystem protein complexes and contains antenna complexes that function

similar to light harvesting complexes. Also, it synthesizes chlorophyll a and carotinoids for use as pigment and energy absorption molecules. Its use of water as a primary electron source and creating oxygen as a byproduct mirrors photosynthesis in higher plants.

Physiological properties of *Synechocystis* also favor its use in the laboratory. It has a relatively quick doubling time of approximately 5 hours under ideal conditions [4]. Its ability to grow heterotrophically with supplied glucose is particularly helpful in analysis of mutants deficient in or lacking photosynthetic machinery, although 5 minutes of exposure to blue light per day is required [5]. *Synechocystis* is also naturally competent, able to acquire and integrate exogenous DNA into its genome through homologous recombination [6] which facilitates the construction of diverse mutants. Largely due to these physiological properties, *Synechocystis* has a wealth of experimental history upon which researchers can draw. It was the first photosynthetic organism to have its genome sequenced and has a well curated database comprised of gene, protein, and biophysical data [7, 8]. These properties encourage the use of *Synechocystis* as model organism for the study of photosynthesis, metabolism, and physiology.

1.3 Photosystem II – light driven charge separation and oxygen evolution

Within the thylakoid membranes of *Synechocystis*, Photosystem II (PSII) is the initial source for electrons entering the photosynthetic electron transport chain (Figure 1.1). To initiate photosynthetic electron transport, PSII removes electrons from a special pair of chlorophyll a molecules, and regenerates the donor molecule with an electron extracted from water. The byproduct of this reaction is the eventual formation of dioxygen, O_2. The electrons removed from chlorophyll a/water are used to create reducing equivalents, usually a reduced quinol. The

structure and function of PSII allow this reaction to proceed, but the exact mechanisms are still being elucidated. A number of crystal structures for the PSII complex have been solved, with the most recent, and highest resolution, resolved at 1.9Å from the cyanobacterium *Themosynechococcus vulcanus* [9-13].

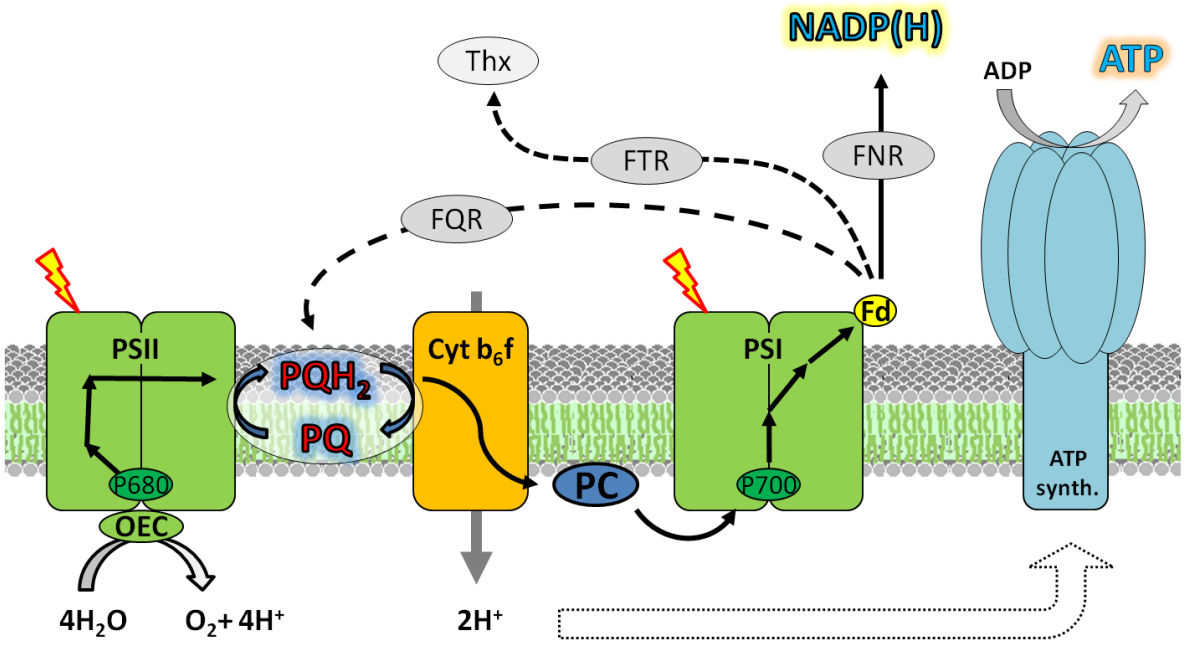

Figure 2.1 The photosynthetic electron transport chain in *Synechocystis*. The path of electron transport (black arrows) originates within photosystem II (PSII) on the special chlorophyll molecule P680 when light-induced charge separation occurs. Electrons from water replace the electron hole on the chlorophyll molecule via activity of the oxygen evolution complex (OEC). From PSII, electrons are donated to the soluble quinone plastoquinone (PQ). This serves as a donor molecule to the cytochrome b_6f, whose activity is similar to that of the respiratory cytochrome bc1 comlex. Electrons are transferred to the soluble electron carrier plastocyanin (PC) which serves to regenerate the special chlorophyll molecule P700 within photosystem I. Similar to PSII, light-driven charge separation removes an electron from P700 and is transferred to ferredoxin. In canonical linear electron transport electrons are transferred to NADP+ to form NADPH via ferredoxin:NADP reductase (FNR). Alternate pathways include transfer to thioredoxin (Thx) via ferredoxin:thioredoxin reductase (FTR) to serve regulatory functions, or return to the plastoquinone pool through ferredoxin:quinone reductase (FQR) or other pathways of cyclic electron transport. The proton motive force generated from the activity of PSII and cyt b_6f serve to synthesize ATP at the ATP synthase.

Cyanobacterial PSII is a protein complex of approximately 350kDa comprised of at least 19 subunits. It consists of 17 transmembrane helices and resides in the thylakoid membrane. The

PSII core complex houses 35 chlorophyll a and 11 β-carotene molecules [13]. A majority of these chlorophyll molecules reside in subunits CP47 and CP43 [13]. Here, they serve in an energy capture role by absorbing photons. Alternatively, and more frequently, these molecules may be excited through resonance energy transfer from excited molecules in large light harvesting complexes called phycobilisomes. This resonance transfer is due to the close proximity of these molecules, and is crucial for efficient light harvesting. The excitation energy is transferred towards a set of 2 modified 'special pair' of chlorophyll molecules comprising the reaction center; one chlorophyll molecule resides in the D1 subunit and another in the D2 subunit. Upon excitation, one of these chlorophyll molecules, P680, becomes a strong reducing agent, P680* [14]. The P680 molecule serves as the bridge between energy transfer and redox chemistries.

The excited P680* molecule reduces a pheophytin (Phe) molecule. This event creates the $Phe^{\bullet -}$ radical, which quickly reduces the plastoquinone molecule associated with the D2 protein (Q_A). In the millisecond time range, the reduced Q_A radical (Q_A^-) transfers its electron to a second plastoquinone within the D1 protein of the PSII core, Q_B. The electron resides on the reduced Q_B^- molecule until a subsequent photochemical turnover of the reaction center transfers a second electron, creating Q_B^{2-}, when it is then fully protonated, creating plastoquinol, and released into the membrane. These transfers occur on the picosecond to millisecond time scale, and can be probed spectroscopically. In order for the second electron to become available, the P680 molecule must be regenerated, through the oxidation of a water molecule.

The oxidation of water occurs at the oxygen evolving complex (OEC). Residing within the OEC is the manganese cluster, comprised of four manganese, one calcium, and five oxygen ions

(Mn_4CaO_5). Recent crystallography studies have provided adequate structural data on the cluster, but photoreduction by X-ray damage may have altered its presumed structure [13, 15]. Regardless of structural details, the oxidation of water and eventual production of O_2 requires the energy from four photons of light. With the energy from each photon, an electron is extracted from water to replenish the electron released from P680* through a tyrosine residue in the D1 subunit (Y_Z). The manganese cluster serves to hold and stabilize the radical intermediates that are created through the oxidation of water. For the evolution of one oxygen molecule, four light flashes and two water molecules are required. This results in the extraction of 4 electrons, reducing two plastoquinone (PQ) to two plastoquinol (PQH_2) molecules. The overall formula for PSII activity can be described with the following formula:

$$2H_2O + 2PQ + 4H^+_{stroma} \xrightarrow{4hv} O_2 + 2PQH_2 + 4H^+_{lumen}$$

Oxygen evolution can be used as a measure of PSII activity, since it is dependent upon plastoquinone availability and downstream electron transport efficiency. Analysis of oxygen evolution is a useful tool in probing the effect of PSII mutations (for example [16, 17]), and as will be discussed below, can be used to measure carbon availability and electron transport [18].

1.4 Cytochrome b_6f – the bridge between photosystems

Residing between photosystems II and I, in order of electron transfer, is the cytochrome b_6f complex (cyt b_6f), another multi-subunit electron transport protein complex. Cytochrome b_6f serves to generate a proton motive force (*pmf*) through the oxidation of PQ, reduction of plastocyanin (PC), and proton transfer reactions. The electron and proton transfer reactions of cyt b_6f, and its homologous respiratory counterpart cytochrome bc1, are collectively termed the Q-

cycle [19]. In the first phase of the Q cycle a reduced PQ molecule, PQH_2, binds to the p-site of cyt b_6f. Its two protons are released into the lumen while the two electrons are transferred to the cyt b_6f complex. The first is destined for heme *f*, where it will be used to reduce PC. The second electron is transferred to heme b_n, where it is used to reduce a PQ molecule residing in the n-site, creating a semiquinone radical that accepts a proton from the stromal side of the membrane. The cycle is repeated, donating two protons to the lumenal side of the membrane, transferring one electron to PC and one electron to the semiquinone. The semiquinone accepts one proton from the stroma and is released as PQH_2. The net results from these reactions are seen in the equation:

$$2PQH_2 + 2PC(Cu^{2+}) + 2H^+(\text{stroma}) \rightarrow PQH_2 + PQ + 2PC(Cu^+) + 4H^+(\text{lumen})$$

Two PQH_2 molecules are oxidized in the process, but are used to reduce another PQ molecule, resulting in one net oxidation. Two plastocyanin, or alternatively, two cytochrome c553 molecules receive an electron each and 2 net protons are released into the lumen. Thus, an important function of the cyt b_6f complex is to participate in the establishment of a *pmf*, and the eventual synthesis of ATP.

1.5 Photosystem I – the second photosystem

Downstream of PSII is photosystem I (PSI), a trimeric supercomplex similar to PSII. Like PSII, PSI uses absorbed excitation energy from light to induce charge separation and electron extraction from a special pair of chlorophyll molecules within the complex. The PSI monomer is a multi-subunit complex also situated in the thylakoid membrane. Its intramolecular electron transport chain consists of 6 chlorophylls, 2 phylloquinones, and 3 iron-sulfur (4Fe4S) clusters. Each PSI monomer contains a lumenal projection from the membrane to provide a docking site

for plastocyanin, the electron donor, as well as a stromal projection for electron donation to ferredoxin.

Energy from absorbed photons excites an electron in the special pair chlorophylls, P700, and the electron is transferred to the first stable acceptor A0. The electron is transferred to a phylloquinone molecule, and eventually to the three 4Fe-4S clusters designated F_X, F_A, and F_B, in that order. Residing in the PsaC subunit, F_B serves as the ferredoxin (Fd) interacting and electron donation site [20]. In order to reduce the $P700^+$ chlorophyll generated, reduced PC is used as the electron donor. Since the mobile electron carriers PC and Fd alter the oxidation states of metal ion ligands to act as stable electron holders, and both hold single electrons, the overall reaction equation becomes:

$$4\mathrm{PC}(\mathrm{Cu}^{2+}) + 4\mathrm{Fd}(2\mathrm{Fe}^{3+}, 2\mathrm{Fe}^{2+}) \xrightarrow{4\mathrm{h}\nu} 4\mathrm{PC}(\mathrm{Cu}^{3+}) + 4\mathrm{Fd}(1\mathrm{Fe}^{3+}, 3\mathrm{Fe}^{2+})$$

where PC and Fd are the mobile electron carriers plastocyanin and ferredoxin, and the atoms in parentheses indicate the oxidation state of their metal ligands. Notice that no proton transfer or translocation is involved in PSI activity, so no *pmf* is generated solely from the mechanism of PSI. Photosystem I does have some sensitivity to pH; however this sensitivity appears to extend beyond the pH ranges explored in this work (reviewed in [21]).

1.6 Plastoquinone and plastocyanin – mobile electron carriers

In order to transfer electrons between these large protein complexes, cyanobacteria employ a number of small, mobile electron carriers. By using these small molecules to shuttle electrons between complexes, the stoichiometry of each system can be regulated as needed. In addition,

these smaller molecules can serve as transient reservoirs of electrons. By analyzing the redox poise of these carrier molecules, *Synechocystis* can regulate and adjust cellular functions to maintain ideal photosynthetic electron flow.

After accepting electrons from PSII, plastoquinol (PQH_2), the reduced form of plastoquinone (PQ; also used to refer generically to the combined population of plastoquinol and plastoquinone) is released from PSII and diffuses through the thylakoid membrane. Plastoquinone primarily serves as an electron shuttle from PSII to the proton-pumping cytochrome b_6f membrane complex. However, regulatory and physiological functions regulated by the redox poise of the plastoquinone pool have been discovered. For instance, distribution of excitation energy into the electron transport chain through state transitions (the translocation of light harvesting antennae) is likely mediated by the redox state of plastoquinone in *Synechocystis* [22]. The redox state of plastoquinone has also been implicated in altering protein phosphorylation in cyanobacteria, a process important in regulating state transitions in higher plants, although it is uncertain whether protein phosphorylation has a similar effect in cyanobacteria [23]. The redox state of plastoquinone has also been implicated in altering the PSII/PSI ratio in many cyanobacteria (reviewed in [24]). Important to the research presented herein, the redox state of the PQ pool may play a significant role in cyclic electron flow (discussed below) [25].

There is a surprisingly large amount of interchange between the photosynthetic and respiratory electron transport chains in cyanobacteria. The photosynthetic cytochrome b_6f and respiratory cytochrome bc_1 complex share the same quinone molecule, plastoquinone [26]. This allows two pathways for excess reductant to become consumed. Similarly, the acceptor side of cytochrome b_6f can donate electrons to plastocyanin or cytochrome c553 and both molecules can donate

electrons to P700 [27]. Which molecule is being expressed appears to be regulated by copper availability [28], but it was seen that in a deletion mutant of one soluble electron carrier, activity was supplemented by the other, implying that both molecules can function in photosynthetic and respiratory activity [29, 30]. It would appear cyanobacteria favor the flexibility allowed from multiple destinations of electrons, rather than the strict control that could be obtained over stringently distinct pathways. However, specifics as to how or why electrons are destined for specific electron transport pathways are still elusive.

1.7 Ferredoxin and NADPH – the end of the Z-scheme

The immediate electron acceptor of PSI is the small iron-sulfur protein ferredoxin (Fd). The ferredoxin proteins are ubiquitous in electron transfer reactions of a diverse range of organisms [31]. *Synechocystis* contains nine ferredoxin isoforms, which vary in iron-sulfur center composition and their expression during various environmental stimuli [32]. It is the first isoform, Fed1, encoded by the *petF* gene, that is of concern for this work. It is the primary isoform responsible for photophosphorylation in both linear and cyclic (discussed below) electron transport; as such it is found in high quantities and is essential for cellular viability, under both autotrophic and heterotrophic growth conditions [33]. Under conditions of linear electron transport, ferredoxin accepts electrons from PSI and transfers them to $NADP^+$, using the enzyme ferredoxin:$NADP^+$ reductase (FNR) [32].

The FNR protein appears to play a major role in determining the routes of electron flow in *Synechocystis*. The FNR gene, *petH*, is transcribed into either a long or short form [34]. Interestingly, the long gene transcript is translated into the shorter protein product due to

formation of an RNA secondary structure blocking an early start codon in the long transcript [35]. This gives rise to the FNR_L and FNR_S isoforms, which vary in their localization and activity [34]. Both isoforms share the same catalytic domain, but the long isoform, FNR_L, has an additional N-terminal extension. This extension has similarity to the CpcD-phycobilisome linker polypeptide, and as a result localizes FNR_L to the light harvesting phycobilisome complex [36]. While the exact mechanism of isoform length and localization with its activity in reducing $NADP^+$ is not fully understood, experiments with *Synechocystis* mutants expressing only one isoform have begun to elucidate its properties. While the mutant expressing only FNR_L behaved similarly to the wild-type strain under photoautotrophic conditions, the mutant expressing only FNR_S showed a growth impairment and a higher NADP+/NADPH ratio [37]. This has led to the model that FNR_s may be associated with respiratory or cyclic electron transport, transferring electrons directly to those complexes, and FNR_L promotes linear electron transfer to $NADP^+$.

NADP(H) is a cofactor that primarily serves as a reducing agent in anabolic reactions of cyanobacterial metabolism. Its specific role in each process will be elaborated in later sections, but $NADP^+$ serves as the terminal electron acceptor in linear electron transport. The NADP(H) pool appears to serve as a reservoir of electrons, where the rates of production and consumption reach a steady-state redox poise. Unsurprisingly, the redox state and concentration of $NADP^+$/NADPH has been found to play a regulatory role in CO_2 fixation and assimilation [38, 39]. NADPH may also serve as an electron donor to power NAD(P)H-dehydrogenase (NDH) complexes, although some uncertainty exists as to whether donation occurs from ferredoxin, FNR, NADPH or some combination [40]. Nevertheless, the primary role of NADPH is in acting

as a reducing equivalent in assimilating inorganic carbon through the Calvin-Benson-Bassham (CBB) cycle.

1.8 The Calvin-Benson-Bassham cycle – assimilation of inorganic carbon

The major pathway for inorganic carbon assimilation in plants, algae, and cyanobacteria is the Calvin-Benson-Bassham (CBB) cycle (Figure 1.2) [41]. In this cyclical series of reactions, CO_2 is affixed onto a pentose phosphate molecule. The resulting hexose splits into two triose molecules that undergo phosphorylation and reduction events. The incorporation of three CO_2 molecules results in six triose phosphate molecules. One of the triose phosphates is 'free' to be used in cellular metabolism, while the other five triose phosphates are regenerated into three pentose phosphates ready for CO_2 fixation.

The enzyme ribulose-1,5-bisphosphate carboxylase/oxygenase (RubisCO) is thought to be one of the most abundant proteins on Earth. RubisCO is a key enzyme in the CBB cycle, where it facilitates the incorporation of CO_2 onto the pentose phosphate ribulose-1,5-bisphosphate (RuBP). It is also amongst the slowest and least efficient enzymes, with a low substrate specificity that permits O_2 use as a substrate and creation of a wasteful byproduct, 2-phosphoglycolate (2PG) [42]. In order to minimize the oxygenase activity of the enzyme, RubisCO is localized to the carboxysome, a proteinaceous microcompartment found in the cyanobacterial cytoplasm. Within the carboxysome, there also resides a carbonic anhydrase, which converts the high intracellular concentrations of bicarbonate (HCO_3^-) into CO_2, thereby saturating the active site of RubisCO with CO_2, minimizing its oxygenase activity [43, 44]. After

carboxylation of RuBP, an unstable, transient six carbon molecule is formed, but quickly dissociates into two 3-carbon molecules of 3-phosphoglycerate (3PGA).

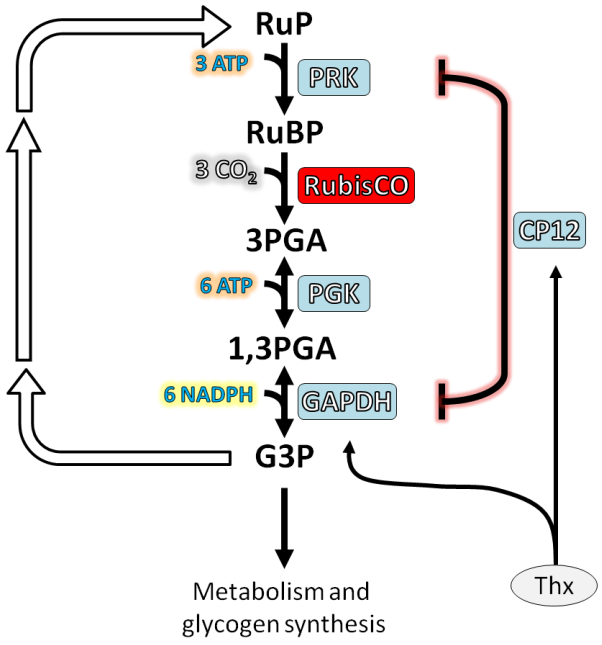

Figure 1.2 Simplified pathway map of the reductive Calvin-Benson-Bassham cycle. Progression through the reductive side of the CBB cycle requires the input of energy at multiple steps. Due to the reversibility of some of these reactions and their use in oxidative pathways, the activity of some enzymes are tightly regulated. The activity of the CP12 protein acts as a scaffold protein to inhibit the activity of PRK and GAPDH. The scaffolding activity in turn is regulated by thioredoxin (and NADPH) illustrating further redox control of carbon metabolism. Abbreviations: RuP, ribulose 5-phosphate; RuBP, ribulose 1,5-bisphosphate; 3PGA, 3-phosphoglycerate; 1,3PGA, 1,3-bisphosphoglycerate; G3P, glyceraldehydes 3-phosphate; PRK, phosphoribulokinase; RubisCO, ribulose 1,5-bisphosphate carboxylase/oxygenase; PGK, phosphoglycerate kinase; GAPDH, glyceraldehydes-3-phosphate dehydrogenase.

Following three carboxylation reactions, six molecules of 3PGA have been formed. These six molecules are phosphorylated by the enzyme phosphoglycerate kinase (PGK), resulting in 6 molecules of 1,3-bisphosphoglycerate (1,3BPGA). During this activity, 3 ATP molecules are converted to ADP. Phosphoglycerate kinase also has reverse activity, and will dephosphorylate 1,3BPGA during the catabolic reactions of glycolysis. Within pea plants, this activity was found to be modulated by the energy charge of the cell [45]. Therefore during photosynthesis, when ATP concentrations would be high, PGK phosphorylates 3PGA, and in the absence of light, lower ATP levels would lead to glycolytic activity and dephosphorylation. A similar regulatory mechanism is likely involved in cyanobacteria as well.

Two additional CBB cycle enzymes are worth mentioning for their roles in energy consumption and CBB activity. The first, glyceraldehyde-3-phosphate dehydrogenase (GAPDH), catalyzes the reduction of 1,3BPGA to glyceraldehyde-3-phosphate (G3P, or GAP) using an electron from NADPH, with dephosphorylation also occurring. Since three carboxylation reactions result in the formation of six 1,3BPGA molecules, six molecules of NADPH are consumed to create the resulting six molecules of G3P. Glyceraldehyde-3-phosphate plays an important role in amino acid synthesis and cellular metabolism, as such, it is often considered an end product of the CBB cycle. Since G3P serves a pivotal role in glycolysis and gluconeogenesis, the reaction is reversible, therefore GAPDH activity must be regulated (discussed below). In order to maintain the cyclical nature of the CBB cycle, of the six resulting G3P molecules, five are used to regenerate CBB substrates, while one is 'free' to participate in cellular metabolism. This occurs through the activity of a number of enzymes that convert the five 3-carbon G3P molecules to three 5-carbon ribulose 5-phosphate (RuP) molecules. In the final regenerating step of the CBB cycle, three RuP molecules are phosphorylated by the enzyme phosphoribulokinase (PRK), resulting in three molecules of ribulose-1,5-bisphosphate (RuBP), the starting substrate to which CO_2 will be fixed by RubisCO. Three ATP molecules are consumed in the process, bringing the total number of NADPH and ATP consumed to 6:9 for three CO_2 molecules fixed. Together with GAPDH, the activity of PRK is regulated by the activity of the CP12 protein in order to regulate the activation of the CBB cycle [38].

Since a number of enzymes are shared in the anabolic reactions of the CBB cycle and the catabolic reactions of glycolysis, it is important that these antagonistic activities remain distinct. Many CBB enzymes have their activity regulated by the thioredoxin system, which obtains

electrons through either reduced Fd or NADPH [46, 47]. The ferredoxin:thioredoxin reductase (FTR) or NADPH:thioredoxin reductase (NTR) enzymes facilitate the transfer of electrons to thioredoxin, which is used to reduce a disulfide bond on the molecule. In this manner, the thioredoxin system acts to transform an electron signal into a disulfide/dithiol bond signal. The activity of CBB enzymes through disulfide bond breakage and formation has been linked to the regulatory control of fructose-1,6-bisphosphatase, NADP-malate dehydrogenase (found in the tricarboxylic acid cycle), and GAPDH [46]. Thioredoxin, in addition to NADP(H), was found to regulate the activity of the intrinsically unstructured CP12 protein, whose activity causes the formation of a complex between GAPDH and PRK, greatly diminishing both their activities [38, 48].

Since the activity of the CBB cycle is controlled by availability of high energy molecules (reduced Fd, NADPH, and ATP) created by the reactions of photosynthesis, it is advantageous for photosynthetic organisms to modulate the production of these molecules. One mechanism by which this is accomplished is through cyclic electron flow (CEF).

1.9 Cyclic electron flow – balancing NADPH and ATP

If a stoichiometric accounting of the CBB cycle is performed, then a 2:3 ratio of NADPH to ATP molecules will be found. There is some debate over whether linear electron transport can fulfill this ratio (briefly reviewed in [49]). Firstly, the uncertainty of the number of protons necessary to produce one ATP molecule by the ATP synthase makes theoretical determination of the amount of ATP synthesized by the *pmf* generated from the electron transport chain difficult. Secondly, practical complications arise when environments that facilitate or impair electron flow may be

encountered: pH extremes, limited carbon availability, and extremes in light availability. As such, photosynthetic organisms have evolved methods of returning electrons to the electron transport chain, thereby increasing *pmf* without producing net NADPH. Collectively, these mechanisms are referred to as cyclic electron flow (CEF).

There are a number of various pathways of CEF in cyanobacteria, but their common mechanism relies on taking electrons downstream of PSI and returning them to the PQ pool. In doing so, no net NADPH is produced and electrons can again move through the cytochrome b_6f complex and PSI, generating a net gain in *pmf* and subsequent ATP.

A minor contributor to cyclic electron flow in cyanobacteria is an antimycin A-sensitive pathway. A major source of CEF in chloroplasts [50], this pathway depends on a *pgr5* homolog encoded by ORF *ssr*2016 [51]. It is also dependent on an elusive ferredoxin-quinone reductase (FQR) which was identified by its ability to induce CEF around PSI by ferredoxin oxidation [52]. Recent evidence suggests FQR may be the PGRL1 protein in plants [53], but this has not been yet investigated at the biochemical or mechanistic level in cyanobacteria.

A pathway of cyclic electron flow intimately related to inorganic carbon metabolism relies on the NDH-$1_{3/4}$ complexes. These are specialized NAD(P)H dehydrogenases that are comprised of core NDH subunit proteins, and an associated putative reverse carbonic anhydrase protein CupA or CupB with adjoining NdhD3/F3/CupS or NdhD4/F4 subunits, respectively (reviewed in [54]). These complexes are localized to the thylakoid membrane, where they catalyze the hydration of CO_2 into bicarbonate. The role of these NDH-1 complexes in inorganic carbon acquisition will be discussed in a later section. While there is some uncertainty as to their specific mechanism of

action, these complexes oxidize NADPH and reduce PQ [55]. While the NDH-1 complexes in cyanobacteria have a specificity for NADPH over NADH [55], there is still uncertainty what role FNR plays in their operation. Localization and activity of FNR suggests the short isoform participates in NADPH oxidase activity [35] and co-precipitation with NDH-1 complexes has been reported [56]. There is also some recent evidence to suggest that the NdhS protein, may modulate the electron input activity of the NDH complex and its electron donor [57].

It should be noted that while not a source of CEF per se, the respiratory and photosynthetic electron transport chains utilize a common quinone for electron transport: plastoquinone. As such, electrons coming from respiratory substrates (NADH and succinate) can cross to the photosynthetic pathway and vice versa. In mutants of the respiratory NADH and succinate dehydrogenase complexes, the PQ pools were much more oxidized than those of the wild-type strain, implicating their activity as a significant source of electron flow in photoautotrophic conditions [58].

1.10 The cyanobacterial CO_2-concentrating mechanism – saturating RubisCO with CO_2

The CO_2 concentrating mechanism (CCM) within cyanobacteria exists to saturate the active site of RubisCO with CO_2, thereby minimizing the oxygenase activity of the enzyme (see Figure 1.3). One constituent of the CCM, the carboxysome, houses RubisCO and a carbonic anhydrase. The carboxysome allows free diffusion of HCO_3^- into the compartment, but has putatively limited CO_2 permeability [59]. In order to allow the conversion of HCO_3^- into CO_2, cyanobacteria maintain their intracellular concentrations of bicarbonate to over 500 times that of the

extracellular environment [60]. They accomplish this feat through the second component of the CCM, a suite of constitutive and inducible inorganic carbon transporters.

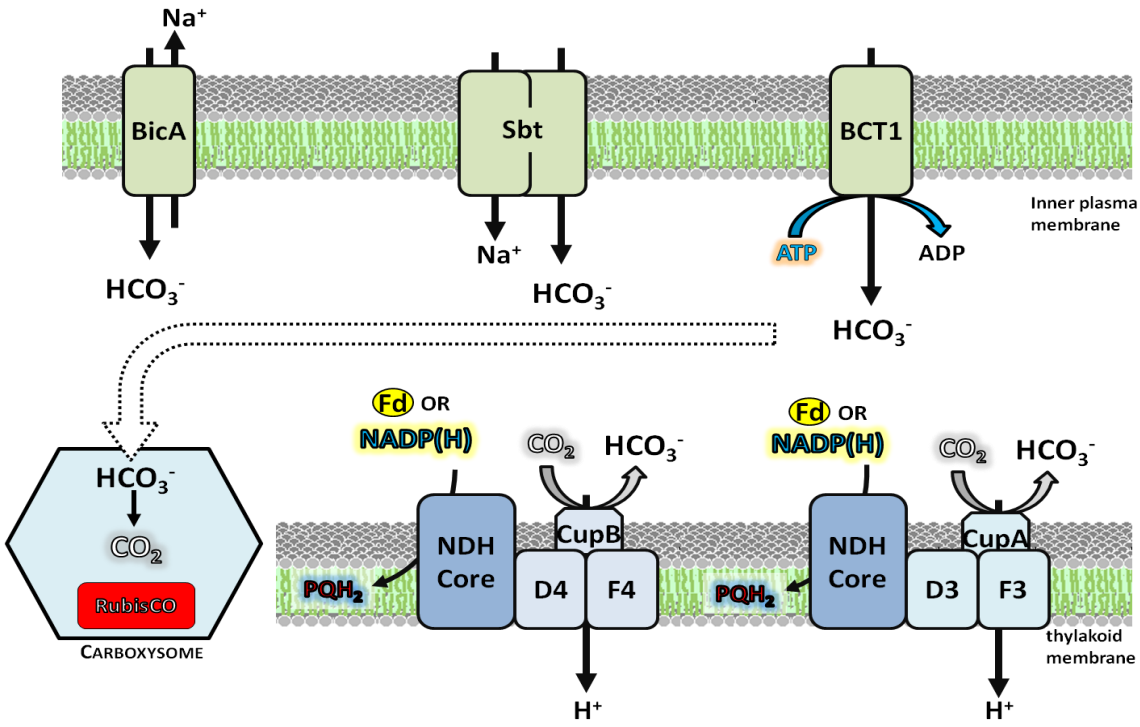

Figure 1.3 The CO_2-concentrating mechanism of *Synechocystis* functions to saturate the active site of RubisCO with CO_2. RubisCO is localized to the carboxysome, a protein microcompartment that allows free diffusion of HCO_3^-, but limited CO_2 diffusion. In order to increase the intracellular concentration of HCO_3^-, a suite of carbon transporters are used. The BicA, Sbt, and BCT1 complexes transport HCO_3^- directly, energized by either sodium co-transport or ATP hydrolysis. Another class, the NDH-1 complexes, uses reducing equivalents to power the hydrogenation of CO_2 and proton translocation. These complexes consist of a common core of Ndh proteins and variable membrane domain. The BicA and CupB complexes are constitutively expressed, while the Sbt, BCT1, and CupA complex are induced under carbon limitation.

Inorganic carbon transporters of cyanobacteria can be divided into which species of inorganic carbon is being transported: HCO_3^- or CO_2. Within each class, there exist high-affinity and low-affinity analogs, with the low-affinity transporter being relatively constitutive in its expression, and the high-affinity transporter being induced in periods of limited carbon availability.

There are two CO_2-specific inorganic carbon transporters in *Synechocystis*, the NDH-$1_{3/4}$ complexes previously described in their role in cyclic electron flow. These two multi-subunit complexes reside in the thylakoid membrane and have a number of electron acceptor subunits in common. They differ however in the composition of their membrane and CO_2-hydration domain, specifically the NdhF, NdhD, and Cup proteins. The NDH-1_4 complex is composed of the NdhF4, NdhD4, and CupB proteins and participates in constitutive low-affinity, high flux CO_2 hydration [61]. Whereas the NDH-1_3 complex is composed of homologous NdhF3, NdhD3, CupA, and CupS proteins and is induced under carbon limitation due to its high-affinity, but low flux, properties [62]. The NdhF/D proteins of these complexes share homology to the NdhF/D proteins found in respiratory NDH complexes, and their localization in the membrane implicates a role in proton pumping [63]. The CupA/B proteins are essential in the CO_2-hydration mechanism, and likely function similar to a carbonic anhydrase, although their mechanism has not been fully elucidated [64]. Because cyanobacteria often inhabit slightly alkaline environments, dissolved CO_2 is not as prevalent as HCO_3^-, therefore the activity of NDH-1 complexes are also thought to play a major role in recycling leaked CO_2 from the carboxysome [65, 66]. Although these complexes certainly obtain diffused CO_2 of an extracellular origin, cyanobacteria also heavily rely on transporters specific to HCO_3^- as well.

In addition to CO_2 hydration, cyanobacteria increase their intracellular bicarbonate levels through transporters specific to HCO_3^-. All the bicarbonate transporters reside on the inner plasma membrane, rather than the thylakoid membrane as the NDH-1 complexes do. The BicA transporter belongs to the SulP family of anion transporters [67], and appears to be constitutively expressed [68]. Its activity was also found to be sodium concentration dependent, implicating Na^+

as its antiporter co-substrate, and has an affinity constant value and V_{max} that would classify it with the other low-affinity, high flux transporter NDH-1_4 [67]. The SbtA transporter is a high-affinity, low flux Na^+/HCO_3^- symporter that relies on the NtpJ Na^+/K^+ antiporter in order to transport bicarbonate into the cell [69]. It is inducible under periods of low carbon availability and shows little to no expression under carbon-replete growth. The final bicarbonate transporter, BCT1, is a multi-subunit ABC-type bicarbonate transporter encoded by the *cmpABCD* genes [70]. Belonging to the ATPase family, it uses ATP hydrolysis to transport bicarbonate and belongs to the inducible, high-affinity suite of carbon transporters.

In carbon replete conditions, there is very little expression of the high-affinity suite of carbon transporters (BCT1, SbtA, NDH-1_3), however, within 1-3 hours of low carbon availability transcripts for carbon transporters and carboxysome-related genes rapidly accumulate [68]. It has been found that the high-affinity carbon transporters of the inducible CCM are under the transcriptional control of two LysR-type transcriptional regulators (LTTRs): NdhR and CmpR. The CmpR protein acts as a transcriptional activator of the *cmpABCD* operon, encoding subunits of the BCT1 complex [71]. The NdhR protein acts as a transcriptional repressor for a number of CCM-related genes, including *sbtA/B* and the *ndhD3/F3/cupA/cupS* operon [72]. An interesting feature of LTTRs is that their activity is often modulated by small molecule co-inducers, allowing sensing of the environment and establishment of feedback inhibition or activation [73]. For the CmpR protein, the co-activators RuBP and 2PG were found to increase CmpR binding affinity to its promoter region [74] and the molecules $NADP^+$ and 2-oxoglutarate (2OG or alpha-ketoglutarate, αKG) were found to have a similar effect on promoter binding by NdhR [39]. The finding that these molecules act as a sensory mechanism of carbon limitation should not be

surprising. During periods of carbon limitation, an increase in RuBP, the substrate to which CO_2 is fixed, would be expected to accumulate, and evidence shows that 2PG synthesis, the product of the oxygenase activity by RubisCO, does increase [75]. This would result in the transcriptional activation of the BCT1 complex through CmpR. Similarly, under carbon limitation, the NADP(H) pool would become more reduced, as CBB activity slowed and the consumption of NADPH diminishes. The resulting lower $NADP^+$ concentration would lead to release of transcriptional repression by the NdhR protein.

Regulation of CCM induction is not solely under the control of LTTRs and their co-inducer metabolites. Recent evidence of anti-sense RNA to CCM genes has been reported, and their role in post-transcriptional regulation has been proposed [76, 77]. Evidence of post-translation modification of some carbon transporters is also beginning to emerge [78].

1.11 Carbon metabolism – storage and recovery of electrons

The glyceraldehyde-3-phosphate (G3P) produced in the CBB cycle is not the terminal electron/carbon storage molecule in cyanobacteria. Glycogen, a branching glucose polymer chain, serves this role. G3P is converted to glucose-6-phosphate (G6P) by gluconeogenesis pathway enzymes. G6P is then converted to glucose-1-phosphate by phosphoglucomutase. The enzyme glucose-1-phosphate adenylyltransferase (GlgC) then transfers an ADP moiety onto glucose, creating ADP-glucose. The GlgA (glycogen synthase) and GlgB (branching enzyme) proteins then polymerize these glucose monomers into glycogen. Deletion of either *glgC* alone, or *glgA* and *glgB* together, has been shown to eliminate glycogen production [79].

The acclimation to low carbon conditions brings with it alterations in carbon metabolite concentrations. In periods of high carbon growth, glycogen is stored in granules observable through electron microscopy. During the transition to low carbon availability, these granules disappear [80], with the proposed function of replenishing CBB metabolites [75]. A similar role for glycogen is observed upon long-term exposure to darkness [81]. In low carbon conditions, glycolytic pathways are strongly induced, as demonstrated by increased levels of dihydroxyacetonephosphate and phosphoenolpyruvate [75].

It has also been shown that early in the transition to low carbon acclimation, an increase in photorespiratory substrates, termed a photorespiratory burst, was observed [77]. Levels of 2PG in low carbon cells were measured to be 5 times those in high carbon cells and remained high 24 hours later. Such an observation gives evidence to the principle of metabolite control over high-affinity carbon transport induction. The same study [77] showed a decrease in 2OG during this time as well, however previous results by the same authors show increase in this metabolite [75].

1.12 The Δ*glgC* mutant – closing a carbon sink

Impairment of glycogen synthesis creates a number of phenotypes in Δ*glgC* mutants. One of these phenotypes, the 'energy spilling' response, is marked by the excretion of pyruvate and 2OG into the extracellular medium. The response is observed during nitrogen limitation [79, 82] and photomixotrophic growth [79]. The amount of carbon excreted in this manner accounts for 20-60% of carbon that would otherwise have been utilized in glycogen synthesis. The level of photosynthetic activity, as measured by oxygen evolution, in the Δ*glgC* mutant is 70-80% lower in *Synechocystis* [79, 83] and 33% lower in *Synechococcus* [84] compared to the wild-type strain

in nutrient replete conditions. In *Chlamydomonas*, it was found that lowered photosynthetic activity in the mutant was due to electron donation downstream of the electron transport chain [85]. Glycogen appears to serve as a source to replenish CBB cycle intermediates, as a *Synechocystis* mutant deficient in glycogen synthesis displays a delay in CBB activation when acclimated to darkness [81]. Although the effect of light and nitrogen availability has been studied in the Δ*glgC* mutants of cyanobacteria, the response to carbon availability has received less attention, with the exception of glucose addition, which displayed a modest growth impairment and energy spilling phenotype [79].

1.13 The JU547 mutant – engineering a carbon sink

Another carbon sink mutant has been used in this research. In the case of the JU547 mutant, a carbon sink pathway has been inserted, rather than closed. This mutant has the gene for the ethylene forming enzyme (EFE) inserted into the genome [86]. The EFE uses 2OG and arginine to produce ethylene and succinate as products. Since ethylene is a volatile compound, it escapes from the cell into the atmosphere, or headspace of the culturing vessel. As such, its production does not accumulate intracellularly, where it may cause regulatory or metabolic stress. It has also been found that growth of *Synechocystis* was not impaired when grown in concentrations of up to 95%, with the remaining 5% comprised of air and CO_2 [86]. Therefore ethylene synthesis provides a continually open sink for electron and carbon flux. The production of succinate also provides an alternative to 2-oxoglutarate decarboxylase and succinic semialdehyde dehydrogenase in the tricarboxylic acid cycle recently described in cyanobacteria [87]. In addition, succinate provides a means of electrons entering the photosynthetic and respiratory electron transport chains through succinate dehydrogenase.

1.14 Open questions and goals

My research aims to investigate the photosynthetic electron transport efficiency and redox poise of cyanobacteria in response to altered carbon availability. This project resulted in two major studies. In the first, presented in Chapter 3, the redox state of wild-type *Synechocystis* was examined as photosynthesis facilitated the consumption of inorganic carbon available in the medium. The results identified carbon-sensitive features of chlorophyll and NADPH fluorescence and were helpful in future analyses of *Synechocystis* mutants. The aims were to understand the changes in the electron transport chain as carbon becomes limiting, specifically:

- What changes in the redox poise of electron 'pools' are observed during carbon limitation? Are transient effects seen that are lost during longer term acclimation?
- What carbon-dependent features are seen in chlorophyll and NADPH fluorescence transients?

In the second study, presented in Chapter 4, the response of mutants with alterations in carbon metabolism was examined in response to changes in carbon availability. The study of mutants with altered carbon sinks is typically done with the objective of increasing bioproduct formation. Research into carbon limitation in bioproduction strains is limited, since inorganic carbon is easily supplemented in research and industrial settings. Increased understanding of how photosynthetic activity and carbon uptake efficiency are connected is needed, especially since one proposed use of engineered strains is atmospheric CO_2 sequestration and conversion into useful products. Researching the photosynthetic response to carbon limitation may give insight into the relative efficiency of the electron transport chain and its plasticity towards future engineering

endeavors. In addition, examination of mutants under different carbon regimes can allow analysis of CCM induction and activity, allowing inferences to intracellular metabolite levels. With these goals in mind, the following questions were addressed:

- How does the transition into low carbon environments affect photosynthetic electron transport?
- How is CEF affected by the availability of a carbon sink in high and low carbon conditions?
- Does each mutant's interaction with 2OG affect CCM induction? Do carbon sink mutants have misregulated carbon transporters?

1.15 Chapter 1 References

1. Stanier, R.Y. and G.C. Bazine, *Phototrophic Prokaryotes: The Cyanobacteria.* Annual Review of Microbiology, 1977. **31**(1): p. 225-274.

2. Rippka, R., et al., *Generic Assignments, Strain Histories and Properties of Pure Cultures of Cyanobacteria.* Journal of General Microbiology, 1979. **111**(Mar): p. 1-61.

3. Stanier, R.Y., et al., *Purification and properties of unicellular blue-green algae (order Chroococcales).* Bacteriol Rev, 1971. **35**(2): p. 171-205.

4. Zavrel, T., et al., *Characterization of a model cyanobacterium Synechocystis sp PCC 6803 autotrophic growth in a flat-panel photobioreactor.* Engineering in Life Sciences, 2015. **15**(1): p. 122-132.

5. Anderson, S.L. and L. Mcintosh, *Light-Activated Heterotrophic Growth of the Cyanobacterium Synechocystis Sp Strain Pcc-6803 - a Blue-Light-Requiring Process.* Journal of Bacteriology, 1991. **173**(9): p. 2761-2767.

6. Vermaas, W., *Molecular genetics of the cyanobacterium Synechocystis sp. PCC 6803: Principles and possible biotechnology applications.* Journal of Applied Phycology, 1996. **8**(4-5): p. 263-273.

7. Kaneko, T., et al., *Sequence analysis of the genome of the unicellular cyanobacterium Synechocystis sp. strain 6803. II. Sequence determination of the entire genome and assignment of potential protein-coding regions.* DNA Research, 1996. **3**: p. 109-136.

8. Nakamura, Y., T. Kaneko, and S. Tabata, *CyanoBase, the genome database for Synechocystis sp. strain PCC6803: status for the year 2000.* Nucleic Acids Res, 2000. **28**(1): p. 72.

9. Zouni, A., et al., *Crystal structure of photosystem II from Synechococcus elongatus at 3.8 Å resolution.* Nature, 2001. **409**(6821): p. 739-43.

10. Ferreira, K.N., et al., *Architecture of the photosynthetic oxygen-evolving center.* Science, 2004. **303**(5665): p. 1831-8.

11. Guskov, A., et al., *Cyanobacterial photosystem II at 2.9-Ångstrom resolution and the role of quinones, lipids, channels and chloride.* Nature Structural & Molecular Biology, 2009. **16**(3): p. 334-342.

12. Kamiya, N. and J.R. Shen, *Crystal structure of oxygen-evolving photosystem II from Thermosynechococcus vulcanus at 3.7-Å resolution.* Proc Natl Acad Sci U S A, 2003. **100**(1): p. 98-103.

13. Umena, Y., et al., *Crystal structure of oxygen-evolving photosystem II at a resolution of 1.9 Ångstrom.* Nature, 2011. **473**(7345): p. 55-U65.

14. Barber, J., *Photosystem II: the engine of life.* Q Rev Biophys, 2003. **36**(1): p. 71-89.

15. Cox, N., et al., *Biological water oxidation.* Acc Chem Res, 2013. **46**(7): p. 1588-96.

16. Chu, H.-A., A.P. Nguyen, and R.A. Debus, *Site-directed mutagenesis of photosynthetic oxygen evolution: Instability or inefficient assembly of the manganese cluster in vivo.* Biochemistry, 1994. **33**: p. 6137-6149.

17. Dilbeck, P.L., et al., *The D1-D61N Mutation in Synechocystis sp PCC 6803 Allows the Observation of pH-Sensitive Intermediates in the Formation and Release of O-2 from Photosystem II.* Biochemistry, 2012. **51**(6): p. 1079-1091.

18. Badger, M.R. and T.J. Andrews, *Photosynthesis and inorganic carbon usage by the marine cyanobacterium, Synechococcus sp.* Plant Physiol, 1982. **70**(2): p. 517-23.

19. Mitchell, P., *The protonmotive Q cycle: a general formulation.* FEBS Lett, 1975. **59**(2): p. 137-9.

20. Fischer, N., P. Setif, and J.D. Rochaix, *Site-directed mutagenesis of the PsaC subunit of photosystem I. F(b) is the cluster interacting with soluble ferredoxin.* J Biol Chem, 1999. **274**(33): p. 23333-40.

21. Hope, A.B., *Electron transfers amongst cytochrome f, plastocyanin and photosystem I: kinetics and mechanisms.* Biochim Biophys Acta, 2000. **1456**(1): p. 5-26.

22. Mao, H.B., et al., *The redox state of plastoquinone pool regulates state transitions via cytochrome b(6)f complex in Synechocystis sp PCC 6803.* Febs Letters, 2002. **519**(1-3): p. 82-86.

23. Allen, J.F., et al., *Chloroplast Protein-Phosphorylation Couples Plastoquinone Redox State to Distribution of Excitation-Energy between Photosystems.* Nature, 1981. **291**(5810): p. 25-29.

24. Murakami, A., S.-J. Kim, and Y. Fujita, *Changes in Photosystem Stoichiometry in Response to Environmental Conditions for Cell Growth Observed with the Cyanophyte Synechocystis PCC 6714.* Plant and Cell Physiology, 1997. **38**(4): p. 392-397.

25. Alric, J., J. Lavergne, and F. Rappaport, *Redox and ATP control of photosynthetic cyclic electron flow in Chlamydomonas reinhardtii (I) aerobic conditions.* Biochim Biophys Acta, 2010. **1797**(1): p. 44-51.

26. Aoki, M. and S. Katoh, *Oxidation and Reduction of Plastoquinone by Photosynthetic and Respiratory Electron-Transport in a Cyanobacterium Synechococcus Sp.* Biochimica Et Biophysica Acta, 1982. **682**(3): p. 307-314.

27. Ho, K.K. and D.W. Krogmann, *Electron-Donors to P700 in Cyanobacteria and Algae - an Instance of Unusual Genetic-Variability.* Biochimica Et Biophysica Acta, 1984. **766**(2): p. 310-316.

28. Zhang, L., H.B. Pakrasi, and J. Whitmarsh, *Photoautotrophic growth of the cyanobacterium Synechocystis sp. PCC 6803 in the absence of cytochrome c553 and plastocyanin.* J Biol Chem, 1994. **269**(7): p. 5036-42.

29. Duran, R.V., et al., *The efficient functioning of photosynthesis and respiration in synechocystis sp. PCC 6803 strictly requires the presence of either cytochrome c6 or plastocyanin.* J Biol Chem, 2003.

30. Binder, A., R. Hauser, and D. Krogmann, *Respiration in Energy-Transducing Membranes of the Thermophilic Cyanobacterium Mastigocladus-Laminosus .1. Relation of the Respiratory and Photosynthetic Electron-Transport.* Biochimica Et Biophysica Acta, 1984. **765**(3): p. 241-246.

31. Sticht, H. and P. Rosch, *The structure of iron-sulfur proteins.* Prog Biophys Mol Biol, 1998. **70**(2): p. 95-136.

32. Cassier-Chauvat, C. and F. Chauvat, *Function and Regulation of Ferredoxins in the Cyanobacterium, Synechocystis PCC6803: Recent Advances.* Life (Basel), 2014. **4**(4): p. 666-80.

33. Poncelet, M., et al., *Targeted deletion and mutational analysis of the essential (2Fe-2S) plant-like ferredoxin in Synechocystis PCC6803 by plasmid shuffling.* Mol Microbiol, 1998. **28**(4): p. 813-21.

34. van Thor, J.J., K.J. Hellingwerf, and H.C. Matthijs, *Characterization and transcriptional regulation of the Synechocystis PCC 6803 petH gene, encoding ferredoxin-NADP+ oxidoreductase: involvement of a novel type of divergent operator*. Plant Mol Biol, 1998. **36**(3): p. 353-63.

35. Thomas, J.C., et al., *A second isoform of the ferredoxin:NADP oxidoreductase generated by an in-frame initiation of translation.* Proc Natl Acad Sci U S A, 2006. **103**(48): p. 18368-73.

36. Nakajima, M., T. Sakamoto, and K. Wada, *The complete purification and characterization of three forms of ferredoxin-NADP(+) oxidoreductase from a thermophilic cyanobacterium Synechococcus elongatus.* Plant Cell Physiol, 2002. **43**(5): p. 484-93.

37. Korn, A., et al., *Ferredoxin:NADP+ oxidoreductase association with phycocyanin modulates its properties.* J Biol Chem, 2009. **284**(46): p. 31789-97.

38. Tamoi, M., et al., *The Calvin cycle in cyanobacteria is regulated by CP12 via the NAD(H)/NADP(H) ratio under light/dark conditions.* Plant J, 2005. **42**(4): p. 504-13.

39. Daley, S.M.E., et al., *Regulation of the Cyanobacterial CO2-Concentrating Mechanism Involves Internal Sensing of NADP(+) and alpha-Ketogutarate Levels by Transcription Factor CcmR.* Plos One, 2012. **7**(7).

40. Ma, W. and T. Ogawa, *Oxygenic photosynthesis-specific subunits of cyanobacterial NADPH dehydrogenases.* IUBMB Life, 2015. **67**(1): p. 3-8.

41. Bassham, J.A., A.A. Benson, and M. Calvin, *The path of carbon in photosynthesis.* J Biol Chem, 1950. **185**(2): p. 781-7.

42. Spreitzer, R.J. and M.E. Salvucci, *Rubisco: structure, regulatory interactions, and possibilities for a better enzyme.* Annu Rev Plant Biol, 2002. **53**: p. 449-75.

43. Badger, M.R. and G.D. Price, *Carbonic Anhydrase Activity Associated with the Cyanobacterium Synechococcus PCC7942.* Plant Physiol, 1989. **89**(1): p. 51-60.

44. Price, G.D., J.R. Coleman, and M.R. Badger, *Association of Carbonic Anhydrase Activity with Carboxysomes Isolated from the Cyanobacterium Synechococcus PCC7942.* Plant Physiol, 1992. **100**(2): p. 784-93.

45. Pacold, I. and L.E. Anderson, *Energy charge control of the Calvin cycle enzyme 3-phosphoglyceric acid kinase.* Biochem Biophys Res Commun, 1973. **51**(1): p. 139-43.

46. Dai, S., et al., *Structural Basis 7of Redox Signaling in Photosynthesis: Structure and Function of Ferredoxin:thioredoxin Reductase and Target Enzymes.* Photosynth Res, 2004. **79**(3): p. 233-48.

47. Hishiya, S., et al., *Binary reducing equivalent pathways using NADPH-thioredoxin reductase and ferredoxin-thioredoxin reductase in the cyanobacterium Synechocystis sp. strain PCC 6803.* Plant Cell Physiol, 2008. **49**(1): p. 11-8.

48. Howard, T.P., et al., *Thioredoxin-mediated reversible dissociation of a stromal multiprotein complex in response to changes in light availability.* Proc Natl Acad Sci U S A, 2008. **105**(10): p. 4056-61.

49. Kramer, D.M. and J.R. Evans, *The importance of energy balance in improving photosynthetic productivity.* Plant Physiol, 2011. **155**(1): p. 70-8.

50. Munekage, Y., et al., *Cyclic electron flow around photosystem I is essential for photosynthesis.* Nature, 2004. **429**(6991): p. 579-82.

51. Yeremenko, N., et al., *Open reading frame ssr2016 is required for antimycin A-sensitive photosystem I-driven cyclic electron flow in the cyanobacterium Synechocystis sp. PCC 6803.* Plant Cell Physiol, 2005. **46**(8): p. 1433-6.

52. Endo, T., et al., *Donation of electrons to plastoquinone by NAD(P)H dehydrogenase and by ferredoxin-quinone reductase in spinach chloroplasts.* Plant and Cell Physiology, 1997. **38**(11): p. 1272-1277.

53. Hertle, A.P., et al., *PGRL1 is the elusive ferredoxin-plastoquinone reductase in photosynthetic cyclic electron flow.* Molecular cell, 2013. **49**(3): p. 511-523.

54. Battchikova, N. and E.M. Aro, *Cyanobacterial NDH-1 complexes: multiplicity in function and subunit composition.* Physiol Plant, 2007. **131**(1): p. 22-32.

55. Mi, H., et al., *Thylakoid membrane-bound, NADPH-specific pyridine nucleotide dehydrogenase complex mediates cyclic electron transport in the cyanobacterium Synechocystis sp. PCC 6803.* Plant and Cell Physiology, 1995. **36**(4): p. 661-668.

56. Hu, P., et al., *Enzymatic characterization of an active NDH complex from Thermosynechococcus elongatus.* FEBS Lett, 2013. **587**(15): p. 2340-5.

57. Battchikova, N., et al., *Identification of Novel Ssl0352 Protein (NdhS), Essential for Efficient Operation of Cyclic Electron Transport around Photosystem I, in NADPH:plastoquinone Oxidoreductase (NDH-1) Complexes of Synechocystis sp. PCC 6803.* Journal of Biological Chemistry, 2011. **286**(42): p. 36992-37001.

58. Cooley, J.W. and W.F.J. Vermaas, *Succinate dehydrogenase and other respiratory pathways in thylakoid membranes of Synechocystis sp strain PCC 6803: Capacity comparisons and physiological function.* Journal of Bacteriology, 2001. **183**(14): p. 4251-4258.

59. Reinhold, L., R. Kosloff, and A. Kaplan, *A Model for Inorganic Carbon Fluxes and Photosynthesis in Cyanobacterial Carboxysomes.* Canadian Journal of Botany-Revue Canadienne De Botanique, 1991. **69**(5): p. 984-988.

60. Miller, A.G. and B. Colman, *Active transport and accumulation of bicarbonate by a unicellular cyanobacterium.* J Bacteriol, 1980. **143**(3): p. 1253-9.

61. Ohkawa, H., H.B. Pakrasi, and T. Ogawa, *Two types of functionally distinct NAD(P)H dehydrogenases in Synechocystis sp. strain PCC6803.* J Biol Chem, 2000. **275**(41): p. 31630-4.

62. Klughammer, B., et al., *The involvement of NAD(P)H dehydrogenase subunits, NdhD3 and NdhF3, in high-affinity CO2 uptake in Synechococcus sp. PCC7002 gives evidence for multiple NDH-1 complexes with specific roles in cyanobacteria.* Mol Microbiol, 1999. **32**(6): p. 1305-15.

63. Friedrich, T. and D. Scheide, *The respiratory complex I of bacteria, archaea and eukarya and its module common with membrane-bound multisubunit hydrogenases.* Febs Letters, 2000. **479**(1-2): p. 1-5.

64. Maeda, S., M.R. Badger, and G.D. Price, *Novel gene products associated with NdhD3/D4-containing NDH-1 complexes are involved in photosynthetic CO2 hydration in the cyanobacterium, Synechococcus sp PCC7942.* Molecular Microbiology, 2002. **43**(2): p. 425-435.

65. Reinhold, L., M. Zviman, and A. Kaplan, *A Quantitative Model for Inorganic Carbon Fluxes and Photosynthesis in Cyanobacteria.* Plant Physiology and Biochemistry, 1989. **27**(6): p. 945-954.

66. Price, G.D., et al., *Advances in understanding the cyanobacterial CO(2)-concentrating-mechanism (CCM): functional components, Ci transporters, diversity, genetic regulation and prospects for engineering into plants.* Journal of Experimental Botany, 2008. **59**(7): p. 1441-1461.

67. Price, G.D., et al., *Identification of a SulP-type bicarbonate transporter in marine cyanobacteria.* Proc Natl Acad Sci U S A, 2004. **101**(52): p. 18228-33.

68. Wang, H.L., B.L. Postier, and R.L. Burnap, *Alterations in global patterns of gene expression in Synechocystis sp PCC 6803 in response to inorganic carbon limitation and the inactivation of ndhR, a LysR family regulator.* Journal of Biological Chemistry, 2004. **279**(7): p. 5739-5751.

69. Shibata, M., et al., *Genes essential to sodium-dependent bicarbonate transport in cyanobacteria: function and phylogenetic analysis.* J Biol Chem, 2002. **277**(21): p. 18658-64.

70. Omata, T., et al., *Identification of an ATP-binding cassette transporter involved in bicarbonate uptake in the cyanobacterium Synechococcus sp. strain PCC 7942.* Proc Natl Acad Sci U S A, 1999. **96**(23): p. 13571-6.

71. Omata, T., et al., *Involvement of a CbbR homolog in low CO2-induced activation of the bicarbonate transporter operon in cyanobacteria.* J Bacteriol, 2001. **183**(6): p. 1891-8.

72. Figge, R.M., et al., *Characterization and analysis of an NAD(P)H dehydrogenase transcriptional regulator critical for the survival of cyanobacteria facing inorganic carbon starvation and osmotic stress.* Molecular Microbiology, 2001. **39**(2): p. 455-468.

73. Maddocks, S.E. and P.C.F. Oyston, *Structure and function of the LysR-type transcriptional regulator (LTTR) family proteins.* Microbiology-Sgm, 2008. **154**: p. 3609-3623.

74. Nishimura, T., et al., *Mechanism of low CO2-induced activation of the cmp bicarbonate transporter operon by a LysR family protein in the cyanobacterium Synechococcus elongatus strain PCC 7942.* Molecular Microbiology, 2008. **68**(1): p. 98-109.

75. Eisenhut, M., et al., *Metabolome Phenotyping of Inorganic Carbon Limitation in Cells of the Wild Type and Photorespiratory Mutants of the Cyanobacterium Synechocystis sp Strain PCC 6803.* Plant Physiology, 2008. **148**(4): p. 2109-2120.

76. Mitschke, J., et al., *An experimentally anchored map of transcriptional start sites in the model cyanobacterium Synechocystis sp. PCC6803.* Proc Natl Acad Sci U S A, 2011. **108**(5): p. 2124-9.

77. Klahn, S., et al., *Integrated transcriptomic and metabolomic characterization of the low-carbon response using an ndhR mutant of Synechocystis sp. PCC 6803.* Plant Physiol, 2015.

78. Du, J., et al., *Characterisation of cyanobacterial bicarbonate transporters in E. coli shows that SbtA homologs are functional in this heterologous expression system.* PLoS One, 2014. **9**(12): p. e115905.

79. Grundel, M., et al., *Impaired glycogen synthesis causes metabolic overflow reactions and affects stress responses in the cyanobacterium Synechocystis sp PCC 6803.* Microbiology-Sgm, 2012. **158**: p. 3032-3043.

80. Eisenhut, M., et al., *Long-term response toward inorganic carbon limitation in wild type and glycolate turnover mutants of the cyanobacterium Synechocystis sp strain PCC 6803(1[W]).* Plant Physiology, 2007. **144**(4): p. 1946-1959.

81. Shimakawa, G., et al., *Respiration accumulates Calvin cycle intermediates for the rapid start of photosynthesis in Synechocystis sp. PCC 6803.* Bioscience Biotechnology and Biochemistry, 2014. **78**(12): p. 1997-2007.

82. Carrieri, D., et al., *Photo-catalytic conversion of carbon dioxide to organic acids by a recombinant cyanobacterium incapable of glycogen storage.* Energy & Environmental Science, 2012. **5**(11): p. 9457-9461.

83. Miao, X.L., et al., *Changes in photosynthesis and pigmentation in an agp deletion mutant of the cyanobacterium Synechocystis sp.* Biotechnology Letters, 2003. **25**(5): p. 391-396.

84. Suzuki, E., et al., *Carbohydrate Metabolism in Mutants of the Cyanobacterium Synechococcus elongatus PCC 7942 Defective in Glycogen Synthesis.* Applied and Environmental Microbiology, 2010. **76**(10): p. 3153-3159.

85. Krishnan, A., et al., *Metabolic and photosynthetic consequences of blocking starch biosynthesis in the green alga Chlamydomonas reinhardtii sta6 mutant.* Plant Journal, 2015. **81**(6): p. 947-960.

86. Ungerer, J., et al., *Sustained photosynthetic conversion of CO2 to ethylene in recombinant cyanobacterium Synechocystis 6803.* Energy & Environmental Science, 2012. **5**(10): p. 8998-9006.

87. Zhang, S. and D.A. Bryant, *The tricarboxylic acid cycle in cyanobacteria.* Science, 2011. **334**(6062): p. 1551-3.

CHAPTER II

Experimental procedures

2.1 Growth and culturing

Wild-type and mutant strains of *Synechocystis* sp. PCC 6803 (hereafter *Synechocystis*) were used for all experimental assays. Wild-type stains were obtained from in-lab frozen glycerol stocks that were obtained from Louis Sherman (Purdue University, Indiana). The Δ*glgC* knock-out mutant and JU547 EFE mutant were gifts from the Yu lab at the National Renewable Energy Lab (Golden, CO), and detail of their construction has been previously published [1, 2].

Synechocystis cultures were maintained in BG11 medium [3]. Cultures from frozen glycerol stocks were spread onto BG11 plates supplemented with 1.4% agar. Cultures were grown until isolated colonies were observed (~7-14 days) and transferred to 100 mL of BG11 medium in a 250 mL Erlenmeyer flask. These cultures were grown on a rotary shaker (~200 rpm) at a modest light intensity (~80 μE). Selective pressure for mutant strains were maintained using 20 μg/mL spectinomycin for the JU547 mutant and 10 μg/mL gentamycin for the Δ*glgC* mutant. The medium for the Δ*glgC* mutant was also supplemented with 20 mM HCO_3^- when grown with antibiotics.

For experimental assays, cultures were transferred to a modified BG11 medium (termed LC7 medium). The medium is strongly buffered with 40 mM HEPES, using KOH to bring the medium to pH 7.0. Sodium carbonate (Na_2CO_3) is omitted from the medium as well. These modifications allow the inorganic carbon availability to be more easily manipulated during culturing, since the lower pH increases the amount of dissolved CO_2 and decreases the concentration of HCO_3^- existing in solution. Therefore, inorganic carbon availability can be adjusted through altering the concentration of CO_2 in the gassing mixture used to aerate cultures.

For growing cultures to be used in experimental assays, strains were grown in 1 L Roux bottles containing 800 mL of modified BG11. Inorganic carbon was delivered by gassing mixtures with ambient air (~0.03% CO_2) or a 3% CO_2/air mixture filtered through 0.2 μm filters. Culture bottles were kept in a 30°C water-bath and were kept under moderate white-light illumination (~50 μE) supplied by fluorescent bulbs. Cultures grown under 3% CO_2 gassing do not express the high-affinity carbon transport complexes, but expression of these proteins can be induced upon switching to ambient air gassing [4]. Cultures grown under 3% CO_2 gassing are denoted as high-carbon grown (HC), while those gassed with ambient air are referred to as low-carbon grown (LC).

Wild-type cell cultures were maintained under constant HC growth during in situ analysis of redox changes accompanying inorganic carbon limitation (Paper I; see Chapter 3). Cells were passaged by dilution into sterile LC7 media every 3 days, in order to minimize alterations in photosynthesis due to cell shading in dense cultures. Samples were harvested at OD_{750} ~0.6 (approximately 2 days growth) to perform assays. When the analysis of carbon metabolism mutants was performed, cells were cultured in similar HC conditions, and harvested for sample collection when OD_{750} = 0.6-1.0, due to differences in growth rates. In order to induce the high-affinity CCM carbon transporters, 2 day old cell cultures (OD_{750} = 0.6-1.0) were switched to air gassing (LC) for 24 hours and then harvested to perform assays.

2.2 Sample harvesting and preparation

Approximately 200-250 mL of each cell culture were harvested by centrifugation at 6,000 x g for 10 minutes in 250 mL plastic bottles. When analyzing cultures during the transition from high-carbon to low-carbon conditions (Paper I; see Chapter 3), samples were resuspended in LC7 medium that had been bubbled with 3% CO_2 for at least one hour. Samples were resuspended to a dense cell concentration corresponding to 50-200 μg chlorophyll·mL^{-1} and placed on a rotary shaker under moderate illumination (~100 μE). When cultures were also to be analyzed for their carbon uptake properties (Paper II; see Chapter 4), samples were resuspended in 2 mL LC7 medium that had been bubbled with CO_2-free air (79% N_2/21% O_2). Samples were transferred to 2 mL test tubes and centrifuged at 10,000 x g for 5 minutes. Samples were resuspended and washed in media in this manner two more times. After the third wash, samples were resuspended to a dense chlorophyll concentration corresponding to 50-200 μg Chl · ml^{-1} and placed on a rotary shaker under moderate illumination (~100 μE).

The chlorophyll content of these dense cell preparations was estimated by measuring the optical density of a 1 mL 1:20 dilution of sample to buffer. Optical density measurements were made by a UV–Vis Scanning Spectrophotometer (UV-2101PC, Shimadzu, Japan) which had been blanked using buffer or water (BG11 and water have equivalent absorption properties). During the blanking of the spectrophotometer and measurement of samples, office tape was applied in a manner so that the sample and reference beam passed through tape and samples. This modification helps to reduce the effect of cell scattering when measuring the absorption properties. Optical density values at three wavelengths were used to estimate chlorophyll content using the following equation [5]:

$$[\mathrm{Chl}] = \left(14.96 * (\mathrm{A}_{678} - \mathrm{A}_{750})\right) - \left(0.607 * (\mathrm{A}_{620} - \mathrm{A}_{750})\right) * dilution$$

Where A_{620}, A_{678}, and A_{750} are absorbance values at those 620, 678, and 750 nm and *dilution* is the dilution factor of the measured samples (i.e. 20). This estimated chlorophyll concentration was used to dilute the dense cell preparations to a density corresponding to 5 μg Chl · ml^{-1} using assay buffer.

In order to determine the actual chlorophyll concentration of samples, 1 mL of sample was centrifuged at 10,000 x g for 10 minutes. The supernatant was decanted and cells were resuspended in 1 mL of cold (4°C) methanol by vortexing. Samples were incubated 20 minutes at 4°C. Samples were centrifuged at 10,000 x g for 10 minutes at 4°C. The optical density of the supernatant was measured by UV-Vis spectroscopy at 650 and 720 nm wavelengths. The chlorophyll concentration was determined by the following equation [6]:

$$[\mathrm{Chl}] = 12.9447 * (A_{650} - A_{720})$$

2.3 Chlorophyll fluorescence spectroscopy

Chlorophyll fluorescence was measured using a Walz DUAL-PAM 100 (Walz, Germany) outfitted with a DUAL-DR photodetector and LED module. The DUAL-DR uses a single red LED (620 nm) in order to provide an adjustable, low-intensity measuring light. The unit also contains an array of 24 red (635 nm) LEDs used to provide illumination for actinic light, saturating flashes, and multiple turnover flashes. The fluorescence signal is detected by an internal photodiode that is protected by a long-pass filter (RG9 glass), effectively blocking light at wavelengths below 680 nm. Cell samples were prepared in an optical glass cuvette (1 cm cross section) and placed into an enclosure that omits exogenous light. Sample agitation is provided with a magnetic stir bar and stirrer controlled by the DUAL-PAM software. Using DUAL-PAM software, measuring traces (triggered runs) were programmed to deliver actions (e.g. actinic illumination, saturating pulses, stir bar, etc.) at specific time points, ensuring replicate traces encounter identical conditions.

In order to follow chlorophyll fluorescence as cells experience carbon limitation (Paper I; see Chapter 3), cell preparations were diluted in an optical glass cuvette to a density corresponding to 5 μg Chl · ml^{-1} in LC7 medium that had been bubbled with CO_2 for at least one hour. The sample was placed into the DUAL-PAM sample holder and stirred at a rate that maintained cells in suspension, but did not cause excessive aeration of the sample. The measuring light was turned on at a low setting (12 μE) and actinic light was turned on at a moderate light intensity (~100 μE). After 15 minutes the stirrer and actinic illumination was terminated, and a triggered run measuring trace was recorded (discussed below). After the triggered run was completed, sample stirring and actinic illumination resumed. Measuring traces were repeated in this manner for 16 hours to analyze chlorophyll fluorescence in response to the depletion of inorganic carbon available in the media.

The triggered run performed every 15 minutes was designed for the cell samples to experience periods of darkness, actinic illumination, and then darkness again, a measuring protocol termed the Kautsky transient [7]. Measurement of chlorophyll fluorescence initiated at t=0, 30 seconds after actinic illumination and stirring was terminated. Dark-adapted fluorescence was measured for 1 minute, and then actinic illumination (100 μE) was provided (t=60 s). Actinic illumination was provided for 270 seconds, at which point actinic illumination was terminated (t=330 s) and measurement of chlorophyll fluorescence continued for 80 additional seconds. At this point (t=410 s) measurement traces terminated and sample stirring and actinic illumination (100μE) resumed, allowing photosynthesis to resume consumption of inorganic carbon available in the media. Multiple turnover flashes (20,000 μE) were delivered at 30, 310, and 400 seconds; two in darkness, and one during actinic illumination. This triggered run pattern was delivered every 15 minutes over 16 hours.

In order to analyze chlorophyll fluorescence of the wild-type and mutant strains (Paper II; see Chapter 3) under high and low inorganic carbon availability, a similar triggered run pattern was

used. Cell samples were diluted in an optical glass cuvette to a density corresponding to 5 μg Chl · ml^{-1} in LC7 medium that had been bubbled with CO_2-free air for at least one hour. Samples were supplemented with 5 mM Na_2HCO_3 and stirred under actinic illumination (53μE) for 4 minutes. Actinic illumination was terminated and samples were allowed to dark-adapt for 5 minutes before measuring traces were started. Dark-adapted chlorophyll fluorescence was measured for 60 seconds, at which point actinic illumination (53 μE) was provided for 300 seconds and then terminated (t = 360 s). Post-illumination fluorescence was measured for an additional 140 seconds (t = 500 s) and terminated. Multiple turnover flashes (20,000 μE) were provided at 15 and 310 seconds.

Samples were also subjected to shorter periods of actinic illumination. In these traces, the chlorophyll fluorescence of dark-adapted cells was measured for 30 seconds in darkness, 60 seconds of actinic illumination (53μE), and 60 seconds in darkness. No multiple turnover flashes were provided as these might interfere with post-illumination transients.

2.4 NADPH fluorescence

Blue-green fluorescence was measured using Walz DUAL-ENADPH (emitter) and DUAL-DNADPH (detector) units (Walz, Germany). The DUAL-ENADPH unit has a 365 nm measuring light, while the Dual-DNADPH unit has a blue-sensitive photomultiplier with a filter sandwich transmitting from 420-550 nm. Although NADH shows fluorescence activity at these wavelengths, no evidence has been shown that significant changes in blue-green fluorescence transients measured in cyanobacteria is attributable to NADH [8, 9].

Due to the difference of excitation and emission wavelengths between NADPH and chlorophyll, both chlorophyll and NADPH fluorescence could be measured simultaneously. The DUAL-PAM apparatus is arranged so that the DUAL-DR and DUAL-ENADPH units are set on opposing sides of the sample cuvette, and the DUAL-DNADPH device is oriented perpendicular to the DUAL-

ENADPH unit. Therefore all triggered runs and programs used the same sequence of actions, actinic light patterns and intensities, and sample preparation conditions as those described in measuring chlorophyll fluorescence (see above).

2.5 P700 absorbance

P700 absorbance was measured in a JTS-10 spectrophotometer (Bio-Logic, France) using a 620 nm actinic light and a 705 nm interference filter over the detection and reference photodetectors. Samples were diluted to a density corresponding to 5 μg Chl · ml^{-1} in a 1 cm quartz cuvette using LC7 medium that had been bubbled with CO_2-free air for at least one hour and supplemented with 5 mM Na_2HCO_3. In order to measure cyclic electron flow of cell samples, 10 μM DCMU was also added. Samples were acclimated to darkness for 5 minutes while being stirred with a magnetic stirrer. Stirring was terminated before measurements and the beam aperture was adjusted to a level where the voltage difference between the measuring and reference photodetector was <0.1 V. Absorbance measurements were followed for 10 seconds in darkness, in order to establish a minimum value of P700 oxidation, during a 5 second illumination (2050 μE), and for 8.5 seconds in darkness. This was performed using the following JTS-10 program:

```
3(10msD)10sD2(10msD)10msG200μsD1msD1msD3msD{3ms,30,5s,
D}100μsH200μsD{2ms,20,8s,D}
```

In order to assay steady-state P700 activity during illumination, samples were placed in the JTS-10 cuvette holder and stirred while under mild actinic illumination (45 μE). Stirring was terminated after 10 minutes and the beam aperture was adjusted as previously described. Two series of three detection pulses were applied 10 seconds apart, in order to establish a baseline level of P700 oxidation during illumination. Illumination was terminated as a 200 μs saturating pulse (2500 μE) was delivered to fully oxidize P700. The rereduction of P700 was followed for 8

seconds in order to obtain the absorbance value of fully reduced P700. The following JTS-10 program formula was used:

```
3(10msD)10sD2(10msD)10msH300µsD20µsE{3ms,30,200ms,D}
100µsF200µsD{2ms,20,8s,D}50msD3(1msD)
```

The chlorophyll content for sample loading of the JTS-10 was estimated spectroscopically, so fluorescence transients were normalized to chlorophyll content as measured by methanol extraction, as spectroscopic estimation of chlorophyll content was more variable in the mutant strains. Half-times were measured using JTS-10 software (Bio-Logic, France) and converted into rate constants, k, by dividing the natural log of 2 by the half-time value. The percent of reduced P700 ($P700_{red}/P700_{tot}$; Φ_{PSI}) was determined by dividing the baseline absorbance value during illumination by the difference between maximum and minimum absorbance values (i.e. during the saturating pulse and during darkness). The given values are mean values of three biological replicates and error bars are the standard deviation of these values.

2.6 Oxygen evolution assays

Oxygen evolution assays were performed using a Clark-type oxygen electrode. Assays were performed in a temperature controlled water jacket maintained at 30°C. Samples were diluted to a density corresponding to 5 µg Chl · ml^{-1} in LC7 medium that had been bubbled with CO_2-free air for at least one hour. Whole chain electron transport and respiration was measured in the presence of 5 mM $NaHCO_3^-$. Maximum rates of oxygen evolution were measured in the presence of 1 mM DCBQ and 1 mM potassium ferricyanide to act as electron acceptors from PSII, thereby liberating its activity from the photosynthetic electron transport chain. Oxygen evolution was measured under saturating light (~10,000 µE) for 90 seconds. A linear regression fit from 40 to 80 seconds were used to determine rates of oxygen evolution, as earlier time points have an artefactual rise due to heat. Rates of respiration were obtained after rates of oxygen evolution, so

that respiration was measured during 80 seconds of darkness after approximately 90 seconds of illumination. Rates of respiration were obtained from linear regression fits from values obtained 40 to 80 seconds after illumination was terminated. Results are presented as the mean of three biological replicates, with error bars representing standard deviation values.

In order to test the delayed induction of the Calvin-Benson-Bashamm cycle, samples were diluted to a density corresponding to 5 μg Chl · ml^{-1} in LC7 medium that had been bubbled with CO_2-free air for at least one hour. Samples were supplemented with 5 mM $NaHCO_3$, and when noted, 5 mM glucose. Oxygen evolution was measured for 900 seconds while samples were under illumination (180 μE). Linear regression fits were made over 30 second time ranges in order to obtain rates of oxygen evolution. Linear and sigmoidal curve fits were determined from rates of oxygen evolution using Kaleidagraph software (Synergy Software) and are presented to highlight general trends of data, not as determinate models of activity.

Bicarbonate affinity measurements were made using oxygen evolution as an indicator of electron transport and carbon uptake, similar to methods employed by other researchers [10]. The oxygen evolution of samples at a density corresponding to 5 μg Chl · ml^{-1} in carbon-free LC7 medium that had been bubbled with CO_2-free air for at least one hour was monitored under continuous illumination (~1500 μE) until oxygen was no longer evolved. At this point, the CO_2 compensation point, rates of oxygen evolution and oxygen consumption are equivalent due to a limitation in carbon availability [11]. This consumption of residual inorganic carbon in the medium typically took 5-10 minutes. While illumination was maintained, known concentrations of $NaHCO_3$ were added in increasing concentrations while oxygen evolution was monitored. Rates of oxygen evolution at each concentration were obtained by taking linear regression of values between 10 seconds after inoculation and 10 seconds before the inoculation of the next concentration (40 seconds total). Rates of oxygen evolution were fitted to the Michaelis-Menton equation using Kaleidagraph software (Synergy Software). Values of V_{max}, the maximum rate of

oxygen evolution, and K_s, the concentration at which the rate of oxygen evolution is half of V_{max}, are presented as mean values of at least three biological replicates and error bars are standard deviations of these values.

2.7 Immunoblot assays

Approximately 200 mL of cell culture was harvested from HC or LC grown cells and centrifuged at 10,000 x g for 10 minutes. Samples were resuspended in 1 mL of 25 mM Tris-HCl/5 mM EDTA pH 7.5 (hereafter TE), transferred to 2 mL centrifuge tubes, and stored at -20°C until protein analysis was performed. Cells were diluted to a density corresponding to 1 mg Chl · ml^{-1} and benzamidine, ε-amino-η-caproic acid, and phenylmethanesulfonyl fluoride were added to 1 mM concentrations in order to inhibit protease activity. An equal volume of zirconium beads were washed with TE buffer and decanted. The cell suspension was added to beads and mixed well. Cells were lysed at 4°C using a Mini-BeadBeater (BioSpec Products, Bartlesville, OK, USA) using 1 minute of beating, followed by 5 minutes in an ice water bath. The 1 minute beating and 5 minute cooling was repeated one time. The samples were gently centrifuged at 600 x g and the cell lysate was removed from the settled beads. Beads were washed one time with 25 mM Tris, and allowed to settle. The lysate was collected and added to the first collected fraction. The chlorophyll content of the cell lysate was measured using methanol extraction and samples were diluted in TE to a density corresponding to 100 μg Chl · ml^{-1}. Samples were aliquoted, frozen in liquid nitrogen, and stored at -80°C.

Proteins were separated on a Laemmli type SDS-PAGE gel comprised of an 8% stacking gel and 12% resolving gel. A sample volume corresponding to 1 μg Chl was added to 2x SDS sample buffer (125 mM Tris-HCl pH 7.5, 20% glycerol, 2% SDS, 0.02% bromophenol blue, 5% β-mercaptoethanol) and loaded onto the gel. Electrophoresis was performed at a constant 100 V for

approximately 2 hours, until the sample loading dye front and low molecular weight protein marker had reached the end of the gel.

Proteins separated by SDS-PAGE were transferred to a PVDF membrane using a semi-dry electrophoretic transfer apparatus (Bio-Rad) with Towbin buffer (25 mM Tris, 192 mM glycine, 20% methanol) supplemented with 0.03% sodium dodecylsulfate (w/v). Before transfer, the PVDF membrane was soaked in 100% methanol and equilibrated in Towbin buffer. The acrylamide gel and filter papers were also equilibrated in Towbin buffer before transfer. Transfers were performed under a constant 25 V for 25 minutes. The membranes were washed two times with 5% bovine serum albumin (BSA) in Tris buffered saline (pH 7.5) with 0.2% Tween 20 (TBST) for 15 minutes and blocked by a 45 minute incubation with 5% BSA in TBST under gentle agitation at room temperature. The membranes were incubated overnight in primary rabbit antibody (rabbit anti-PsbC and rabbit anti-Sbta; Agrisera, Sweden) diluted (1:2000 for PsbC; 1:2000 for SbtA) in 5% BSA in TBST at room temperature with gentle agitation. After incubation, membranes were washed three times in 5% BSA in TBST for 15 minutes each wash. Goat anti-rabbit HRP-conjugated secondary antibody (Agrisera, Sweden) was diluted in 5% BSA in TBST (1:3000 dilution) and incubated with membranes for 2 hours at room temperature while gently shaking. After incubation, membranes were washed two times in TBS (no Tween) for 15 minutes.

Visualization of secondary antibodies was performed using the chromogenic substrate 4-chloro-1-napthol (4CN; Bio-Rad) and H_2O_2 as developing agents. Immediately before visualization, 60 mg of 4CN were dissolved into 20 mL of room temperature methanol. Sixty microliters of ice cold 30% H_2O_2 were added to 100 mL of ice cold TBS. The solutions were mixed and applied to the membrane under intermittent gentle shaking. Color development proceeded for 15-30 minutes and was terminated by washing the membrane with deionized water. Membranes were then dried, photographed, and stored at room temperature in the dark.

2.8 Chapter 2 references

1. Carrieri, D., et al., *Photo-catalytic conversion of carbon dioxide to organic acids by a recombinant cyanobacterium incapable of glycogen storage.* Energy & Environmental Science, 2012. **5**(11): p. 9457-9461.

2. Ungerer, J., et al., *Sustained photosynthetic conversion of CO2 to ethylene in recombinant cyanobacterium Synechocystis 6803.* Energy & Environmental Science, 2012. **5**(10): p. 8998-9006.

3. Castenholz, R.W., *Culturing Methods for Cyanobacteria.* Methods in Enzymology, 1988. **167**: p. 68-93.

4. Wang, H.L., B.L. Postier, and R.L. Burnap, *Alterations in global patterns of gene expression in Synechocystis sp PCC 6803 in response to inorganic carbon limitation and the inactivation of ndhR, a LysR family regulator.* Journal of Biological Chemistry, 2004. **279**(7): p. 5739-5751.

5. Williams, J.G.K., *Construction of Specific Mutations in Photosystem-Ii Photosynthetic Reaction Center by Genetic-Engineering Methods in Synechocystis-6803.* Methods in Enzymology, 1988. **167**: p. 766-778.

6. Ritchie, R.J., *Consistent sets of spectrophotometric chlorophyll equations for acetone, methanol and ethanol solvents.* Photosynthesis Research, 2006. **89**(1): p. 27-41.

7. Stirbet, A. and Govindjee, *On the relation between the Kautsky effect (chlorophyll a fluorescence induction) and Photosystem II: Basics and applications of the OJIP fluorescence transient.* Journal of Photochemistry and Photobiology B-Biology, 2011. **104**(1-2): p. 236-257.

8. Mi, H., C. Klughammer, and U. Schreiber, *Light-induced dynamic changes of NADPH fluorescence in Synechocystis PCC 6803 and its ndhB-defective mutant M55.* Plant Cell Physiol, 2000. **41**(10): p. 1129-35.

9. Kauny, J. and P. Setif, *NADPH fluorescence in the cyanobacterium Synechocystis sp PCC 6803: A versatile probe for in vivo measurements of rates, yields and pools.* Biochimica Et Biophysica Acta-Bioenergetics, 2014. **1837**(6): p. 792-801.

10. Price, G.D., et al., *Identification of a SulP-type bicarbonate transporter in marine cyanobacteria.* Proc Natl Acad Sci U S A, 2004. **101**(52): p. 18228-33.

11. Miller, A.G., G.S. Espie, and D.T. Canvin, *Physiological-Aspects of Co2 and Hco3-Transport by Cyanobacteria - a Review.* Canadian Journal of Botany-Revue Canadienne De Botanique, 1990. **68**(6): p. 1291-1302.

CHAPTER III

Redox changes accompanying inorganic carbon limitation in *Synechocystis* sp. PCC 6803[†]

[†]This chapter is reproduced with slight modification from the following publication:

Holland S.C., Kappell, A. D., Burnap, R. L. (2015) Redox changes accompanying inorganic carbon limitation in *Synechocystis* sp. PCC6803. *Biochimica et Biophysica Acta – Bioenergetics 1847*, 355-363. Reprinted with permission.

Abstract

Inorganic carbon (C_i) is the major sink for photosynthetic reductant in organisms capable of oxygenic photosynthesis. In the absence of abundant C_i, the cyanobacterium *Synechocystis* sp. strain PCC6803 expresses a high affinity C_i acquisition system, the CO_2-concentrating mechanisms (CCM), controlled by the transcriptional regulator CcmR and the metabolites $NADP^+$ and α-ketoglutarate, which act as co-repressors of CcmR by modulating its DNA binding. The CCM thus responds to internal cellular redox changes during the transition from C_i-replete to C_i-limited conditions. However, the actual changes in the metabolic state of the NADPH/$NADP^+$ system that occur during the transition to C_i-limited conditions remain ill-defined. Analysis of changes in the redox state of cells experiencing C_i limitation reveals systematic changes associated with physiological adjustments and a trend towards the quinone and NADP pools becoming highly reduced. A rapid and persistent increase in F_0 was observed in cells reaching the C_i-limited state, as was the induction of photoprotective fluorescence quenching. Systematic changes in the fluorescence induction transients were also observed. As with Chl fluorescence, a

transient reduction of the NADPH pool ('M' peak), is assigned to State 2→State 1 transition associated with increased electron flow to $NADP^+$. This was followed by a characteristic decline, which was abolished by C_i limitation or inhibition of the Calvin-Benson-Bassham (CBB) cycle and is thus assigned to the activation of the CBB cycle. The results are consistent with the proposed regulation of the CCM and provide new information on the nature of the Chl and NADPH fluorescence induction curves.

3.1 Introduction

Inorganic carbon (C_i) is an essential and often limiting macronutrient for the growth of organisms performing oxygenic photosynthesis. It serves as the major sink of photosynthetic reductant via incorporation into sugar carbon skeletons of the reductive Calvin-Bassham-Benson (CBB) cycle. Correspondingly, C_i-limitation may result in the accumulation of electrons in carrier pools leading to the production of damaging reactive oxygen intermediates as well as the loss of overall photosynthetic efficiency due to photorespiration. Photorespiration results from the competition between CO_2 and O_2 at the active site of ribulose bisphosphate carboxylase-oxygenase (RuBisCO) with the former giving the productive carboxylation reaction of ribulose bisphosphate (RuBP) and the latter leading to the wasteful oxygenation of RuBP. Accordingly, low CO_2 or high O_2 concentrations favor the oxygenation reaction over the carboxylation reaction. In aquatic environments, the potential for C_i limitation is particularly acute due to the low solubility and diffusivity of dissolved C_i. To avoid this, cyanobacteria and algae have evolved a CO_2-concentrating mechanism (CCM). The CCM may have emerged in the progenitors of contemporary cyanobacteria as they adapted to cope with increased photorespiration and lower efficiency carbon fixation accompanying a drop in CO_2 levels and a rise in O_2 levels during the Phanerozoic eon about 350 million years ago [1, 2] or an earlier epoch [3]. These adaptations include transport mechanisms for the active uptake of C_i [reviewed in [4, 5]] that work together within a micro-compartment, known as the carboxysome, to localize and increase the local

concentration of CO_2 around RuBisCO, thereby improving the efficiency of CO_2 fixation [reviewed in [6]]. Such mechanisms are highly effective and result in the accumulation of C_i over 1000-fold within the cyanobacterial cell relative to its environment [7, 8]. Recent biotechnological efforts now consider utilizing the cyanobacterial CCM components as a model and source of molecular components for improving plant productivity [5, 9, 10].

The existence of two distinct physiological states defined by different C_i affinities was identified in *Chlamydomonas* depending upon whether cells were grown in air or CO_2-enriched air [11]. Studies with cyanobacteria revealed that they also exhibit an inducible high affinity CCM [8, 12, 13]. The cyanobacterium *Synechocystis* sp. PCC 6803 (hereafter *Synechocystis*) exhibits a basal, lower affinity CCM when grown under C_i sufficient conditions (e.g. gassing with air enriched with 3% v/v air, high C_i, HC) and this depends upon low affinity C_i transporters that are constitutively expressed [14, 15]. The constitutively expressed low affinity uptake mechanism is comprised of multiple transporters, including Na^+/HCO_3^- symporters and a redox powered CO_2-hydration enzyme, CupB (ChpX) that couples to the NADPH dehydrogenase complex (NDH-1) that collectively elevate the cytoplasmic concentration of HCO_3^-. This form of the NDH-1 complex is denoted NDH-1_4 in reference to the alternative pair of intrinsic membrane protein D4/F4 subunits that are postulated to be involved in proton pumping based on homology with known structures [16] and bind the CupB (ChpY) protein [17]. Exposure of *Synechocystis*, and many other cyanobacterial species, to C_i–limited growth conditions elicits the expression of a supplementary high affinity system. Under limiting C_i conditions (bubbling with ambient air, low C_i, LC) there is an induced increase in affinity for C_i achieved through transcriptional up-regulation of transport activities and carboxysome components and, possibly, kinetic modification of existing transporters accounting for the higher affinity physiological state mentioned above. Alternative high affinity suites of proteins, including high affinity Na^+/HCO_3^- symporters and the high affinity CO_2-hydration enzymes, are expressed when cyanobacteria are grown under C_i-

limiting conditions. The increase in transporter affinity for C_i during limiting conditions is due to the transcriptional induction of the genes encoding the ATP dependent BCT1 high affinity HCO_3^- transporter encoded by the *cmp* operon, Na^+-dependent SbtA HCO_3^- symporter, and the specialized NADPH dehydrogenase complex NDH-1_3 high affinity CO_2-hydrating system encoded by the *ndhF3/ndhD3/cupA/cupS* operon. The NDH-1_3 complex is similar to the NDH-1_4 complex except that three specialized membrane intrinsic subunits, D4/F4/CupB, are replaced by their high affinity paralogs, the D3/F3/CupA subunits. The transcriptional regulation of the inducible transporters is controlled by the two self-regulating LysR-type transcriptional regulators known as CcmR (NdhR) [18-20] and CmpR [21, 22]. The signal for induction of the transporter encoded by the *cmp* operon through CmpR has been identified as the co-activators ribulose-bisphosphate (RuBP) and 2-phosphoglycolate (2PG) [21]. The signals for the repression of the putative CcmR regulon controlling the expression of the *sbtA* gene, *ndhF3* operon, and the expression of a putative NDH-I dependent Na^+ transporter are the co-repressors, α-ketoglutarate (α-KG) and oxidized nicotinamide adenine dinucleotide ($NADP^+$) [20]. Thus, the internal metabolic state provides the regulatory cues for expressing the high-affinity system rather than inorganic carbon species *per se*.

The aim of the present study is to understand physiological changes that accompany, and potentially trigger, changes in the regulation of CCM genes and to provide additional physiological context for previous experiments [14, 19, 23-26]. Because of the central role of NADPH in metabolism and because it acts as a critical signaling molecule in the regulation of the CCM, it is important to understand the dynamics of the redox state of the cellular pool of NADPH/$NADP^+$ in response to changes in the availability of C_i. Previous studies have shown that the NADP pool is more reduced in cells grown in low-carbon conditions than in those grown under high-carbon conditions [27]. However, the physiological basis for this change is not fully understood. Furthermore, it is important to understand the dynamic properties of the redox state

of NADP under fluctuating environmental conditions due to it role in regulating cellular processes. Blue green fluorescence has been developed as an approach to monitor changes in the redox state of the pyridine nucleotide pools in isolated intact chloroplasts and leaf fragments [28, 29]. Similarly, the dynamics of redox changes in pyridine pools in cyanobacteria has yielded information on the role of NADPH in cyclic electron flow (CEF) [30]. The commercial availability of a DUAL-PAM-100 (Walz, Germany) allows for the simultaneous measurement of chlorophyll a and NADPH fluorescence [31], which permits the simultaneous *in vivo* investigation of the photosynthetic reducing equivalents of plastoquinone (PQ) and NAD(P)H. A recent investigation of *Synechocystis* NADPH transients has provided important insights into the quantitative use of this instrument and how the levels of NADPH fluctuate in response to different light regimes [32]. Importantly, that study also revealed, for the first time, the extent and kinetic properties of electron transfer occurring from PSI to NADPH via ferredoxin NADP reductase (FNR).

This study aims to use these techniques in order to investigate cellular response to nutrient limitation (i.e. high and low carbon availability). Simultaneous chlorophyll and NADPH fluorescence provides insight into the relationship between the redox state of the PSET chain and its dependence on downstream metabolic processes, namely the CBB cycle.

3.2 Methods

3.2.1 Cell cultures and growth conditions

Experiments sampled 800 mL cultures of wild-type *Synechocystis* sp. PCC 6803 that were grown under 3% CO_2 bubbling conditions in 1L Roux bottles in a modified BG11 medium [33] as described previously [19]. Modified media was identical to standard BG11 except omitting Na_2CO_3, adding HEPES to a concentration of 40 mM, and adjusting the pH to 7.0 using KOH, rather than NaOH.

3.2.2 Fluorescence measurements probing cells during the transition to C_i-limited growth

A 250 mL sample of 3% CO_2 grown cells was centrifuged at 10,000g for 5 minutes. Cells were gently re-suspended in fresh, CO_2 bubbled, low-C_i BG-11 media to a chlorophyll concentration of 5 μg/mL in a 2 mL sample. The sample was placed in a 10 mm open quartz cuvette with a small stir bar. Cells were exposed to red actinic light (~100 μE) and stirred for up to approximately 16 hours. Stirring occurred at a pace that maintained cells in suspension, but did not cause excessive aeration of the sample and therefore inorganic carbon concentrations within the sample could not be replenished at a rate that can keep pace with consumption by cells in the sample performing photosynthesis. Accordingly, samples exhibited fluorescence characteristics of indicative of C_i-limitation approximately eight hours into the experiment.

Every 15 minutes during the approximately 16 hour assay, the stirring and actinic light would be turned off. After 30 seconds of this dark acclimation period, a measuring trace would initiate recording the fluorescence yield from the measuring beam in the dark. Dark period fluorescence was measured for one minute, with an intense 300 ms multiple turnover (MT) flash occurring at 35 seconds. At 60 seconds, the actinic light was turned on. The sample was exposed to actinic light for 270 seconds, with a MT flash occurring 250 seconds after the actinic light exposure. Post-illumination measurement continued for 80 seconds, with a MT flash occurring 70 seconds after stopping illumination. Nine seconds after the (MT), actinic light exposure and stirring resumed. As shown in Supplemental Figure 3.1, growth of cells was maintained although gradual and in a manner consistent with previous observations in normal growth bottles used for gene expression experiments [19]. The parameters of Chl fluorescence characterizing the induction curves follow the calculation and nomenclature described by Campbell *et al* [34].

3.3 Results and Discussion

3.3.1 PAM fluorescence measurements of redox changes in cells during C_i-limitation

To investigate the changes in the cellular redox state in response to C_i-limitation, pulse-amplitude modulated (PAM) fluorometry was utilized (Figure 3.1). Chlorophyll fluorescence is widely used for the analysis of both linear electron flow (LEF) and cyclic electron flow (CEF) and thus the PAM technique provides information on basic photosynthetic parameters. The use of PAM fluorometry to track changes in the redox state of NAD(P)H as blue-green fluorescence is not as widely used, but the technique has the potential to uncover possible redox transients *in vivo* with high time resolution [28, 29, 31] as realized in recently reported work [32]. Because NADPH and NADH possess virtually identical fluorescence characteristics, it is impossible to distinguish which species is responsible for the fluorescence transients, and though physiological investigations have indicated that the transients observed under light changes are largely due to NADPH [30], this limitation remains. Simultaneous monitoring of chlorophyll and NAD(P)H fluorescence of samples was performed in a PAM-100 device (Walz) and a HC→LC downshift routine was developed to roughly emulate the C_i-downshift conditions used previously [19]. For PAM fluorometry, small samples (2 mL) of culture were maintained directly in the optical cuvette and allowed to deplete the media of C_i under illumination with red LEDs and stirring. Another difficultly lies in potential cell growth during the assay. The cells appear to behave in a manner consistent with earlier transcriptional profiling experiments [19], with growth becoming negligible after carbon depletion (Supplemental Figure 3.1). Thus, it appears that the application of the biophysical techniques described below should be a reasonable approximation to the experimental conditions utilized earlier for the gentle C_i downshift experiment global gene expression profiling and therefore it should be possible to connect the biophysical changes with those of the transcriptional changes.

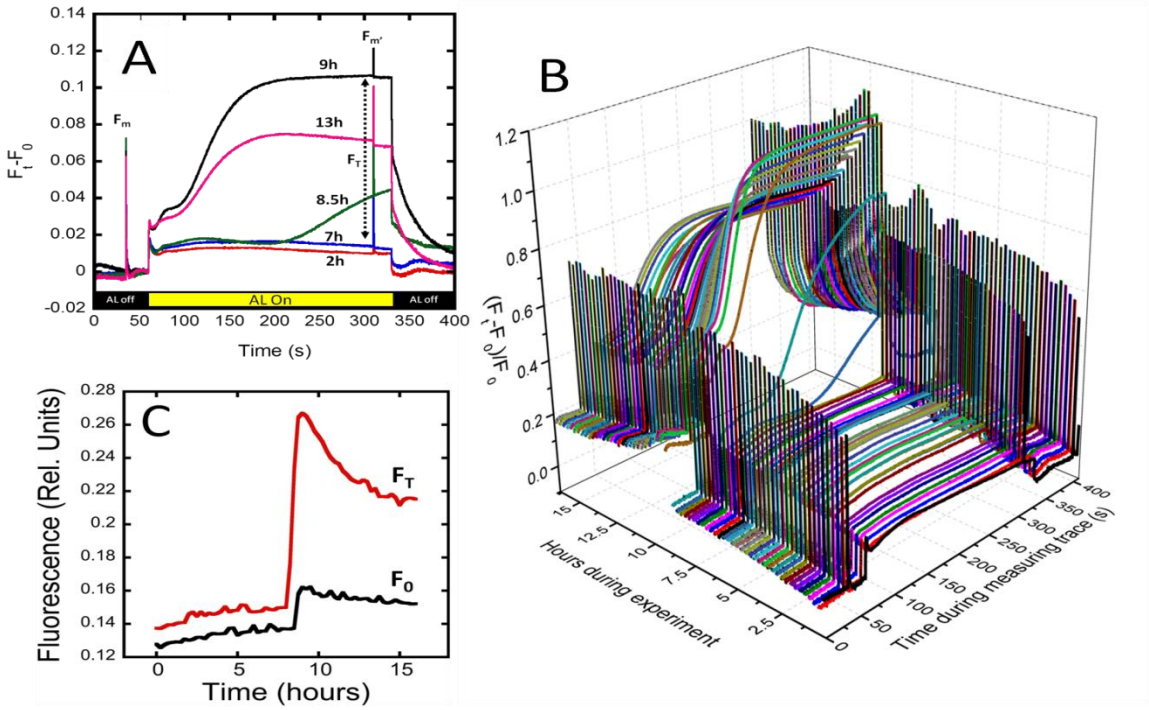

Figure 3.1. Changes in the Chl induction kinetics during the course of inorganic carbon limitation of *Synechocystis* cells. Panel A: Chlorophyll fluorescence traces of cells switched from bubbling with 3% CO_2 enriched air to stirring under illumination in a 10 mm cuvette of a sample undergoing C_i depletion in a PAM fluorometer. Cells were illuminated with actinic red illumination at 110 □E except during the intermittent dark periods at the beginning and end of the actinic light periods of data acquisition. Selected chlorophyll fluorescence induction curves at the time points of 2 (red), 7 (blue), 8.5 (green), 9 (black), and 13 (pink) hours after changing the C_i conditions. After a 60 second dark adaptation (first repetitive intermittent dark period, black bar), actinic light was turned on at 60 seconds (yellow bar) and turned off at 330 seconds for the post-actinic illumination portion of the data collection trace (second repetitive intermittent dark period, second black bar). Multiple turnover flashes were performed during the dark interval and actinic illumination periods at the 30 and 310 time points in the trace (F_m and F_m', respectively). **Panel B:** Overall perspective showing all chlorophyll fluorescence transients during the C_i-deprivation experiment. **Panel C:** Changes in F_0 and F_T during the course of the C_i deprivation, Black line: F_0, chlorophyll fluorescence value 1 second before actinic illumination; Red line: F_T, steady state fluorescence during actinic illumination defined at the 300 sec time point.

Figure 3.1A shows selected chlorophyll fluorescence induction traces at different stages of C_i-limitation. Early in the experiment, while the cells have sufficient C_i, the briefly dark-adapted cells exhibit a characteristic fluorescence induction profile when actinic illumination is resumed. Actinic light powers photosynthetic electron transport, resulting in an increase in chlorophyll fluorescence, indicative of an increase in the number of 'closed' PSII reaction centers, corresponding to an increase in the concentration of reduced acceptor, Q_A^- and, correspondingly,

a higher yield of chlorophyll fluorescence [34]. This reflects a quasi-steady state balance of rates corresponding to the actinic excitation rate generating Q_A^- (Q_A reduction rate) and the rate of forward electron transfer of electron into the PQ pool via the PSII Q_B site (Q_A^- oxidation rate). CBB cycle activation, state transitions, and other bioenergetic and metabolic processes influence their rates and result in additional transients that eventually dampen to a steady state fluorescence level that is maintained throughout the remainder of the actinic illumination period.

Early in the C_i-deprivation experiment, upon illumination of briefly dark adapted cells, a steady state fluorescence level is reached after ~20 seconds of actinic illumination (~80 sec point on the trace) and remains low compared to maximal fluorescence (denoted F_M') in the C_i-replete cells shown as the red trace in Fig. 3.2A. This corresponds to a largely oxidized PQ pool under these illumination conditions, which were designed to approximate the growth light intensities. Correspondingly, this allows the efficient re-oxidization of Q_A^-, thereby maintaining, on balance, about 85% of PSII centers in the open condition (i.e. photochemical quenching, $q_P \sim 0.85$). This situation changes dramatically as discussed below, when the cells proceed into the C_i-limited state, where PSII is found mostly in the closed state under actinic illumination. Saturating multiple turnover flashes were given, one during the dark adaptation (F_m) and one toward the end of the actinic illumination period (F_m'), with the latter having a considerably larger amplitude. This indicates that the cells are undergoing state transitions during the light-dark cycling with cells reaching the State 2 condition in the dark period and then reverting back to State 1 in the light. State 2 corresponds to the molecular configuration where excitation energy from the phycobilisome is increasingly directed to PSI, which is a more efficient quencher of excitation energy than PSII. Resumption of actinic illumination drives the State 2→State 1 transition resulting in more excitation energy from the phycobilisome being directed to PSII providing the higher fluorescence yields seen with the second saturating flash, F_m' (Figure 3.1A). Recent work has assigned the slow S-M fluorescence rise occurring during the first 20 seconds after

application of actinic illumination rise to the State 2→State 1 transition [35]. This assignment is consistent with our experiments where an additional MT flash is given 25 seconds after the re-initiation of actinic illumination (at the 85 sec time point), where it was observed that the higher yield of fluorescence is already elicited indicating that State 2→State 1 transition has already occurred at the end of the S-M phase of the induction curve (Supplemental Figure 3.3).

As the availability of C_i decreases later in the experiment (Figure 3.1, hours 8.25 and after), the characteristic fluorescence induction profile begins to exhibit a new secondary rise phase in the fluorescence yield (Figure 3.1A). This secondary phase first appears late in the actinic illumination period, but as the cells become progressively more C_i-limited, the secondary rise phase is observed earlier and earlier in the actinic illumination portion of the measuring trace (Figure 3.1A, green, black, and pink traces). At the 9 hour trace (Fig 3.1A, black trace), the increase in fluorescence yield begins within 25 seconds of switching on actinic illumination and its level soon approaches maximal fluorescence (F_m'), indicating nearly complete closure of all PSII reaction centers under actinic illumination. Thus, upon reaching the fully C_i-limited condition, virtually all PSII centers are in the closed state (mostly Q_A^-) as the availability of PSII electron acceptor vanishes with all the PQ pool having been converted to the reduced form. This is reflected in the decrease in the re-oxidation rates deduced from the post-actinic illumination fluorescence decays as discussed in the next section. It is also consistent with observations that maximal chlorophyll fluorescence occurs in cyanobacterial cells when they reach the CO_2 compensation point [36-38]. This over-reduced condition is due to C_i-limitation, since the addition of bicarbonate to the cells in the sample cuvette restores the lower fluorescence and kinetic features observed early in the experiment (Supplemental Figure 3.2) [37, 39-42]. We conclude that as C_i limitation becomes progressively more severe, the second rise phase commences progressively earlier as a consequence of an increasingly smaller pool of oxidized

CBB cycle intermediates, the major sink of photosynthetic reductant, consistent with earlier observations [36-38].

Figure 3.1B illustrates the overall experiment, allowing the visualization of these and other trends in the form of a 3D plot that stacks the individual Chl fluorescence measuring traces collected over the entire course of the C_i-limitation experiment. It can be seen that the transition from the low fluorescent to high fluorescent state occurs within a period of about thirty minutes starting at the 8.25 hour time point. It is also clear that upon reaching the C_i-limited state, protective mechanisms involving the induction of some form of non-photochemical quenching (q_N) are elicited. This is evidenced by the decrease in maximal fluorescence starting after 8.25 hours (compare magnitude of fluorescence at 9 hours, black trace versus the lower level at 13 hours in Fig. 3.2A). This is more clearly seen in a plot of F_T, the steady state level of fluorescence under actinic illumination (Figure 3.1C, red trace). Here, F_T is defined as the level of fluorescence at the 300 second point in the overall trace as indicated by the vertical dotted line in Figure 3.1A. F_T reaches a maximum approaching that of maximal fluorescence (F_m'), indicating most PSII centers are closed due to the absence of oxidized acceptor in the over-reduced PQ pool as the lack of available C_i reaches a critical point. However, after reaching this maximum, there is then a steady decline of F_T as protective non-photochemical (q_N) processes are mobilized (Figure 3.1C, red trace). This likely reflects increased activity of photoprotective processes including the action of the flavodiiron proteins, which are associated with the phycobilisome and are proposed to dissipate excess reductant from NADPH and PSII [36, 43-45]. On the other hand, the orange carotenoid protein (OCP), involved in dissipative phycobilisome fluorescence quenching, is not likely involved since red light served as the actinic source and blue-green light activates OCP [46]. This is one possible mechanism for the observed induction of photochemical quenching. Nevertheless, other alternatives also not depending upon OCP cannot be yet excluded as an explanation for the strong gradual decline in maximal fluorescence after cells reach the C_i-limited

state. For example, the dissipation of reductant via the induction of the NDH complexes associated with the CCM may contribute to the quenching [47].

Another redox feature associated with the transition to the C_i-limited physiological state is the occurrence of a sharp increase in F_0 seen beginning at the 8.25 hours trace (Figure 3.1C, black trace). This increase in F_0 is not reversed by the addition of bicarbonate (Supplemental Figure 3.2). Because the post-illumination decay occurs more slowly in C_i-limited cells (Figure 3.2), there existed a possibility that the higher F_0 occurred as a consequence of the slow decay of F_0 due to the absence readily available oxidized carriers and processes that donate electrons to the PQ pool during the dark adaption phase of the light dark cycle. To test this, the dark acclimation interval between measuring traces was increased from 30 to 120 seconds, yet the fluorescence still decayed asymptotically to the higher F_0 position (not shown), indicating the new higher level of F_0 induced by the C_i deprivation corresponds to a relatively long-lived physiological state. Additionally, the higher F_0 does not appear to be due to a state transition since these are observed to occur in a cyclic fashion, as noted above, and the higher F_0 due to C_i depletion persists during the light-dark cycles of the experimental regime. Thus, the origin of the sharp increase in F_0 remains unresolved. It could be speculated that the higher F_0 might be a result of uncoupling of part of the phycobilisome antennae (e.g. partial disassembly of rods) in a process distinct from state transitions. Alternatively, it could relate to an increased redox state of the PQ pool from increased activity of cyclic electron flow or by increased flow through the oxidative pentose phosphate pathway, as sugars are being consumed to compensate for carbon limitation. These alternatives remain hypothetical, yet the phenomenon of increased F_0 does appear to be a novel finding regarding the process of adaptation to nutrient deprivation.

3.3.2 Post-illumination chlorophyll fluorescence kinetics

When the actinic illumination light is switched off, the decline in fluorescence is not monotonic, but exhibits fluctuations during the return to the F_0 level (Figure 3.2). As shown previously, these post-illumination fluctuations in the PQ pool redox state are strongly influenced by CEF and the flow of reductant to the membranes from oxidative metabolism (e.g. pentose phosphate pathway) [30, 48-51]. Upon termination of the actinic light (Figure 3.2, downward arrow, 330 sec), fluorescence drops as reaction centers open due to re-oxidation of Q_A^- by electron transfer to PQ in the Q_B site. The exchange into and out of the Q_B site occurs in the ~5 millisecond time range, which is too fast for the time resolution of these measurements, where the data was collected at a rate of 1 point/ms and with noise levels of about 20% of this comparatively small decaying signal (~15% F_m). However, this poorly resolved fast phase was gradually accompanied by the development of slower phases (Figures 3.2 and Supplemental Figure 3.5) during the course of depletion. The decay of accumulated Q_A^- became multiphasic: the fast fluorescence decay phase ($t_{1/2}$~5 ms) remained about the same relative amplitude as before, but the descent was from the much higher fluorescence level (F_T) of the C_i-starved state and dominated by slower decay processes. Two new decay phases with half times of ~240 ms and ~29 seconds, comprise about 30% and 60%, respectively of the total decline from F_T from cells in the C_i-depleted state (Supplemental Table 3.1 and Supplemental Figure 3.5). These rate constants are only considered as apparent rates due to the presumed complexity of the underlying redox mechanisms, which may include a rate limitation of oxidation of the PQ pool by O_2-dependent oxidases [52]. Nevertheless, the net effect is that the slowdown of Q_A^- oxidation accounts for the accumulation of Q_A^- and the high F_T from cells in the C_i-depleted state as the CBB cycle becomes a less efficient sink for electrons.

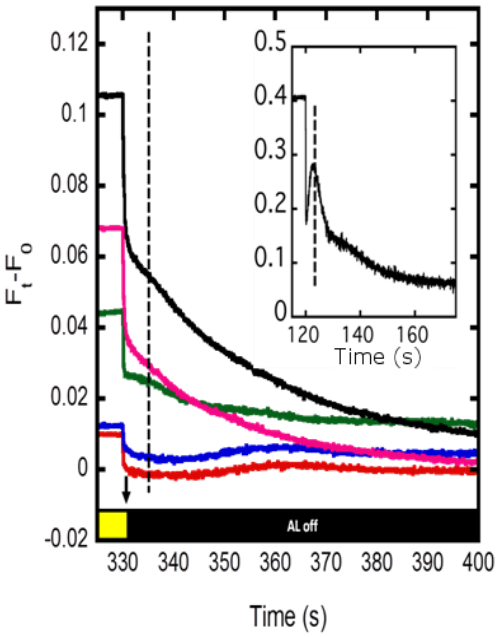

Figure 3.2. Post- actinic illumination fluorescence transients during the course of inorganic carbon limitation of *Synechocystis* cells. Selected chlorophyll fluorescence post-illumination transients at the time points of 2 (red), 7 (blue), 8.5 (green), 9 (black), and 13 (pink) hours after changing the C_i conditions. Post-illumination Chl fluorescence transients show that C_i-limitation enhances the peak occurring ~5 seconds after the cessation of actinic illumination (vertical dotted line). This peak in Chl fluorescence is attributed to cyclic electron transfer [29, 46, 48, 49]. **Inset:** Post-illumination Chl fluorescence peak is most readily observed with shorter actinic illumination periods and in cells grown under low C_i conditions (BG-11 media, slow air bubbling, pH 7), which induces the high affinity CCM including NDH-1_3.

During the first 10 seconds of the post-illumination period there is a kinetic 'shoulder' in the decline of fluorescence, depending on C_i availability (Figure 3.2, inset). This dark increase in fluorescence has been attributed to CEF, predominantly through NDH-1 complexes [30, 48, 50, 51, 53]. Under the current experimental conditions, this peak is not observable early in in the experiment (undetectable in the red and blue traces of Figure 3.2). However, as C_i–limiting conditions prevail later in the experiment, it is possible to observe this increase (Figure 3.2, green and black traces, indicated with a vertical dotted line). This shoulder becomes apparent at ~5 sec after actinic light is switched off (Figure 3.2, denoted with the vertical dotted line). This kinetic feature becomes more pronounced as CEF fluxes increase under conditions where the expression of NDH-1_3 complexes is maximized (i.e. growing cells under LC conditions for several days). This is illustrated in the inset of Figure 3.2, showing the corresponding trace obtained from *Synechocystis* cells grown under LC conditions and giving results very similar to recent experiments [48, 51]. Note the increase in fluorescence ~5 sec after actinic light is switched off, denoted vertical dotted line in the inset of Figure 3.2. In contrast, the present experimental cultures were grown under C_i-replete conditions and switched to C_i-limiting conditions. Because

we have not measured the expression of the NDH-1_3 complexes [see e.g. [25]], it is not possible to determine whether the observed shoulder is due to NDH-1_3 complexes or whether other routes of CEF account for the peak [53]. However, it does seem likely that NDH-1_3 complexes are beginning to be expressed and accumulated as C_i becomes limiting given the similarity to previous experiments [19, 25]. As the cells become more thoroughly C_i–limited and as PQ pool becomes more reduced, the post-illumination shoulder is obscured by the very slow decay phase in the decline of fluorescence yield discussed above (Figure 3.2, pink trace). Besides the 5-10 second post-illumination peak and the slow decay features that increase with C_i-deprivation, it is also interesting to notice an additional kinetic feature: a low amplitude and broad fluorescence increase that occurs approximately 35 seconds after the actinic light is switch off. This roughly corresponds to a similar feature seen in the NADPH post-illumination traces (Figure 3.3B) and probably corresponds to an influx of metabolic reductant into the PQ pool from oxidative carbon metabolism in the cytoplasm as discussed below.

3.3.3 Spectroscopic probes of NADPH during C_i-limitation

Blue-green fluorescence has been used as a tool to analyze NADPH levels *in vivo* [28-30, 32]. Changes in blue-green fluorescence could potentially be due to NADH fluorescence also occurring at these wavelengths. However, Mi *et al*. (2000) noted in *Synechocystis* that short-term changes in fluorescence during actinic illumination were eliminated by treatment with DCMU and DBMIB consistent with the main contribution to the transients as being that from NADPH. Recently, the increase in blue-green fluorescence due to single turnover flashes was best explained by the transfer of electrons from PSI to NADPH via FNR [32]. As shown in Figure 3.3, the shape of the transients produced by actinic illumination during the C_i-limitation experiment shows several similar features with the Chl fluorescence transients acquired in parallel. As with the Chl fluorescence induction profile, blue-green fluorescence quickly rises upon the resumption of actinic illumination (Figure 3.3A, 60 second time point) and is followed

by multiphasic modulations in amplitude that reflect multiple cellular processes that affect the redox state of the NAD(P)H pool. During the first 30 seconds of actinic light exposure, similar multiphasic changes are observed over all periods of carbon availability. For all traces during the experiment, an initial rise occurs quickly due to PSI reduction of $NADP^+$, falls slightly during the ensuing ~8 seconds, and then rises again to a maximal point, labeled 'N_M' in Figure 3.3A. This secondary rise, N_M, peaks ~25-30 seconds after the initial fast rise initiated by resumption of actinic illumination. Similar kinetic features are observed for Chl fluorescence induction kinetics, and there is solid evidence that the corresponding secondary rise to what is referred to as the 'M' peak, corresponds to the State 2→State 1 transition in cyanobacteria [35]. Moreover, the Chl fluorescence experiment described above, where a measuring flash was inserted at the M peak, also provides evidence for this assignment. The State 2→State 1 transition is the adjustable light-harvesting configuration where excitation energy is increasingly directed to PSII at the expense of PSI excitation. Correspondingly, the increased excitation of PSII with cells in State 1 will tend to maximize the rate of whole chain LEF further increasing the level of NADPH in the process. The assignment of the secondary NADPH increase (the N_S to N_M rise) to an increased rate of LEF due to the State 2→State 1 transition, which is consistent with the observation that this secondary peak lags the Chl fluorescence M peak by several seconds, as might be expected from the proposed causal sequence with NADPH redox kinetics lagging behind PQ redox kinetics. Therefore, the rise in NAD(P)H fluorescence to the N_M peak is likely a consequence of the excitation energy redistribution of the State 2→State 1 transition.

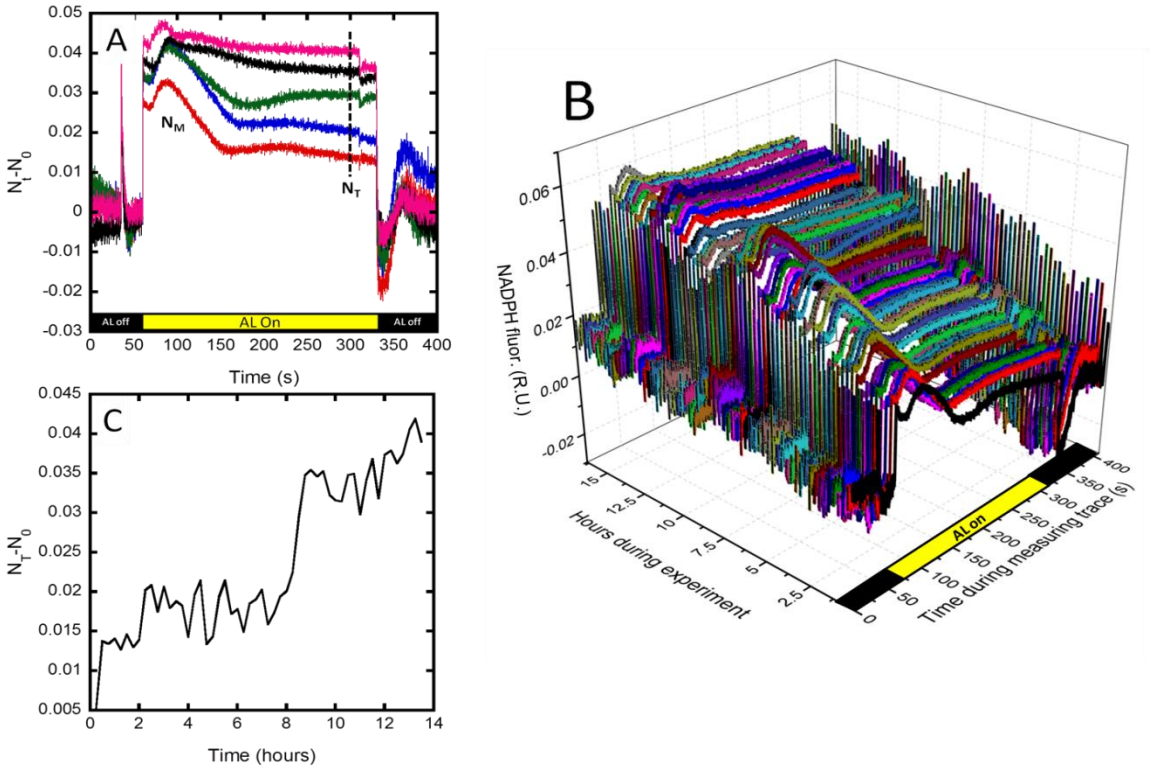

Figure 3.3. Changes in the NAD(P)H kinetics during the course of inorganic carbon limitation of *Synechocystis* cells. Panel A: Selected NAD(P)H fluorescence traces of cells switched from bubbling with 3% CO_2 enriched air to stirring under illumination in a 10 mm cuvette of a sample undergoing C_i depletion in a PAM fluorometer. Cells were illuminated with actinic red illumination at ~100 □E except during the intermittent dark periods at the beginning and end of the actinic light periods of data acquisition. After a 60 second dark adaptation (first repetitive intermittent dark period, black bar), actinic light was turned on at 60 seconds (yellow bar) and turned off at 330 seconds for the post-actinic illumination portion of the data collection trace (second repetitive intermittent dark period, second black bar). The selected traces are for the time points at 2 (red), 7 (blue), 8.5 (green), 9 (black), and 13 (pink) hours after changing the C_i conditions. N_M represents the maximum occurring after resumption of actinic illumination by analogy with 'M' of the Chl fluorescence induction nomenclature (see text). **Panel B:** Overall perspective of NAD(P)H fluorescence transients of a cell sample exposed to C_i limitation. C **Panel C:** Changes in N_T during the course of the C_i deprivation, N_T is here defined as the terminal steady state NAD(P)H fluorescence during actinic illumination, sampled at the 300 sec time point (vertical dotted line).

After ~25 seconds of actinic light exposure (Figure 3.3A), striking differences between NAD(P)H fluorescence traces from C_i-replete and C_i-limited cells are observed. Before the onset of carbon limitation, a pronounced drop in reduced NADPH is observed after reaching the maximum, N_M (Figure 3.3A). This re-oxidation of the NAD(P)H pool after N_M may be attributed to activation of

the CBB cycle by analogy with suggestions from Chl fluorescence transients [54]. This decline in NAD(P)H fluorescence proceeds for approximately 60 seconds before reaching a new lower steady state level under the C_i-replete conditions. Presumably, the new lower level corresponds to a balance in rates of production of NADPH by LEF and the rate of consumption by CO_2 fixation in the fully activated CBB cycle. Provided that the resultant sugars also have a sufficient utilization sink, this steady-state level of NADPH would continue without further modulations. Support for this assignment comes from the observation that as cells become increasingly C_i-starved, this decline disappears and instead, the steady state level of NAD(P)H fluorescence remains at a high value close to the N_M peak (Figure 3.3A, 7 hour and later traces). This is likely due to a hindered CBB cycle resulting in less NADPH being oxidized. This assignment is also supported by the observation that the addition of the CBB cycle inhibitor GLY abolishes this decline after the N_M peak (Figure 3.5). The limitation in available oxidizers of NADPH is reflected in the parameter N_T, defined as the steady state NAD(P)H fluorescence during actinic illumination defined at the 300 sec time point (Figure 3.3A, vertical dotted line). This limitation is illustrated in the plot of N_T as a function of the time during the C_i-deprivation experiment shown in Figure 3.3C. From these data, it can be inferred that illuminated cells have a more reduced NADPH pool in steady-state in C_i-limited conditions, as opposed to those in C_i-replete conditions. Due to the duration of the experiment and uncertainty due to instrument drift, it is difficult to distinguish between the increase in N_0 due to cell growth and that due to change in redox state, yet from the data presented here, and data from previous biochemical studies [27, 55], it can be seen that there is an overall increase in the reduction state of the NAD(P)H pool during the course of depletion. This jump in the level of N_T also appears to slightly precede the sharp jump in F_0 and F_T also observed during the course of C_i–limitation (Figure 3.1C versus Figure 3.3C). So in this case, the change in NADPH redox state precedes the changes in PQ redox state, as might be expected since the accumulation of reductant in the NADP pool occurs

first following the onset of C_i-limitation and the effect propagates backwards and slows the flow of electrons in the electron transport chain as PSI acceptor becomes more sparse.

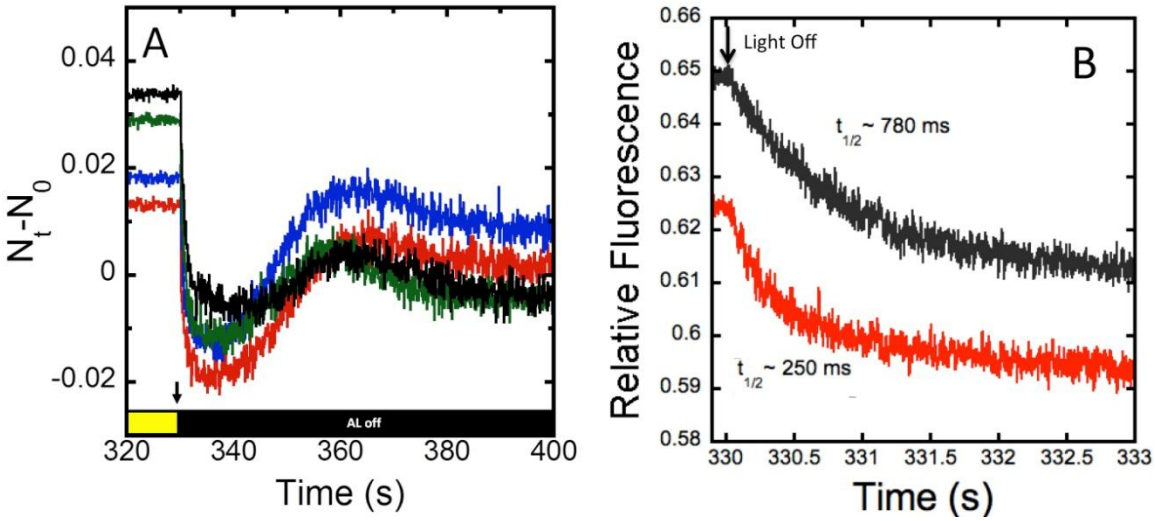

Figure 3.4: Post-illumination changes in NAD(P)H fluorescence. **Panel A:** Selected NAD(P)H fluorescence post-illumination transients at the time points of 2 (red), 7 (blue), 8.5 (green), and 9 (black) hours after changing the C_i conditions. Post-illumination NAD(P)H fluorescence transients exhibit a characteristic oxidation phase followed a re-reduction phase peaking at about 30 seconds after the cessation of the actinic light is switched off at 330 seconds. **Panel B:** Averaged post-illumination decays of NAD(P)H fluorescence during the first three seconds following termination of actinic illumination: Average of 20 traces prior to C_i-depletion (red) and 20 traces after C_i-depletion (black). Downward arrows indicate termination of actinic illumination.

3.3.4 Post-illumination NAD(P)H fluorescence transients

Post-illumination transients in NAD(P)H fluorescence also reveal interesting differences as cells become increasingly C_i-starved (Figure 3.4). After turning off the actinic light (downward arrows), there is a sharp decline in blue-green fluorescence as LEF ceases to drive electrons into the NADPH pool, yet NADPH consumption pathways remain in their active light-adapted state resulting in an undershoot as previously observed [30-32]. These results show that in C_i replete conditions, the NAD(P)H fluorescence decline is rapid ($t_{1/2}$ ~250 ms) indicative of the avidity and high absorptive capacity of these NADPH-utilizing pathways. However, upon carbon limitation, the fluorescence half-time increases to ~780 ms. From a practical perspective, the rapidity of

these declines highlights the difficulty in performing rapid-quench biochemical analysis procedures to evaluate the redox state of the pyridine nucleotide pool.

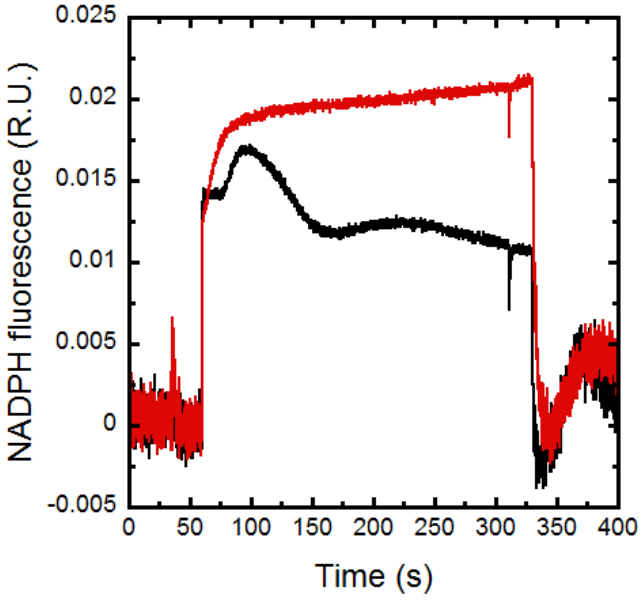

Figure 3.5: The effect of Calvin-Benson-Basham cycle inhibitor glycolaldehyde on NADPH fluorescence induction. NADPH fluorescence transients of a HC cell culture before (black trace) and after (red trace) the addition of 10 mM glycolaldehyde. Cells re-suspended at a concentration of 5 □g Chl mL. Periods of illumination are similar to those previously described except the cells were dark adapted 30 minutes and only 5 cycles of illumination were given and the five traces for each treatment were averaged.

Early in the experiment, the rapid post-illumination decline and 'undershoot' reaches its perigee ~6 seconds after the cessation of actinic illumination followed by a biphasic return to the dark steady state level, N_0. In C_i-replete cells (Figure 3.4, red traces), this biphasic return corresponds to a secondary rise peaking ~35 seconds after the light is switched off. However, as cells proceed into the C_i-limited state, this secondary peak is diminished and shifted to earlier times (Figure 3.4A, black trace). Additionally, the peak corresponds in time to a peak seen in post-illumination Chl fluorescence mentioned above (see also Supplementary Figure 3.4). These peaks are tentatively assigned to the oxidation sugars accumulated in the cytoplasm during the light period which causes the reduction of the pyridine nucleotide pools with electrons transferred the PQ pool for oxidation in the thylakoid located respiratory pathway. As discussed, during chlorophyll fluorescence, a reduction event associated with CEF mediated through NDH-1 complexes becomes more pronounced. Interestingly, very little change occurred within NADPH fluorescence the first 7 seconds after actinic light termination. While the amplitude of the decay

increased, no new transient peaks or shoulders during the decline were observed. The absence of the corresponding feature in the NAD(P)H fluorescence decay occurring 7 seconds after actinic light termination is consistent with the oxidation of NADPH by both the CBB cycle as well as by the respiratory complexes NDH-1 complexes, with the latter contributing to the peak observed during the decay of Chl fluorescence (Figure 3.2).

3.4 Summary and Conclusions

The analysis of changes in the redox state of *Synechocystis* cells experiencing C_i limitation reveals systematic kinetic changes and, as would be expected, a trend towards the quinone and pyridine nucleotide cofactor pools becoming highly reduced. With the ability to measure both chlorophyll and NADPH fluorescence simultaneously, a more complete model of fluorescence kinetics can be created (See Figure 3.6). Changes in NADPH levels are likely to be the major contributor the blue green fluorescence transients observed in response to the changing light and nutrient availability, supporting earlier conclusions based upon inhibitor studies [30] and recent kinetic analyses [32]. Despite many years of observation, the underlying physiological bases for many of the undulations in the Chl fluorescence induction curves are not completely understood. Obviously much is known: starting with the observation that dark-adapted cells will have a basal chlorophyll fluorescence given by the parameter F_0, corresponding to maximal open PSII reaction centers and basal fluorescence due to the decay of excitons in proximal and distal light harvesting antennae, which escape being trapped at the reaction centers. The analogous parameter in NADPH fluorescence, N_0, corresponds to a dark-adapted level of NADPH, where cellular metabolism has reached steady state. Upon illumination, chlorophyll fluorescence undergoes a series of distinct modulations (OJDIP rise, not illustrated in Figure 3.6) before reaching a local peak, F_P within the first 2-3 seconds of illumination. These modulations correspond to intra-molecular electron transfer reactions within PSII but are affected by the rate of re-oxidation of Q_A^- by secondary acceptors [56]. NADPH fluorescence also responds to actinic illumination by

reaching a local maximum, N_P in a similar time frame. It is likely that the kinetic similarities are due to the strong dependence of electron flow through PSI depending upon the flow through PSII with modulation by the state of the intersystem electron transport chain. Similarly, an inhibition of the major sink of photosynthetic electrons, CO_2-fixation via the CBB, results in the accumulation of electrons within the electron transport chain and the consequent diminished ability of the PQ pool to re-oxidize Q_A^-. This intimate connection between the PSII acceptor and the CBB cycle is observed as a larger F_P peak upon reaching the C_i-limited state (Figure 3.1A) and in the presence of glycolaldehyde (not shown). After reaching the F_P peak, chlorophyll fluorescence drops to a local stationary state, F_S. The cause of this decline has been fully resolved [56], but NADPH fluorescence also reaches a local minimum/stationary phase at this time (N_S). From this point, a rise in both chlorophyll and NADPH fluorescence is observed: for Chl fluorescence this is the F_S to F_M rise. This has been attributed to State 2→State 1 transition in cyanobacteria [35]. The subsequent decline from F_M/N_M is not reversion of this state transition, but instead can be attributed to the activation of the CBB cycle, where in C_i-replete conditions NADPH is consumed, and in C_i-limited environments, both Chl and NADPH fluorescence remain high. Photochemical quenching through the activation CBB cycle permits a decline in chlorophyll fluorescence at F_M as regenerated $NADP^+$ remains available as an electron sink. However, when the CBB cycle is impaired, a rise in both chlorophyll fluorescence and NADPH is observed and evolves to higher fluorescence levels (F_T and N_T) upon reaching steady state, which requires about two minutes of actinic illumination in the present experiments (Figures 3.1 and 3.2). As cells reach the C_i–limited state, a rapid and persistent increase in F_0 was observed (Figure 3.1C). The basis for this increase remains to be established, but it may reflect a hitherto unknown protective mechanism for dissipating excess excitation energy, albeit with the possibility of re-absorption. Likewise, an ostensibly photoprotective increase in photochemical quenching is observed upon reaching the C_i –limited state which we tentatively assign to the induction of flavodiiron proteins that dissipate photochemical electron [36, 43-45] and have been

shown to be induced under similar conditions as those studied here [19]. Upon termination of actinic light, chlorophyll and NADPH fluorescence quickly declines, although examination of the decays shows new kinetic features and decreased rates of oxidation as C_i becomes limiting. It is also observed that a small rise in chlorophyll fluorescence (here termed F_N) occurrs 5-10 seconds after actinic light termination. This feature is attributable to cyclic electron flow through NDH complexes ([48, 51], See also Figure 3.2 inset). This feature which is absent under some conditions, but enhanced in cells grown under C_i limitation likely due to the pool of reductant immediately available as reduced ferredoxin and NADPH. Later, a reduction event in chlorophyll and NADPH fluorescence is observed (here termed F_R and N_R), attributed to the oxidation of sugars accumulated in the light and the attendant flow of reductant through the NADP and PQ pools to molecular oxygen consistent with the late (~30 seconds after actinic termination) and protracted kinetics of this feature.

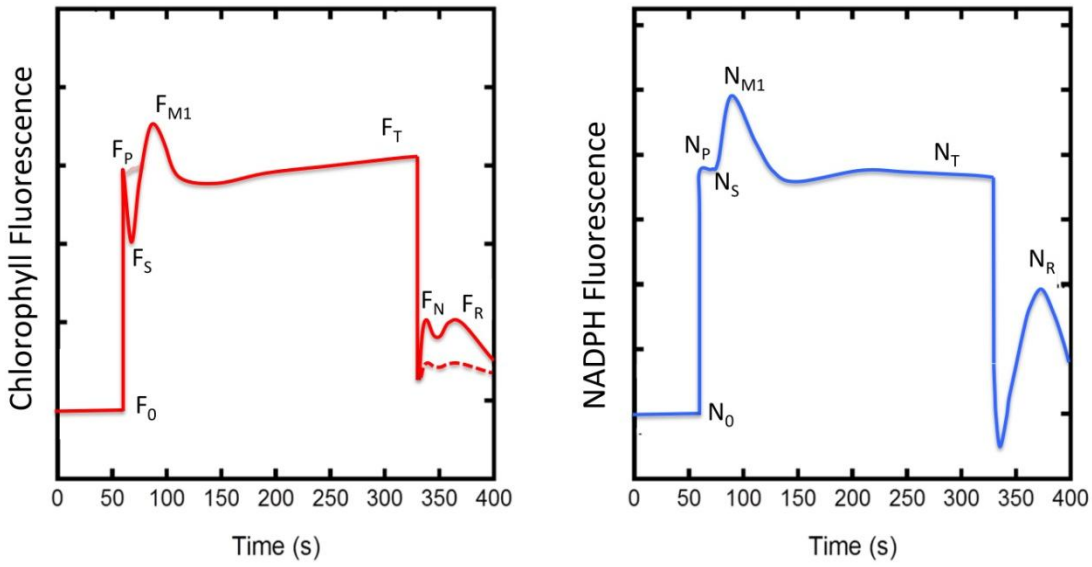

Figure 3.6: Fluorescence transients in cyanobacteria. Left panel: Chlorophyll fluorescence **Right panel:** NADPH fluorescence. Designated points (discussed in the text) may be useful in assaying cellular metabolism.

Finally, the observed increase in the NADPH/$NADP^+$ ratio is consistent with recent findings regarding the mechanism of induction of the high affinity CCM via alterations in the activity of

the transcriptional repressor, CcmR, caused by the interaction of $NADP^+$ and α-KG [20]. The results are consistent with the previous finding that $NADP^+$ acts as an internal sensor of C_i status and inhibits induction of the CCM via its interaction with the transcriptional regulator CcmR. In those experiments, the induction of many genes occurred within 30 minutes of the onset of C_i-limitation, coinciding with the growth inflection and the pronounced changes in fluorescence kinetics observed here.

3.5 Acknowledgements

The authors would like to thank Juliana Artier for her contributions towards developing the PAM fluorescence techniques employed in this study. This work was supported by the United States Department of Energy, Office of Basic Energy Sciences, DE-FG02-08ER15968.

3.6 Supplemental materials

	Chl fluorescence decays		NAD(P)H decay	NAD(P)H decay (10 μs flash)
	halftime	amplitude		
Pre-depletion	4 ms	100%	250 ms	525 ms
C_i -depleted	5 ms	9%	780 ms	924 ms
	240 ms	32%		
	29 sec	59%		
Pre-depletion + 10 mM GLY	240 ms	50%	1800 ms	949 ms
	29 sec	50%		

Supplemental Table 3.1: Kinetics of Post-Illumination Redox Transients Kinetic constants estimated from the chlorophyll and NAD(P)H fluorescence decays following the switch-off of actinic illumination a the end of 270 sec actinic light (~100 μE) illumination period described in the main text (first two columns) and following a 10 μs flash (last column, see figures S3.5, S3.6 also).

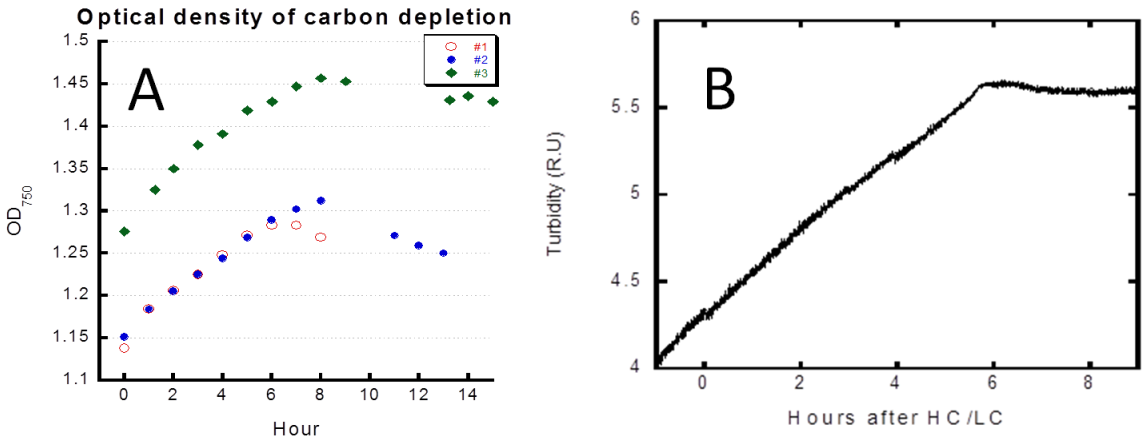

Supplemental Figure 3.1: Optical density measurements during C_i depletion PAM instrument versus in large-scale culture. Panel A: Three different 2 mL samples were subjected to the carbon depletion assay described in the main text. Every hour their absorbance spectra were analyzed. Panel B: Turbidity of a 800 mL cell culture switched from CO2 bubbled growth to air bubbled growth at hour 0 measure under condition similar to previous gene expression experiments [19].

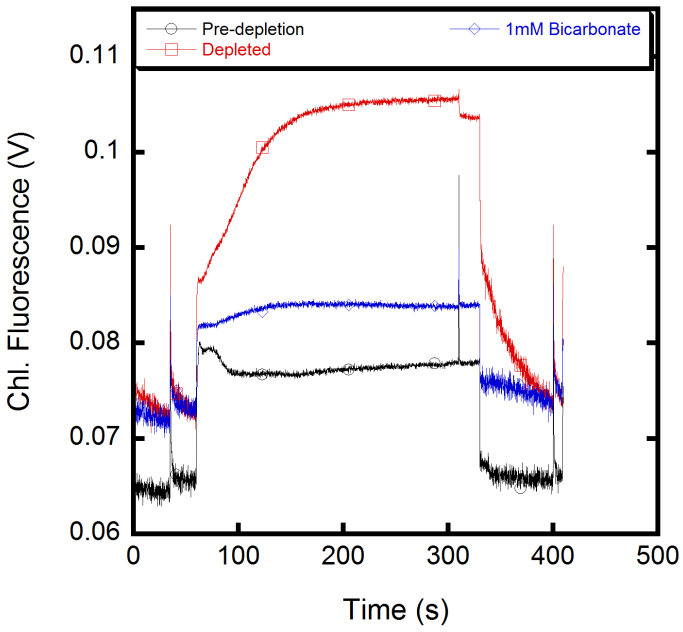

Supplemental Figure 3.2: Alleviation of chlorophyll fluorescence by the addition of sodium bicarbonate to carbon depleted cells. Chlorophyll fluorescence transients of wild-type *Synechocystis* before carbon depletion (black trace), after carbon depletion (red trace), and after the addition of 1mM sodium bicarbonate (blue trace). Cells were carbon depleted using the same light regime described in Figures 2 and 4 of the main text. Bicarbonate was added to the depleted cells in the absence of actinic light and stirred for 30 seconds.

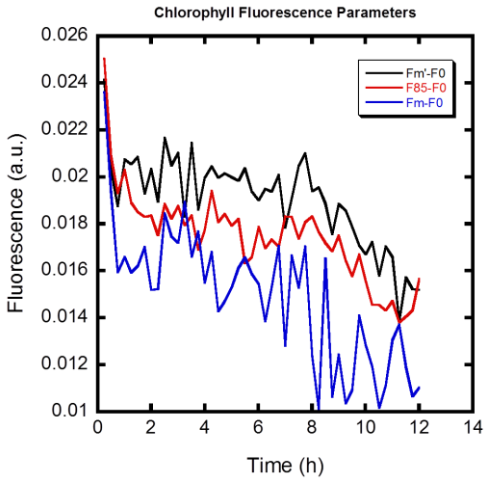

Supplemental Figure 3.3: Amplitudes of multiple turnover flash chlorophyll fluorescence transients. Cells underwent a carbon depletion assay essentially as described (see methods and results), except with the addition of a multiple turnover pulse at 85 seconds (25 seconds after the actinic light was turned on). Displayed are three chlorophyll parameters: $F_{m'}$, F_m, (see text for definitions) and F_{85} (the fluorescence value during a MT flash at 85 seconds) subtracted by F_0.

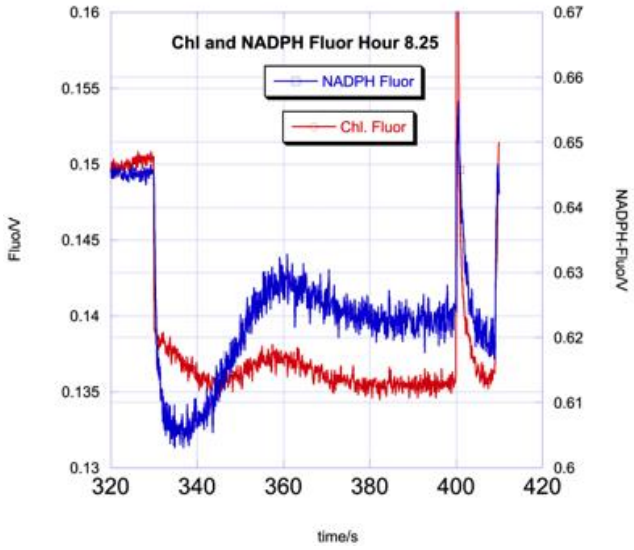

Supplemental Figure 3.4: Comparison of post-illumination chlorophyll and NAD(P)H fluorescence transients. Simultaneous chlorophyll and NADPH fluorescence transients illustrate the timing of metabolic processes that occur post-illumination.

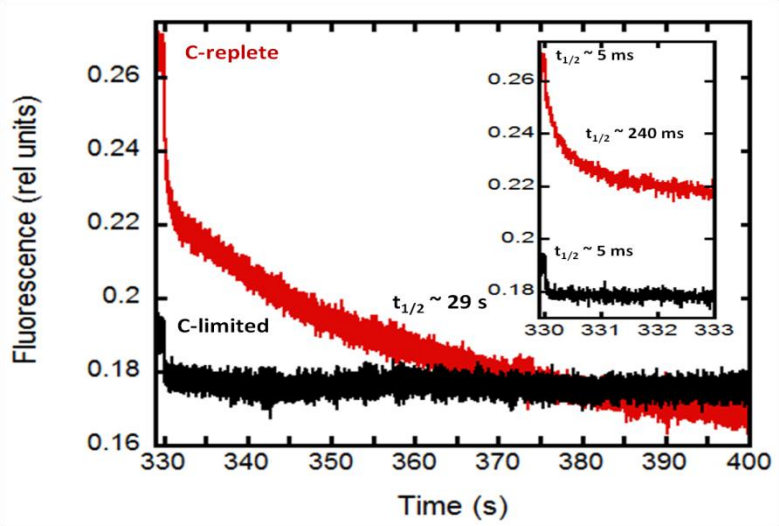

Supplemental Figure 3.5: Post-illumination decays of chlorophyll fluorescence. Traces are derived from the experiment shown in Figure 3.1 of the main text, displaying a carbon replete (black) and carbon limited trace (red). The inset displays the first 3 seconds of each respective trace. Approximate half times of fluorescence decays have been labeled. Also see Table S1.

3.7 Chapter 3 References

1. Badger, M.R., D. Hanson, and G.D. Price, *Evolution and diversity of CO_2 concentrating mechanisms in cyanobacteria.* Functional Plant Biology, 2002. **29**: p. 161-173.

2. Johansson, A.L., et al., *Proton-transport mechanisms in cytochrome c oxidase revealed by studies of kinetic isotope effects.* Biochim Biophys Acta, 2011. **1807**(9): p. 1083-94.

3. Meyer, M. and H. Griffiths, *Origins and diversity of eukaryotic CO2-concentrating mechanisms: lessons for the future.* Journal of Experimental Botany, 2013. **64**(3): p. 769-786.

4. Ogawa, T. and H. Mi, *Cyanobacterial NADPH dehydrogenase complexes.* Photosynth Res, 2007. **93**(1-3): p. 69-77.

5. Price, G.D., et al., *Advances in understanding the cyanobacterial CO_2-concentrating-mechanism (CCM): functional components, Ci transporters, diversity, genetic regulation and prospects for engineering into plants.* J. Exp. Bot., 2008. **59**(7): p. 1441-1461.

6. Yeates, T.O., et al., *Protein-based organelles in bacteria: carboxysomes and related microcompartments.* Nat Rev Microbiol, 2008. **6**(9): p. 681-91.

7. Miller, A.G. and B. Colman, *Active transport and accumulation of bicarbonate by a unicellular cyanobacterium.* J Bacteriol, 1980. **143**(3): p. 1253-9.

8. Badger, M.R. and T.J. Andrews, *Photosynthesis and inorganic carbon usage by the marine cyanobacterium, Synechococcus sp.* Plant Physiol, 1982. **70**(2): p. 517-23.

9. Price, G.D., et al., *The cyanobacterial CCM as a source of genes for improving photosynthetic CO_2 fixation in crop species.* Journal of Experimental Botany, 2013. **64**(3): p. 753-768.

10. Weber, A.P.M. and A. Brautigam, *The role of membrane transport in metabolic engineering of plant primary metabolism.* Current Opinion in Biotechnology, 2013. **24**(2): p. 256-262.

11. Badger, M.R., A. Kaplan, and J.A. Berry, *Internal inorganic carbon pool of Chlamydomonas reinhardtii: Evidence for a carbon dioxide-concentrating mechanism.* Plant Physiol, 1980. **66**(3): p. 407-13.

12. Marcus, Y., et al., *Induction of HCO_3^- transporting capability and high photosynthetic affinity to inorganic carbon by low concentration of CO_2 in Anabaena variabilis.* Plant Physiology, 1982. **69**(5): p. 1008-1012.

13. Kaplan, A., M.R. Badger, and J.A. Berry, *Photosynthesis and intracellular inorganic carbon pool in the blue-green algae Anabaena variabilis: Response to external CO2 concentration.* Planta, 1980. **149**: p. 219-226.

14. Shibata, M., et al., *Distinct constitutive and low-CO_2-induced CO_2 uptake systems in cyanobacteria: genes involved and their phylogenetic relationship with homologous genes in other organisms.* Proc Natl Acad Sci U S A, 2001. **98**(20): p. 11789-94.

15. Klughammer, B., et al., *The involvement of NAD(P)H dehydrogenase subunits, NdhD3 and NdhF3, in high-affinity CO2 uptake in Synechococcus sp. PCC7002 gives evidence for multiple NDH-1 complexes with specific roles in cyanobacteria.* Mol Microbiol, 1999. **32**(6): p. 1305-15.

16. Efremov, R.G., R. Baradaran, and L.A. Sazanov, *The architecture of respiratory complex I.* Nature, 2010. **465**(7297): p. 441-5.

17. Battchikova, N., M. Eisenhut, and E.M. Aro, *Cyanobacterial NDH-1 complexes: novel insights and remaining puzzles.* Biochim Biophys Acta, 2011. **1807**(8): p. 935-44.

18. Figge, R.M., et al., *Characterization and analysis of an NAD(P)H dehydrogenase transcriptional regulator critical for the survival of cyanobacteria facing inorganic carbon starvation and osmotic stress.* Mol Microbiol, 2001. **39**(2): p. 455-68.

19. Wang, H.L., B.L. Postier, and R.L. Burnap, *Alterations in global patterns of gene expression in Synechocystis sp. PCC 6803 in response to inorganic carbon limitation and the inactivation of ndhR, a LysR family regulator.* J Biol Chem, 2004. **279**(7): p. 5739-51.

20. Daley, S.M., et al., *Regulation of the cyanobacterial CO_2-concentrating mechanism involves internal sensing of $NADP^+$ and alpha-ketogutarate levels by transcription factor CcmR.* PLoS One, 2012. **7**(7): p. e41286.

21. Nishimura, T., et al., *Mechanism of low CO_2-induced activation of the cmp bicarbonate transporter operon by a LysR family protein in the cyanobacterium Synechococcus elongatus strain PCC 7942.* Mol Microbiol, 2008. **68**(1): p. 98-109.

22. Takahashi, Y., O. Yamaguchi, and T. Omata, *Roles of CmpR, a LysR family transcriptional regulator, in acclimation of the cyanobacterium Synechococcus sp. strain PCC 7942 to low-CO_2 and high-light conditions.* Mol Microbiol, 2004. **52**(3): p. 837-45.

23. Woodger, F.J., M.R. Badger, and G.D. Price, *Inorganic carbon limitation induces transcripts encoding components of the CO_2-concentrating mechanism in Synechococcus sp. PCC7942 through a redox-independent pathway.* Plant Physiol, 2003. **133**(4): p. 2069-80.

24. Woodger, F.J., M.R. Badger, and G.D. Price, *Sensing of inorganic carbon limitation in Synechococcus PCC7942 is correlated with the size of the internal inorganic carbon pool and involves oxygen.* Plant Physiology, 2005. **139**(4): p. 1959-1969.

25. Zhang, P., et al., *Expression and functional roles of the two distinct NDH-1 complexes and the carbon acquisition complex NdhD3/NdhF3/CupA/Sll1735 in Synechocystis sp PCC 6803.* Plant Cell, 2004. **16**(12): p. 3326-40.

26. Eisenhut, M., et al., *Long-Term Response toward Inorganic Carbon Limitation in Wild Type and Glycolate Turnover Mutants of the Cyanobacterium Synechocystis sp. Strain PCC 6803.* Plant Physiol, 2007. **144**(4): p. 1946-59.

27. Cooley, J.W. and W.F. Vermaas, *Succinate Dehydrogenase and Other Respiratory Pathways in Thylakoid Membranes of Synechocystis sp. Strain PCC 6803: Capacity Comparisons and Physiological Function.* J Bacteriol, 2001. **183**(14): p. 4251-8.

28. Latouche, G., et al., *Light-induced changes of NADPH fluorescence in isolated chloroplasts: a spectral and fluorescence lifetime study.* Biochimica Et Biophysica Acta-Bioenergetics, 2000. **1460**(2-3): p. 311-329.

29. Cerovic, Z., et al., *Simultaneous measurement of changes in red and blue fluorescence in illuminated isolated chloroplasts and leaf pieces: The contribution of NADPH to the blue fluorescence signal.* Photosynthesis Research, 1993. **36**(3): p. 193-204.

30. Mi, H., C. Klughammer, and U. Schreiber, *Light-induced dynamic changes of NADPH fluorescence in Synechocystis PCC 6803 and Its ndhB-defective mutant M55.* Plant Cell Physiol., 2000. **41**(10): p. 1129-1135.

31. Schreiber, U. and C. Klughammer, *New NADPH/9-AA module for the DUAL-PAM-100: Description, operation and examples of application.*, in *PAM Application Notes*2009, Heinz Walz GmbH: Effeltrich, Germany. p. 1-13.

32. Kauny, J. and P. Setif, *NADPH fluorescence in the cyanobacterium Synechocystis sp. PCC 6803: A versatile probe for in vivo measurements of rates, yields and pools.* Biochim Biophys Acta, 2014. **1837**(6): p. 792-801.

33. Allen, M.M., *Simple conditions for growth of unicellular blue-green algae on plates.* Journal of Phycology, 1968. **4**(1): p. 1-4.

34. Campbell, D., et al., *Chlorophyll fluorescence analysis of cyanobacterial photosynthesis and acclimation.* Microbiology and Molecular Biology Reviews, 1998. **62**(3): p. 667–683.

35. Kaňa, R., et al., *The slow S to M fluorescence rise in cyanobacteria is due to a state 2 to state 1 transition.* Biochimica et Biophysica Acta (BBA) - Bioenergetics, 2012. **1817**(8): p. 1237-1247.

36. Miller, A.G., G.S. Espie, and D. Bruce, *Characterization of the non-photochemical quenching of chlorophyll fluorescence that occurs during the active accumulation of inorganic carbon in the cyanobacterium Synechococcus PCC 7942.* Photosynthesis Research, 1996. **49**(3): p. 251-262.

37. Miller, A.G., G.S. Espie, and D.T. Canvin, *Chlorophyll-a fluorescence yield as a monitor of both active CO_2 and HCO_3^- transport by the cyanobacterium Synechococcus UTEX 625.* Plant Physiology, 1988. **86**(3): p. 655-658.

38. Badger, M. and U. Schreiber, *Effects of inorganic carbon accumulation on photosynthetic oxygen reduction and cyclic electron flow in the cyanobacterium Synechococcus PCC7942.* Photosynthesis Research, 1993. **37**(3): p. 177-191.

39. Espie, G.S., A.G. Miller, and D.T. Canvin, *High Affinity Transport of CO(2) in the Cyanobacterium Synechococcus UTEX 625.* Plant Physiol, 1991. **97**(3): p. 943-53.

40. Miller, A.G. and D.T. Canvin, *Glycoaldehyde inhibits CO_2 fixation in the cyanobacterium Synechococcus UTEX-625 without inhibiting the accumulation of inorganic carbon or the associated quenching of chlorophyll a fluorescence.* Plant Physiology, 1989. **91**(3): p. 1044-1049.

41. Bruce, D., G. Samson, and C. Carpenter, *The origins of nonphotochemical quenching of chlorophyll fluorescence in photosynthesis. Direct quenching by P680+ in photosystem II enriched membranes at low pH.* Biochemistry, 1997. **36**: p. 749 55.

42. Price, G.D. and M.R. Badger, *Ethoxyzolamide Inhibition of CO2 Uptake in the Cyanobacterium Synechococcus PCC7942 without Apparent Inhibition of Internal Carbonic Anhydrase Activity.* Plant Physiol., 1989. **89**(1): p. 37-43.

43. Zhang, P., et al., *Operon flv4-flv2 provides cyanobacterial photosystem II with flexibility of electron transfer.* Plant Cell, 2012. **24**(5): p. 1952-71.

44. Allahverdiyeva, Y., et al., *Flavodiiron proteins Flv1 and Flv3 enable cyanobacterial growth and photosynthesis under fluctuating light.* Proc Natl Acad Sci U S A, 2013. **110**(10): p. 4111-6.

45. Bersanini, L., et al., *Flavodiiron Protein Flv2/Flv4-Related Photoprotective Mechanism Dissipates Excitation Pressure of PSII in Cooperation with Phycobilisomes in Cyanobacteria.* Plant Physiology, 2014. **164**(2): p. 805-818.

46. Kirilovsky, D., *Photoprotection in cyanobacteria: the orange carotenoid protein (OCP)-related non-photochemical-quenching mechanism.* Photosynth Res, 2007. **93**(1-3): p. 7-16.

47. Tchernov, D., et al., *Massive light-dependent cycling of inorganic carbon between oxygenic photosynthetic microorganisms and their surroundings.* Photosynth Res, 2003. **77**(2-3): p. 95-103.

48. Battchikova, N., et al., *Identification of Novel Ssl0352 Protein (NdhS), Essential for Efficient Operation of Cyclic Electron Transport around Photosystem I, in NADPH:plastoquinone Oxidoreductase (NDH-1) Complexes of Synechocystis sp. PCC 6803.* Journal of Biological Chemistry, 2011. **286**(42): p. 36992-37001.

49. Gotoh, E., et al., *A qualitative analysis of the regulation of cyclic electron flow around photosystem I from the post-illumination chlorophyll fluorescence transient in Arabidopsis: a new platform for the in vivo investigation of the chloroplast redox state.* Photosynthesis Research, 2010. **103**(2): p. 111-123.

50. Deng, Y., J. Ye, and H. Mi, *Effects of Low CO2 on NAD(P)H Dehydrogenase, a Mediator of Cyclic Electron Transport Around Photosystem I in the Cyanobacterium Synechocystis PCC6803.* Plant and Cell Physiology, 2003. **44**(5): p. 534-540.

51. Schwarz, D., et al., *The gene sml0013 of Synechocystis species strain PCC 6803 encodes for a novel subunit of the NAD(P)H oxidoreductase or complex I that is ubiquitously distributed among Cyanobacteria.* Plant Physiol, 2013. **163**(3): p. 1191-202.

52. Bolyehevtseva, Y.V., et al., *Effects of oxygen and photosynthesis carbon cycle reactions on kinetics of P700 redox transients in cyanobacterium Arthrospira platensis cells.* Biochemistry-Moscow, 2007. **72**(3): p. 275-281.

53. Bernat, G., et al., *Distinct Roles of Multiple NDH-1 Complexes in the Cyanobacterial Electron Transport Network as Revealed by Kinetic Analysis of P700(+) Reduction in Various ndh-Deficient Mutants of Synechocystis sp. Strain PCC6803.* Journal of Bacteriology, 2011. **193**(1): p. 292-295.

54. Renger, G. and U. Schreiber, *Practical applications of fluorometric methods to algae and higher plant research,* in *Light emission by plants and bacteria*, Govindjee, J. Amesz, and D. Fork, Editors. 1986, Academic Press: Orlando, USA. p. 589–616.

55. Tamoi, M., et al., *The Calvin cycle in cyanobacteria is regulated by CP12 via the NAD(H)/NADP(H) ratio under light/dark conditions.* Plant Journal, 2005. **42**(4): p. 504-513.

56. Papageorgiou, G., M. Tsimilli-Michael, and K. Stamatakis, *The fast and slow kinetics of chlorophyll a fluorescence induction in plants, algae and cyanobacteria: a viewpoint.* Photosynthesis Research, 2007. **94**(2): p. 275-290.

CHAPTER IV

Impacts of metabolic pathway engineering on photosynthetic performance. †

†This chapter contains work being prepared for publication. The work contains contributions from the following authors, but the experiments were primarily designed, performed and analyzed by Steven C. Holland.

Steven C. Holland[1], Juliana Artier[1], Neil Miller[1], Melissa Cano[2], Junpeng Yu[2], Maria Ghirardi,[2] Robert L. Burnap[1]*

[1]Department of Microbiology and Molecular Genetics, Oklahoma State University, Stillwater, OK 74078, USA.

[2]Biosciences Center, National Renewable Energy Laboratory, 15013 Denver West Parkway Golden, CO 80401, USA.

Abstract

Genetic engineering of photosynthetic organisms typically redirects native metabolism towards desirable products, which thereby represent new metabolic sinks. There is limited information on how these modifications impact the evolved mechanisms of photosynthetic energy metabolism and cellular growth. Two engineered strains of *Synechocystis* sp. PCC 6803 with altered carbon sink capacity were assayed for their photosynthetic and CO_2 concentrating mechanism properties in conditions of high and low inorganic carbon (C_i) availability. In the Δ*glgC* mutant, glycogen cannot be synthesized and a carbon sink pathway has been effectively removed. The JU547 strain

has been engineered by integration of the *Pseudomonas syringae* ethylene forming enzyme and provides a new sink. When cultured under high carbon conditions, *ΔglgC* displayed diminished photochemical efficiency, a more reduced NADPH pool, delayed initiation of the Calvin-Benson-Bassham cycle, and impairment of linear and cyclic electron flows. It also exhibited a large decrease in photochemical quenching indicative of the accumulation of Q_A^-, normally associated with a reduced PQ pool, but was instead found to be due to saturatable pool of alternative PSII oxidant, presumably for dissipation of excess reductant due to impaired metabolism. In the case of carbon sink integration, JU547 displayed slightly more oxidized PQ and NADPH pools and increased rates of cyclic electron flow and an enhanced demand for inorganic carbon as suggested by increase in the expression of the bicarbonate transporter, SbtA. Overall, the results highlight the importance of the native regulatory network of autotrophic metabolism in governing photosynthetic performance and provide cogent examples of both predicable and difficult to predict phenotypic consequences upon installation of new pathways in autotrophs.

4.1 Introduction

The cyanobacteria have long served as models for studying oxygenic photosynthesis and autotrophic carbon metabolism. This includes recent genetic engineering studies that investigate the feasibility of producing biofuels and economically valuable compounds that represent diversions of photosynthetic products to these alternative products (reviews, see references[1-3]). Presently there is limited information on how such engineered modifications will impact the evolved mechanism of photosynthetic energy metabolism and cellular growth. Conceivably, it is possible that the evolved regulatory mechanisms built into the native enzymes and cell regulatory circuits will be sufficient to accommodate the alterations in photosynthetic and metabolic flux imposed by the engineered pathways. That is, the introduction of genetic modifications leading to desired products or restricting flux to competing pathways may produce little in the way of deleterious or unexpected effects, apart from anticipated losses in cell growth and productivity

due to partitioning of photosynthate away from growth substrate. Such introduced pathway alterations would be considered benign. On the other hand, it is also possible, in principle, that the introduced changes in metabolism will 'inappropriately' interact with the native regulatory mechanisms. In this case, native regulatory mechanisms and flux characteristics that normally give rise to evolutionary fitness and robustness in the natural system instead produce deleterious misregulation of gene and metabolic activity. For example, it was recently observed that carbon fixation capacity was severely diminished upon large diversion of photosynthate towards, 2,3-butanediol, an engineered sink [4]. However, the physiological basis for that observation remained unresolved. Indeed, an understanding of the 'interaction' between introduced pathways and photosynthetic function generally remains poorly understood. An important approach to this question is to examine photosynthetic performance in the face of contrasting limiting nutrient conditions because nutrient or light availabilities may have a strong influence on whether or not these hypothesized metabolic impacts become significant [2-4].

The availability of inorganic carbon (C_i) is very often the limiting factor in the growth of algae and cyanobacteria in natural and engineered settings[5-10]. For cyanobacterial growth, the two main substrate forms are CO_2 and bicarbonate (HCO_3^-). Cyanobacteria have evolved mechanisms to acquire and concentrate both forms in order to saturate the active site of RubisCO with CO_2. The overall mechanism is termed the CO_2-concentrating mechanism (CCM) [11-13]. The CCM consists of a set of HCO_3^- transporters and a set of redox powered CO_2 uptake (Cup) proteins, which together function to supply HCO_3^- to the carboxysome. The latter contains RubisCO, as well carbonic anhydrase [14]. The action of the HCO_3^- transporters and Cup proteins results in high cytoplasmic concentrations of HCO_3^- driving its transport across the carboxysome boundary through selectively permeable pores in the surrounding proteinaceous shell. Carbonic anhydrase within the carboxysome converts incoming bicarbonate into CO_2 thereby supplying RubisCO. The CCM also exists in two forms: a constitutive low affinity, high flux uptake system and an

inducible high affinity system that is controlled by C_i availability via changes in $NADP^+$ and 2-oxoglutarate levels, which are metabolic signals that respond to changes in C_i availability. An additional metabolic interface between the CCM and metabolism relates to the power demands imposed by the operation of the CCM. The CCM requires both ATP and reductant (NADPH or reduced ferredoxin, Fd_{red}), and therefore, the CCM is intimately connected to photosynthetic electron transport. Accordingly, an important metabolic impact of the CCM involves its demands for ATP and Fd_{red}/NADPH production. A stoichiometric accounting of the NADPH and ATP requirements of the Calvin-Benson-Bassham (CBB) cycle shows a 2:3 ratio of NADPH to ATP required for carbon metabolism [15, 16], although there remains debate whether linear electron transport can fulfil this ratio (briefly reviewed in [15]). Nevertheless, the demanded actual ratio, as tuned to metabolism, almost certainly changes in response to changes in the environment: limited inorganic carbon availability and extremes in pH and light intensity very likely modify this ratio. Furthermore, the introduction of new metabolic channels, and/or the closing of other channels, is predicted to impact these demands on the photosynthetic mechanism. To cope with changes in the cellular demand ratio for NADPH/ATP, oxygenic photosynthesizers have evolved mechanisms of returning electrons to the electron transport chain, thereby increasing *pmf* (and therefore producing ATP) without the net production of Fd/NADPH. Collectively, these mechanisms are referred to as cyclic electron flow (CEF; see Fig. 4.1). There are several putative CEF pathways in cyanobacteria, involving SDH, NDH and FNR, but they remain poorly understood. The availability of CEF pathways, combined with energy dissipation pathways provides the photosynthetic electron transport system flexibility required to cope with fluctuations in light intensity and nutrient supply.

Here we perform a detailed analysis probing for possible changes in photosynthetic electron transport to address the question of how two types of engineered modification, one closing a metabolic sink, the other creating a new sink, are tolerated in the face of contrasting availability

of the major photosynthetic macronutrient, inorganic carbon (Ci). Two engineered strains of Synechocystis sp. PCC6803 (hereafter Synechocystis) were chosen as models for analysis of differentially altered carbon metabolism.

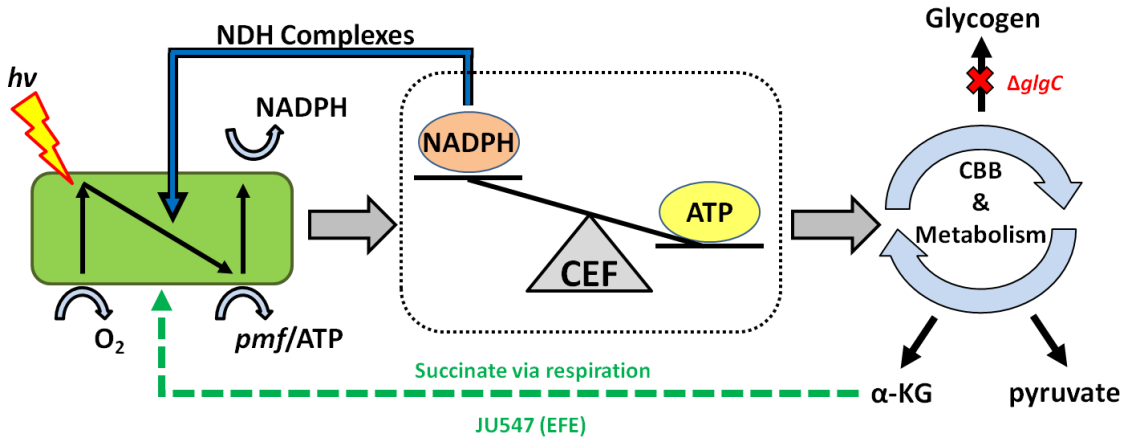

Figure 4.1. Simplified model of electron flow and metabolism in *Synechocystis* sp. PCC 6803. The photosynthetic light reactions obtain electrons from water, producing gaseous oxygen as a result. Electrons are transferred through the photosynthetic electron transport chain ultimately reducing $NADP^+$, forming NADPH. During these reactions, a proton motive force (*pmf*) is established and used to drive the formation of ATP. NADPH and ATP are used to energize the Calvin-Benson-Bassham (CBB) cycle in order to integrate inorganic carbon into cellular metabolism. Cyclic electron flow (CEF) returns electrons back to the electron transport chain and regulates the NADPH/ATP ratio as needed, although the regulatory mechanisms are not fully elucidated. In nutrient replete conditions, glycogen serves as a primary storage molecule for excess electrons and carbon skeletons. In the Δ*glgC* strain (red), an enzyme responsible for glycogen synthesis has been deleted, and glycogen synthesis is removed. In the JU547 strain (green), the ethylene forming enzyme (EFE) gene has been integrated into the genome. As a result, ethylene and succinate are formed as products. Succinate itself may serve as a form of CEF through the succinate dehydrogenase complex (SDH) and return electrons to the electron transport chain.

The first strain, ΔglgC, has a deletion of the gene encoding glucose-1-phosphate adenylyltransferase and cannot synthesize glycogen [17]. Consequently, this mutant lacks a carbon sink available to the wild-type strain. The second strain, JU547, has been engineered to express the ethylene forming enzyme (EFE) from the organism *Pseudomonas syringae* [18]. The ethylene-forming enzyme uses 2-oxoglutarate (2OG, aka α-ketoglutarate) as a cofactor for the synthesis of ethylene, a volatile compound, which escapes the medium as a gas. The JU547 strain therefore has an additional, engineered carbon and electron sink available. Furthermore, the ethylene-

forming reaction also produces succinate in addition to ethylene, which can serve as an electron donor to the plastoquinone pool through the succinate dehydrogenase complex, which may serve as a major donor of electrons during respiration [19]. Appropriately, lower 2OG and higher succinate concentrations have been reported in JU547 [20].

4.2 Methods

4.2.1 Strains used and culturing conditions.

The glucose tolerant *Synechocystis* served as the background control strain and was maintained in standard BG-11 medium [47]. The Δ*glgC* and JU547 strains have been previously described [17, 18]. Experimental cultures were grown in BG-11 medium with the following modifications (here referred as LC7) to allow manipulation of the availability of inorganic carbon. The medium was buffered with 40 mM HEPES-KOH and adjusted to pH 7.0. Sodium carbonate was also omitted from the medium. Prior to inoculation into the modified media, the strains were grown for approximately 5 days in standard BG-11 in shaking flasks under an atmosphere of 3% CO_2 to ensure the cells were in a carbon replete physiological state. These starter cultures were then used to inoculate 700 mL of modified BG-11 in flattened 900 mL flasks, bubbling with 3% CO_2 at a flow rate of ~500 mL min^{-1} and with illumination provided by Cool White fluorescent lamps with an incident intensity of ~ 80 μE m^{-2} s^{-1}. Physiological and biochemical assays were initiated using cultures that had reached an OD_{750} between 0.6 and 1.0. These cultures were designated high carbon cultures (HC). To cause conditions of C_i limitation, the HC cultures were switched to bubbling with ambient air for 18-22 hours to produce low carbon cultures (LC). This mimics the culturing conditions previously used for analysis of transcriptional changes accompanying the downshift in CO_2 availability [48].

4.2.2 Culture harvesting and sample preparation.

Cells were harvested from culture by centrifugation (6000 x g, 10 min). Cells were resuspended in the modified BG-11 medium (above) that had been bubbled with CO_2-free air for at least 1 hour. The cells were washed in this manner two additional times with the final resuspension to a chlorophyll (Chl) concentration of 100-200 μg Chl · mL^{-1}. These dense cell cultures were kept shaking under white light (approx. 50 μE m^{-2} s^{-1}) and aliquots diluted to 5 μg Chl mL^{-1} for assays. Cultures were assayed within 2 to 3 hours after harvesting. Values of Chl were estimated while cells were in suspension as described by Williams [49], and later normalized to actual concentrations determined in methanol extracts using an extinction coefficient of 12.95 [50]. Absorbance spectra and optical density due to scattering at 750 nm were measured with a UV–Vis Scanning Spectrophotometer (UV-2101PC, Shimadzu, Japan). Cell density was estimated using an automatic cell counter (Cellometer Auto X4, Nexcelom Biosciences). Estimates of cell size were obtained using a Nikon Eclipse Ni series differential interference contrast microscope and a digital camera. The relative areas of cells were obtained by using area measurements of manually selected cells using ImageJ software (NIH, Maryland, USA).

4.2.3 Oxygen evolution assays.

Oxygen evolution was measured using a Clark-type electrode system maintained at 30°C. Bicarbonate-dependent oxygen evolution and consumption measurements were routinely performed in the presence of 5 mM sodium bicarbonate, unless otherwise stated. PSII capacity was determined using an oxygen electrode with the addition of 1 mM DCBQ and 1 mM potassium ferricyanide. Oxygen evolution was measured for 90 seconds under saturating illumination (~10,000 μE m^{-2} s^{-1}), and rates of oxygen evolution were obtained from 40 to 80 seconds using a linear regression fit of the computer-acquired datapoints. Respiration was

assayed immediately after rates of oxygen evolution and respiration rates were obtained by cessation of illumination and fitting oxygen consumption to a linear fit model.

4.2.4 P700 spectroscopy.

P700 absorbance was measured with a JTS-10 spectrophotometer (Bio-Logic, France) using a 620 nm actinic light and 705 nm interference filters over the sample and reference photodetectors. Assays were performed on whole cells in LC7 medium supplemented with 5 mM $NaHCO_3$ at a density corresponding to 5 μg Chl mL^{-1} unless otherwise stated. Before illumination, samples were dark-adapted 5 min with stirring. Stirring was terminated one minute before illumination. Basal levels of P700 absorbance were determined with measuring pulses 10 seconds before and immediately before illumination. Samples were then illuminated for 5 seconds at a nominal intensity of 2050 μE m^{-2} s^{-1} actinic light. Re-reduction of P700 was followed for 14 seconds after illumination was terminated. Measuring pulses were applied throughout the illumination and darkness period. Rates of oxidation and reduction were obtained using Bio-Logic software to obtain half times, which were converted to apparent rate constants. Unless noted, transients are representative traces from at least three biological replicates (independent cyanobacterial cultures).

In order to assay P700 activity during illumination (see Fig. 4.8, and Supplemental Fig. 4.1), samples were placed in the JTS-10 cuvette holder and stirred while under actinic illumination (620 nm, 45 μE m^{-2} s^{-1}). Stirring was terminated after 10 min. Detection pulses were applied 10 seconds apart to determine basal levels of P700 oxidation during illumination. Actinic illumination was terminated as a 200 ms saturating pulse (2500 μE m^{-2} s^{-1}) was delivered, fully oxidizing P700. Re-reduction of P700 during darkness was followed for 8 seconds after termination of the saturating pulse. Total P700 was taken as the difference between maximum and minimum absorbance values. Reduced P700 was measured as the difference between the

basal absorbance value and the value at maximum oxidation (during saturating pulse) divided by total P700. Oxidized P700 can be determined by the difference between basal oxidation values (during illumination) and maximally reduced values (during darkness).

4.2.5 PAM spectroscopy.

Experiments utilized a Walz DUAL-PAM 100 (Walz, Germany) with (DUAL-DR) and NADPH (DUAL-(E/D) NADPH) units. Cell samples were diluted in an optical glass cuvette to a density corresponding to 5 μg Chl mL^{-1} in LC7 medium supplemented with 5 mM $NaHCO_3$ and stirred under actinic illumination (nominally 53μE m^{-2} s^{-1}) for 4 minutes. Actinic illumination was terminated and samples were allowed to dark-adapt for 5 minutes before measuring traces were started. Dark-adapted chlorophyll fluorescence was measured for 60 seconds, at which point actinic illumination (53 μE m^{-2} s^{-1}) was provided for 300 seconds and then terminated (t = 360 s). Post-illumination fluorescence was measured for an additional 140 seconds (t = 500 s) and terminated. Multiple turnover flashes (nominally 20,000 μE m^{-2} s^{-1}) were provided at 15 and 310 seconds. Samples were subjected to either a five minute, or one minute measuring sequence. The fluorescence measuring frequency was high during periods of illumination (1000 Hz) but lowered (200 Hz) during periods of darkness in order to minimize actinic effects. Transients as presented have been averaged (500 pts) for clarity, but non-averaged traces were used for calculation of decay rates and physiological parameters (i.e. F_0, $F_{m'}$). Unless noted, transients presented are representative traces from at least three biological replicates.

4.2.6 Immunoblot assays.

Aliquots of cells harvested for physiological analyses were pelleted and stored frozen until protein analysis. Pellets were resuspended to a density corresponding to 1 mg Chl mL^{-1} in 25 mM Tris-HCl (pH 7.5). Cells were lysed in a Bullet Blender 24 microfuge tube agitator (Next Advance Inc, USA) using an equal volume of cell suspension and 0.1 mm glass beads. ε-

aminocaproic acid and PMSF, 1 mM each, were added prior to breakage in order to minimize proteolysis. After cell lysis, glass beads were removed by low speed centrifugation (600 x g) and samples were quickly frozen in liquid nitrogen for later use. Cell extracts were solubilized using 2% SDS, 5 mM dithiothreitol (65^{o}C, 10 min), centrifuged (10,000 x g, 5 min), and loaded at a concentration of 1 μg Chl on a 12% SDS-PAGE gel. Proteins were transferred to a PVDF membrane using a Bio-Rad semi-dry electrophoretic transfer apparatus. Commercially available (Agrisera, Sweden) rabbit antibodies targeting SbtA or PsbC were used as primary antibodies, anti-rabbit HRP-conjugated goat antibody was used as secondary antibody according to manufacturer's specifications, and 5% BSA was used as a blocking agent. Visualization of secondary antibody was performed using the chromogenic substrate 4-chloro-1-naphthol (4CN, Bio-Rad) and H_2O_2 as developing agents.

4.3 Results

4.3.1 Engineered strains differ in basic cell characteristics

In order to understand the effects of altered carbon metabolism on photosynthetic efficiency, we first analyzed Chl content and cell density in each strain under our experimental conditions. The aim was to establish a baseline to better normalize physiological results. Often, results are compared on the basis of Chl concentration or sample turbidity. However, since the latter is sensitive to cell state, especially cell size, collection of additional information may be critical in evaluating differences in phenotype.

Although culture turbidity is a convenient experimental parameter, we noticed consistent patterns of altered Chl concentrations per unit turbidity amongst the different strains. We next counted the number of cells per unit culture volume and found that the number of cells per unit OD_{750} was different in the genetically modified strains (Fig. 4.2A). Moreover, cell counts became higher per OD_{750} for all strains as C_i became more limiting. All of these observations suggest increased

scattering per cell, which could reflect differences in cell size. Using differential interference contrast microscopy, it was found that both engineered strains had a radius approximately 80% that of wild-type, and cell size additionally decreased for all strains after switching to low C_i

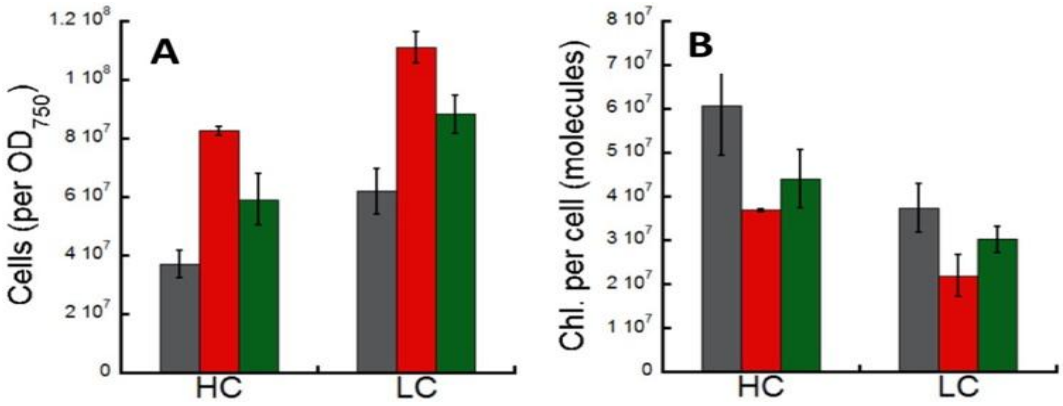

Figure 4.2. Changes in cell culture characteristics as a function of strain and inorganic carbon availability. Grey: WT, Red: Δ*glgC*, Green: JU547. Error bars are standard deviations of three biological replicates. Panel A: Micrograms of chlorophyll per OD_{750} = 1, as measured by methanol extraction. Panel B: Number of cells per OD_{750} = 1. Panel C: Number of molecules per cell, as calculated from Chl determination and cell density counts.

conditions (see Supplemental Fig. 4.2). From these data, the number of Chl molecules per cell was calculated showing that both transformant strains have fewer Chl molecules per cell (Fig. 4.2B). In addition, as C_i becomes more limiting, transformant and WT strains have fewer Chl molecules per cell, and again, the cells themselves appear smaller. Although a detailed study of growth was not performed, growth rates of both genetically modified strains were lower in our hands (Supplementary Fig. 4.3), and an apparent trend worth further study is that faster growing cells were generally larger. Subsequent physiological assays were performed at similar Chl concentrations to simply minimize potential optical differences affecting actinic and measuring lights and, hereafter, cell parameters are normalized and presented on a per microgram of Chl basis. However, these results generally emphasize that interpreting comparative analyses of metabolic activities, such as electron transport, needs to be tempered by findings such as altered Chl per cell in engineered strains.

4.3.2 Carbon sink availability affects oxygen evolution and respiration

Measurements of bicarbonate-dependent oxygen evolution and respiratory oxygen uptake in the dark were used to probe whole chain electron transport coupled to metabolism. Fig. 4.3A shows that the WT and JU547 strains have comparable rates of oxygen evolution and consumption during high carbon growth, normalized to Chl concentration. The Δ*glgC* strain has a pronounced impairment in overall oxygen evolution, similar to that seen in a starch synthesis mutant of *Chlamydomonas reinhardtii* [21]. The Δ*glgC* strain also responded similarly: the artificial electron acceptors DCBQ and PNDA completely alleviated the impairment of electron transport and oxygen evolution (not shown). Moreover, the relative amount of PSII in Δ*glgC* based upon total variable fluorescence due to a single turnover actinic flash is similar to the WT and the decay of fluorescence corresponding to electron transfer from Q_A to Q_B in dark adapted samples was not discernibly affected (not shown). All this points to the conclusion that a normal complement of PSII accumulates in the Δ*glgC* strain and that the impairment of oxygen evolution is due to alterations in downstream sink processes. The rates of oxygen evolution in the JU547 were slightly depressed in high carbon conditions as well. The rates of oxygen evolution per Chl increased in both transformants after the transition to low C_i conditions, however, Δ*glgC* was still lower than the other strains. Rates of respiration, as measured by oxygen consumption in the dark, showed that under high carbon conditions, all strains behaved similarly. On the other hand, the JU547 transformant had an increased rate of respiration under low C_i conditions, perhaps due to extra succinate availability [20, 22].

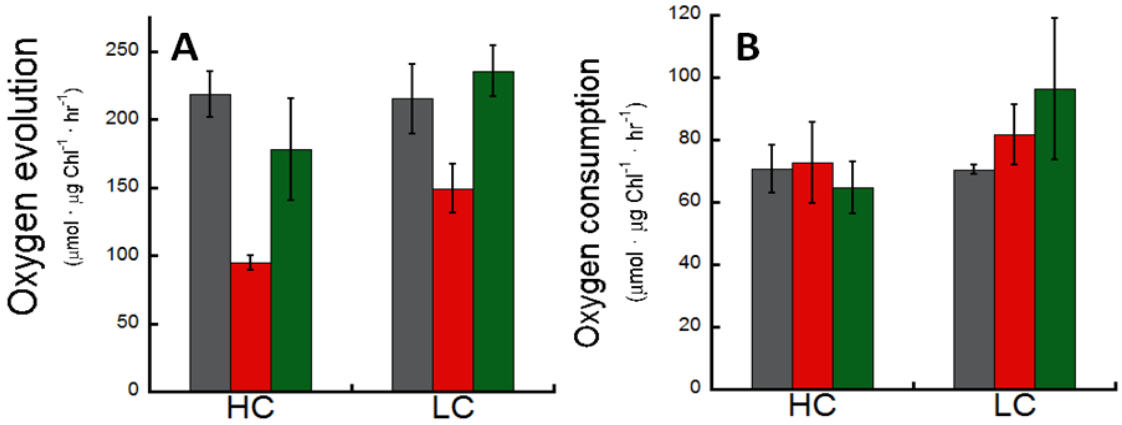

Figure 4.3. Steady-state oxygen evolution and respiration measured in a Clark-type electrode. Grey: WT, Red: Δ*glgC*, Green: JU547. Error bars are standard deviations of three biological replicates. Panel A: Bicarbonate dependent oxygen evolution under saturating light conditions (~10000 μE) measured for 90 seconds. Panel B: Rates of oxygen consumption in 90 seconds of darkness following light exposure.

It has been reported that another glycogen metabolism mutant, Δ*glgP*, exhibits a delay in CBB cycle activation, due to a low internal concentration of CBB metabolites necessary to obtain peak rates of the metabolically autocatalytic CBB cycle activity [23]. In order to test the hypothesis that the Δ*glgC* strain also exhibits a delay in CBB activation, oxygen evolution in the Δ*glgC* strain was monitored over 10 minutes (Fig. 4.4). High carbon grown cultures, in the presence of 5 mM bicarbonate and 180 μE m^{-2} $s^{-1}$of light, had a slow initial rate of oxygen evolution. This rate remained low for just over 5 minutes when rates of oxygen evolution increased to over 3 times their initial levels. When performed in the presence of 5 mM glucose, it is seen that initial rates of oxygen evolution are comparable to the later and fully activated rates seen in the glucose absent samples. Interestingly, low C_i treated Δ*glgC* samples do not display this trend. Rates of oxygen evolution begin high and gradually decrease, possibly due to the sensitivity of Δ*glgC* to photoinhibition.

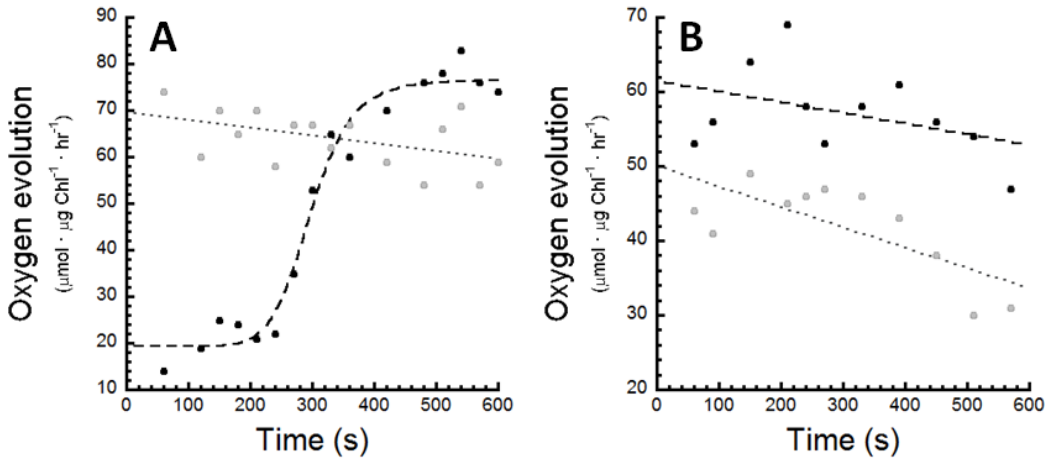

Figure 4.4. Delayed induction of the CBB cycle in Δ*glgC* as assayed by oxygen evolution. Dark adapted cells were exposed to 180μE m^{-2} $s^{-1}$of light (in contrast to saturating intensities used for experiments in Fig. 3) and oxygen evolution was tracked over 10 minutes. Black: bicarbonate only; Grey: addition of 5 mM glucose. Dashed lines represent mathematical curve fits to either sigmoidal or linear equations. Panel A: High carbon grown cultures. Panel B: Low C_i acclimated cultures. These trends were not observed in either the WT or JU547 (not shown).

Addition of glucose to these samples resulted in an overall lowering of oxygen evolution rate, but not a change in trend, similar to WT (not shown). The lack of delay in low C_i acclimated cultures may explain the slight increase in respiration in Δ*glgC* under these conditions (Fig. 4.3B), as the CBB metabolites are accumulated more quickly than in HC cultures during light exposure and are available following cessation of illumination. Overall, this points to a different pattern of metabolite distribution under the two C_i regimes with the LC state tending to have a greater catabolic flux including pathways that communicate with the CBB pathway, thereby allowing it to re-fill more even in the absence of carbon skeletons that are normally derived from the catabolism of glycogen.

Consistent with this interpretation, it was previously observed that the HC→LC transition in WT results in increased levels of glycolytic intermediates including 3-PGA and PEP that appears to occur at the expense of hexoses [24-26]. At the same time, even with this alleviation, the rates were still lower than the wild-type and not commensurate with the content of PSII, which is

similar to the wild-type. Therefore, additional factors are limiting whole chain net oxygen evolution. This could include, for example increased O_2 consumption via the flavodiiron proteins [27, 28].

4.3.3 Chlorophyll fluorescence induction shows interactions with metabolism and responses to C_i availability is different among engineered strains

In order to assay the reduction state at acceptor side of PSII and downstream electron transport chain, Chl fluorescence was measured (Fig. 4.5). Fluorescence transients of the WT strain closely resembled those seen in previous experiments [29]. Chl fluorescence maintains a stable steady-state minimum fluorescence in the dark (F_0). Upon activation of an actinic light source, Chl fluorescence quickly (~1 second) reaches a local peak fluorescence value (F_P), transitioning through standard OJIP phases (not clearly resolved in this study, but for review see [30, 31]). Following the peak in fluorescence at F_P, fluorescence briefly declines to a brief stationary phase (F_S), before rising to a local maximum F_M. The cause of the F_P to F_S decline is still ambiguous in cyanobacteria, but in higher plants it is linked to proton uptake and acidification of the thylakoid lumen [32]. The F_S to F_M rise has been linked to State 2→State 1 transition in cyanobacteria whose regulation is attributed to the oxidation of the PQ pool upon the shift from the dark to light regime [33]. The decline from F_M to a terminal, steady-state fluorescence level, F_T, is highly C_i dependent and is largely due to complete activation of the CBB cycle [29].

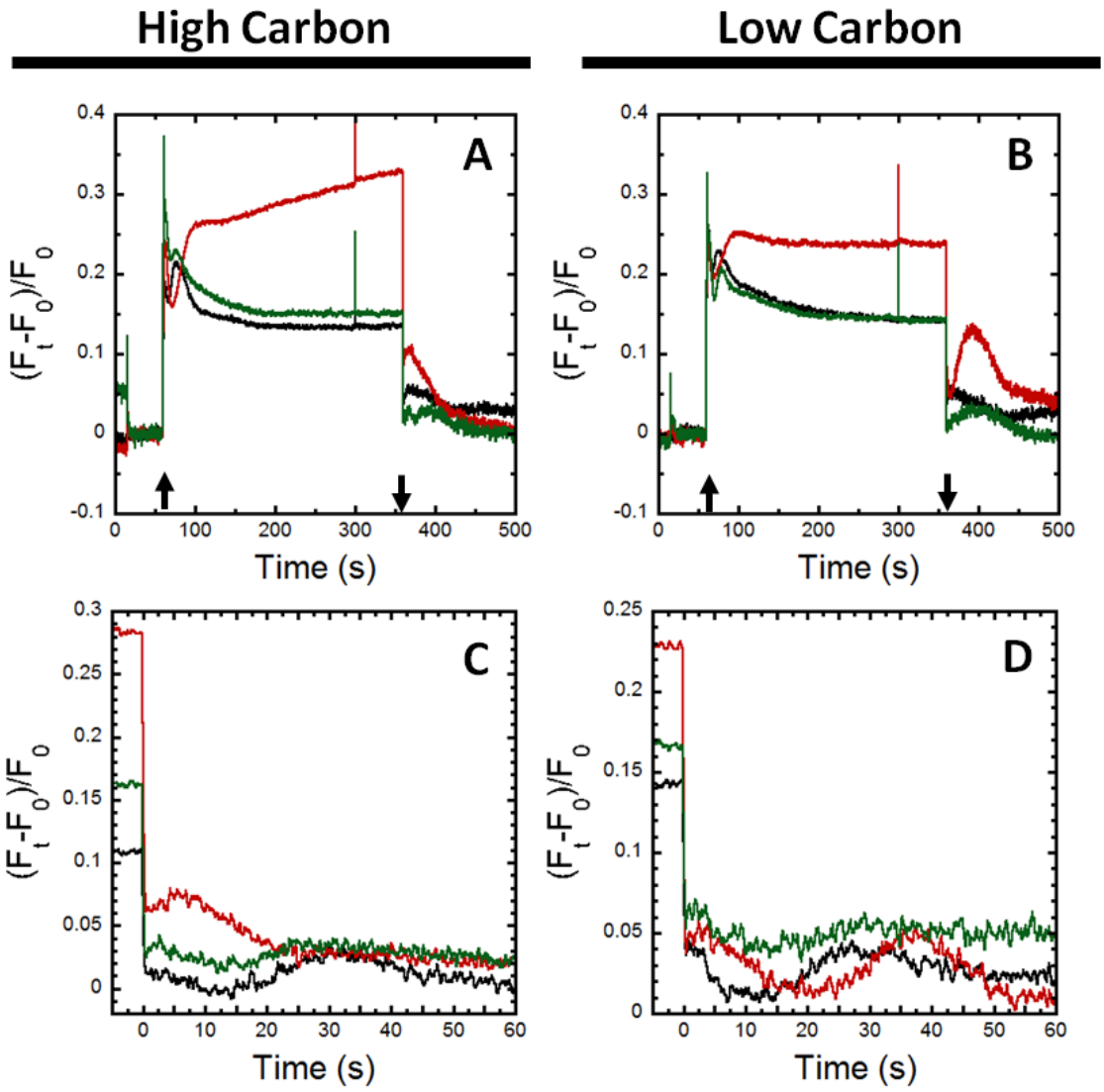

Figure 4.5. Chlorophyll fluorescence transients of HC and LC cultures. Black: WT, Red: Δ*glgC*, Green: JU547. Panels A & B: Chl fluorescence during a five minute exposure to actinic light (53 µE m^{-2} s^{-1}). Actinic light is turned on (up arrow) at 60 seconds and off (down arrow) at 360 seconds. Multiple turnover flashes are given at 15 and 300 seconds. Panels C & D: Chl fluorescence following one minute of actinic light (53 µE m^{-2} s^{-1}). Actinic light is turned off at 0 seconds. Assays were performed in modified BG-11 medium (LC7) supplemented with 5 mM $NaHCO_3$. Calculation of saturation parameters (below) use the light saturated, maximal values. Equal concentrations of Chl (5 µg mL^{-1}) are present and the raw F_0 values in these samples were highly similar.

In Δ*glgC* it is observed that the F_S to F_M rise appears to be delayed, indicating that state transitions may occur more slowly in this strain. The most striking difference seen in the Δ*glgC* mutant compared to WT is that the decline in fluorescence from F_M (~85 s) toward steady state F_T

(~360 s) is replaced by a continued rise in fluorescence, especially in HC cells (Fig. 4.5 A & B). This suggests that the blockage of downstream electron sinks in carbon skeletons prevents the oxidation of PSII, which is usually taken to be diagnostic of a highly reduced PQ pool in the electron transport chain. According to this explanation, electrons, unable to be consumed in the CBB cycle instead have a greater residence time in the intersystem electron transport chain impairing the photooxidation of the PQ pool, which impairs the photooxidation of Q_A^- leading to the high fluorescence state of PSII [34]. Alternative explanations such as increased fluorescence due to state transitions seem unlikely since the drop in fluorescence yield after termination of illumination remains relatively rapid, and not the tens of seconds associated with state transitions. Moreover, the high fluorescent state under active illumination is not due to C_i- limitation since bicarbonate is present in excess [35, 36]. Thus, it would appear that under steady state conditions in actinic illumination at growth light intensities, the PQ pool is abnormally reduced in Δ*glgC*. Furthermore, the fact that an artificial electron acceptor, DCBQ, can completely alleviate the low rates of O_2 evolution (not shown), indicates that an acceptor-side limitation is the cause. Nevertheless, as shown below, the characteristics of P700 reduction kinetics, suggest that a highly reduced PQ pool may actually not exist in Δ*glgC*, and therefore another explanation must be considered.

4.3.4 Post-illumination interactions between metabolism and the PQ pool

Post-illumination kinetics of the three strains were further analyzed after short-term illumination (1 minute, Fig. 5, Panels C & D). The rise in Chl fluorescence 3-7 seconds after actinic illumination, F_N, has been associated with a return of electrons to the PQ pool via NDH-1 complex activity [29, 37]. In addition, a secondary rise, after approximately 30 seconds, F_R, is putatively associated with oxidation of sugars and CBB metabolism [38]. Under the assay conditions here, these post-illumination transients were present, but not very prominent, in the WT and JU547 strains (Figs. 4.5 C & D), suggesting efficient transfer of reductant to the CBB

cycle and towards anabolic metabolism. Nevertheless, these peaks were easily observable in the Δ*glgC* mutant, consistent with a higher amount of photosynthetic reductant accumulated, probably as NADPH and/or reduced Fd. This accumulated reductant rapidly re-reduces the PQ pool ($t_{1/2}$ ~5 sec) after the actinic illumination is terminated probably through NDH-1. In both HC and LC cells, the early NDH-associated peak, F_N, is present. However, under high carbon conditions, the 30 sec F_R rise is absent. Following acclimation to low C_i conditions the 30 sec post-illumination rise returns. This is consistent with the CBB cycle not fully activated for HC cells under these short illumination periods (1 minute). Switching to low C_i culturing eliminates the CBB delay and the F_R rise is observed consistent with the earlier assignment of the 30 sec post-illumination rise as due to the return of reductant via reduced carbon skeletons formed during the actinic period by the CBB [29]. In addition, the intensity of the F_R rise is more pronounced under longer illuminations, and the F_N rise is diminished (Fig. 4.5B), whereas F_N is still observed under shorter illumination (Fig. 4.5D). Although not fully explored here, it seems likely that excess electrons are shunted through NDH complexes (giving the F_N peak) before the CBB cycle becomes fully activated. In this scenario, the more active CBB cycle in the LC cells (Fig. 4.4B) enables the flow of electrons into the form of CBB intermediates and trioses that can later feed reductant back into the PQ pool giving rise to the later F_R post-illumination peak. This corresponds to indirect CEF [39]. The fact that F_R is so pronounced in LC Δ*glgC* suggests that the absence of glycogen synthesis leads to the accumulation of higher levels of sugar that are not readily assimilated into anabolic metabolism and thus provide increased reductant to the membrane system through respiratory pathways. It is also worth noting that induction of the LC physiological state results in shifts in metabolism towards a more 'catabolic configuration' that leads to higher triose levels due to enhanced oxidative pentose phosphate pathway reactions [24-26], as already noted above as an explanation for the better filling of the CBB cycle intermediates in the dark providing for a lag-free induction of oxygen evolution in dark-adapted Δ*glgC* cells, in contrast to the HC condition.

4.3.5 Inorganic carbon availability affects LEF and CEF around PSI differently in engineered strains

Cyclic electron flow functions to balance the stoichiometric requirements of ATP and NADPH [15]. Since these processes return electrons to the PQ pool, changes in PSI activity in the presence and absence of LEF can be used to assay CEF. PSI activity was analysed by measuring absorbance changes at 705 nm (nominally, P700) using a JTS-10 spectrometer (Bio-Logic, France) in the presence of bicarbonate only (LEF + CEF) and with the addition of DCMU to block PSII electron flow (CEF). Again, cells prepared in the HC and LC culture acclimation states are tested, but since excess C_i is present, the differences in P700 redox kinetics reflect differences among the strains and differences in their physiological state (e.g due to gene transcription and allosteric regulation differences) following acclimation to high and low C_i culture conditions.

Upon exposure of the sample to actinic illumination, P700 becomes oxidized, as shown by a decrease in absorbance (Fig. 4.6). High intensity actinic light exposure causes the oxidation of P700 to reach the maximum oxidation level (compare to DCMU trace). The comparative values of oxidation represented by the total negative deflection upon illumination can give relative contents of PSI per Chl, as samples were adjusted to equal Chl concentrations. As can be seen in the presence and absence of DCMU, both Δ*glgC* and Ju547 appear to have comparable concentrations of PSI relative to WT on a per Chl basis. In both transformant strains, rates of oxidation occur faster than in the WT under HC conditions (Fig. 4.7, top). This may reflect some differences in concentration of reduced PSI donor (plastocyanin and/or cytochrome c_{553}) in the PET chain or altered acceptor availability for PSI (i.e. Fd^+, $NADP^+$). It is also seen that switching to low inorganic carbon availability does not appreciably affect the rate of oxidation.

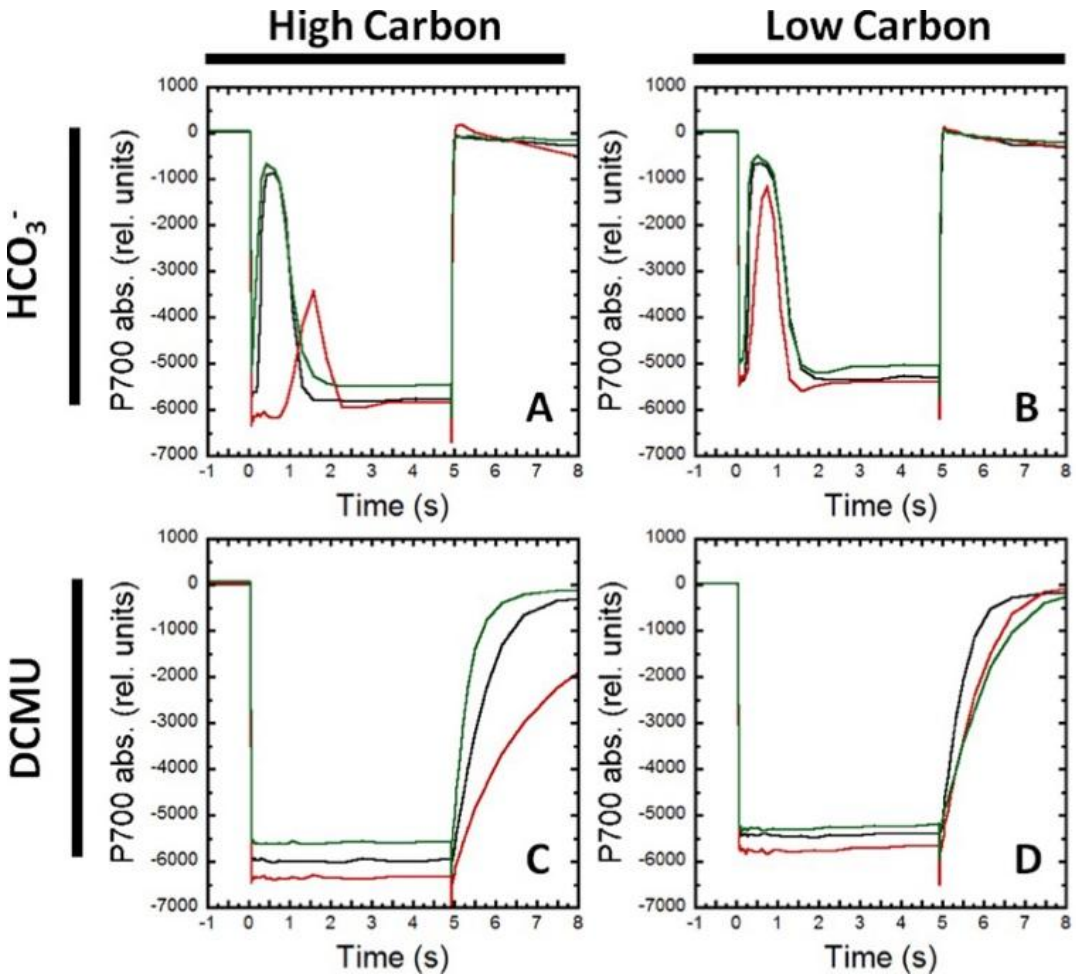

Figure 4.6. P700 absorbance kinetics during 5 seconds of actinic illumination shows different redox states and dynamics among the different engineered strains. Actinic illumination (2050 μE) is turned on at 0 seconds and terminated at 5 seconds. Black/Grey: WT, Red: Δ*glgC*, Green: JU547. Panels A &B: Transients obtained in the presence of 5 mM HCO_3^-. Panels C & D: Transients obtained in the presence of 5 mM HCO_3^- and 10 μM DCMU. The data are presented normalized to measured chlorophyll concentration at a Chl concentration of 5 μg mL^{-1}.

Following oxidation of P700, a transient re-reduction of the resultant $P700^+$ (Fig. 4.6, top) occurs. Before this re-reduction, a brief delay is observed, where P700 remains maximally oxidized. Under HC conditions, this delay lasts ~180-200 ms in the WT strain. The delay is shortest in the JU547 transformant (<100 ms), and in Δ*glgC* the re-reduction is diminished and greatly delayed (~500 ms) (Fig. 4.7A, Fig. 4.8). It appears that the pool of reductant responsible for the transient re-reduction is greatly diminished in Δ*glgC* under HC conditions (see below regarding acceptor

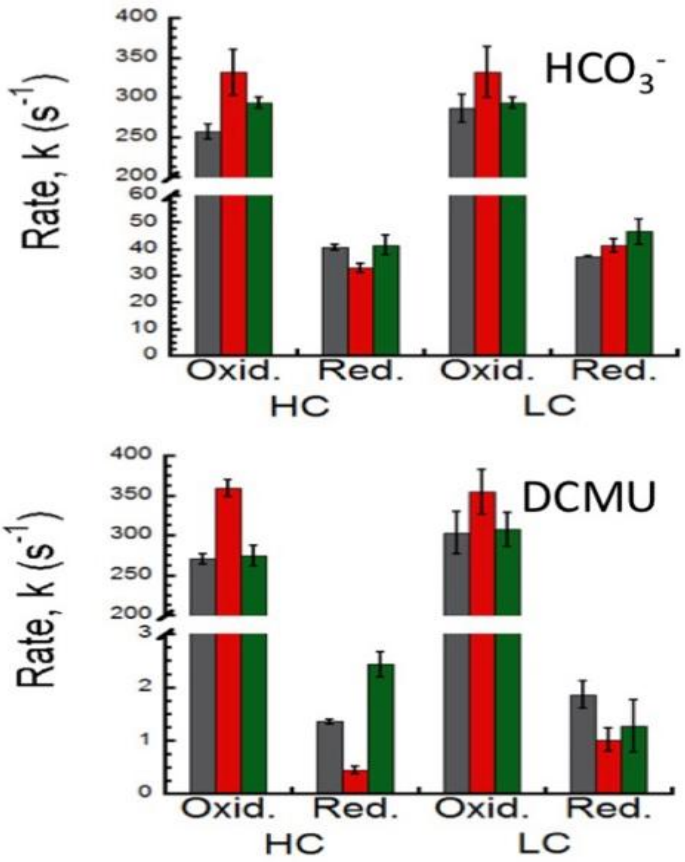

Figure 4.7. Kinetic analysis shows alterations in photosynthetic cyclic electron transport is different in the different strains. Rate constants for $P700^+$ oxidation and re-reduction due to 5 second pulse of saturating illumination in the absence (top) and presence (bottom) of PSII inhibitor, DCMU. Analysis of the kinetic profiles shown is from several experiments similar to that shown in Figure 6. Rate constants of oxidation and re-reduction are plotted for engineered and control strains Black/Grey: WT, Red: Δ*glgC*, Green: JU547. Error bars are standard deviations of three biological replicates. Panel A: Transients obtained in the presence of 5 mM HCO_3^-. Panel B: Transients obtained in the presence of 5 mM HCO_3^- and 10 μM DCMU.

side differences). This loss of the re-reduction transient is highly reminiscent of similar alterations in P700 kinetics upon deletion of succinate dehydrogenase [40]. Interestingly, the diminished re-reduction transient observed in HC Δ*glgC* cells is partially restored by acclimation to low C_i conditions (Fig. 4.7B, Fig. 4.8). Note that the differences are not due to the absence of C_i in the assay, since both HC and LC samples have excess bicarbonate added and therefore, the differences must reflect changes in metabolism/enzyme activity induced by the acclimation to low C_i. While the measurements do not take into account removal of electrons from the intersystem chain through respiratory oxidases, those rates are quite similar among the strains based on oxygen uptake measurements (Fig. 4.3B) except for JU547, which had a somewhat higher rate of respiration in LC conditions. Therefore, the characteristics of the re-reduction transient suggest two alternative, but not mutually exclusive, possibilities: 1.) the transient re-reduction of $P700^+$ is due to the reductant accumulated in the dark and exhausted by actinic

illumination on the time scales used, or 2.) the transient re-reduction feature is due to changes in availability of PSI acceptors, where an oxidized pool of Fd and/or $NADP^+$ rapidly fills with electrons. This creates a transient inability to oxidize $P700^+$ at rates that match the influx of electrons from PSII. The pool of acceptors is then re-oxidized as the 'absorptive flux capacity' of secondary and tertiary acceptors is activated, causing a second phase of oxidation of $P700^+$ following the transient. As shown below, the NADPH pool in Δ*glgC* is more reduced, which should enhance the re-reduction transient, not diminish it as observed. This combined with the fact that it is restored in the LC state associated with increased catabolism and the similarity to the succinate dehydrogenase phenotype support the transient as being strongly dependent upon the flow of electrons into the thylakoid electron transport chain from cytoplasmic catabolic activity and that Δ*glgC* has a diminished flow of reductant via this path into the PQ pool.

In order to analyze CEF in isolation from PSII-dependent linear electron flow, actinic illumination was provided in the presence of DCMU to block electron donation from PSII. The Δ*glgC* mutant exhibits slower re-reduction of $P700^+$ that we attributed to CEF, which again, appears in conflict with the presence of a more reduced PQ pool during actinic illumination (Fig. 4.5). In the JU547, the increased rates of CEF may be explained through the activity of EFE genetic modification that yields ethylene. In addition to ethylene, succinate is a by-product of EFE. With additional succinate being created, succinate dehydrogenase is able to reduce available PQ, leading to indirect CEF to the PQ pool. Upon transition into LC conditions, the rate of $P700^+$ re-reduction in the WT strain remains unchanged, (Fig. 4.6D, Fig. 4.7). For the transformants however, this rate is altered. The LC cells of the Δ*glgC* mutant exhibit a large increase in the rate of re-reduction, probably owing to induction of the high affinity carbon uptake mechanism (see below), the alleviation of CBB cycle activation, and the inferred increase in the flux of reductant towards catabolic pathways [24-26]. This low C_i-induced flux appears to direct metabolism towards inputs into the electron transport chain such as SDH [41] and FNR and thus may not be

related to CEF per se. The LC cells of JU547 exhibit a slight impairment of $P700^+$ re-reduction however, indicating that CEF may be down-regulated in favor of linear electron flow in these conditions.

4.3.6 Glucose feeding confirms a kinetically efficient supply of reductant to the electron transport chain

To further evaluate the conclusion that the slowed rate of $P700^+$ reduction in Δ*glgC* is due to a diminished flow of catabolic reductant into the intersystem electron transport chain, glucose was added to samples of high carbon grown Δ*glgC* and WT and allowed to incubate 5 minutes in darkness before starting the measuring traces (Figure 4.8A). Glucose reduces the PQ pool and thus should hasten the re-reduction of $P700^+$. The addition of glucose had two prominent effects.

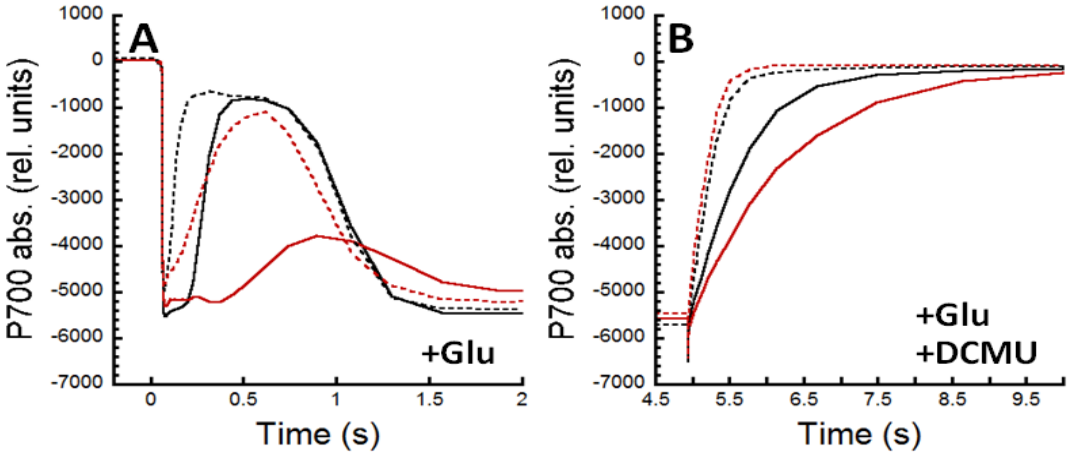

Figure 4.8. P700 absorbance kinetics of WT and Δ*glgC* strains grown under high carbon availability. Samples were incubated 5 minutes in darkness in the absence (solid lines) and presence (dashed lines) of 5 mM glucose before applying a 5 second saturating (2050 μE m^{-2} s^{-1}) actinic illumination. Black: WT; Red: Δ*glgC*. Panel A: Initial oxidation and transient re-reduction of P700 in samples upon actinic illumination. Actinic illumination was turned on at 0 seconds. Panel B: Re-reduction of P700 in samples upon termination of actinic light, with the addition of 10 μM DCMU. Actinic illumination was terminated at 5 seconds. The data are presented in uncorrected form with all samples at a Chl concentration of 5 μg mL^{-1}.

First, the delay in the re-reduction transient is eliminated. In fact, the initial deflection of P700 oxidation does not appear to fully oxidize P700 (compare Figure 4.8A at time 0 seconds versus 2 seconds), implying that glucose is continuously supplying electrons to the electron transport chain, thus slowing the rate of P700 oxidation. Since the main route of catabolic reductant via

glucose addition into the intersystem electron transport chain is succinate dehydrogenase and this enzyme reduces PQ, then it appears that the PQ pool in Δ*glgC* is more oxidized, not more reduced as suggested by the results of Chl fluorescence measurements (Fig. 4.5).

4.3.7 Electron flow during steady-state photosynthesis

To assay the electron flow to PSI during active photosynthesis, cells were illuminated at near growth light intensities (45 μE m^{-2} s^{-1}) for 10 minutes after which a 200 ms saturating pulse was delivered to completely oxidize P700 and illumination was terminated (Supplemental Figure S4.1). Rates of re-reduction after termination of illumination also give insight into the reduction state of the intersystem electron transport chain during steady state photosynthesis. In the illuminated HC cell samples, $P700^+$ re-reduction occurs much more slowly in the Δ*glgC* transformant, with a rate of approximately 40 turnovers per second compared to 70 and 80 in the WT and JU547 strains (Figure 4.9A). These results are similar to the patterns of re-reduction observed during the 5 second illumination, albeit faster due to the build-up of reductant under illumination. The faster rates in all strains under these conditions presumably reflect the higher concentrations of accumulated reductant in this steady state assay. As before, the re-reduction of $P700^+$ in Δ*glgC* in the HC state is comparatively slower than the WT (Fig. 4.9A, red bars). Acclimation to ambient air gassing (LC cells) increases the re-reduction rate in Δ*glgC* almost to that of WT values. The JU547 transformant also shows a slight increase in re-reduction rate as well, indicating that electron flux through the electron transport chain may be increased. Thus, again it is observed that the physiological state elicited during the acclimation to low C_i conditions restores a more WT-like PSI re-reduction flux in the Δ*glgC*.

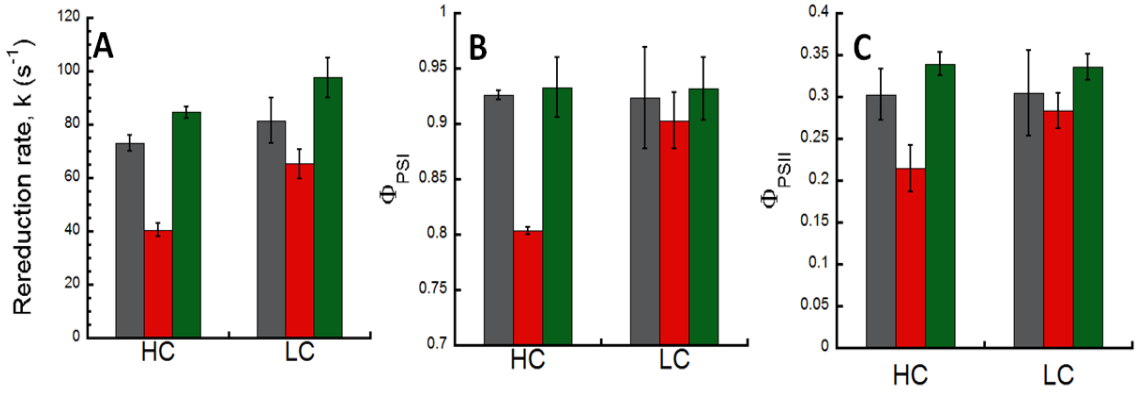

Figure 4.9. Steady-state actinic illumination electron transfer characteristics of photosystems under different carbon availability regimes. Grey: WT, Red: Δ*glgC*, Green: JU547. Error bars are standard deviations of three biological replicates. Panel A: Reaction rates of $P700^+$ re-reduction after a saturating pulse given during continuous 50 μE m^{-2} s^{-1}actinic light. Panel B: Quantum yield of photosystem I, as measured by $P700_{red}/P700_{tot}$. Panel C: Effective quantum yield of photosystem II, as measured by $(F_{m'}-F)/F_{m'}$, obtained from Chl fluorescence (Figure 5).

The observed quantum yield of PSI ($P700_{red}/P700_{tot}$), and relative PSII quantum yield ($[F_{m'}-F_s]/F_{m'}$) during steady state actinic illumination were obtained using saturating pulse techniques tracking P700 absorbance and Chl fluorescence (Fig. 4.9B & 4.9C). Overall, the quantum yields for JU547 are similar to the wild-type, whereas they are markedly lower in Δ*glgC*. Greater than 90% of PSI are in a reduced condition (open) during steady-state photosynthesis in the WT and JU547 strains, whereas Δ*glgC* has only approximately 80% of PSI centers reduced under these relatively low actinic light conditions (~50 μE m^{-2} s^{-1}) consistent with a more oxidized PSI donor pool. The relative quantum yield of PSII is evaluated on the basis of the remaining fraction of PSII centers in the sample that are not in a high fluorescent state (Q_A^-), but can be converted to that state by giving a saturating, high intensity flash. On this basis, JU547 has relatively open reaction centers, whereas Δ*glgC* has a considerably higher fraction of closed PSII centers. The latter is typically interpreted to indicate that the PQ pool is more reduced and is not keeping pace with the rate of electron flow from water to Q_A However, the PQ pool appears relatively oxidized, not more reduced in Δ*glgC* based on the $P700^+$ re-reduction characteristics. This apparent discrepancy is further underlined upon consideration of photochemical quenching, q_P, which is

calculated as ([$F_{m'}$- F_s]/$F_{m'}$- F_0]). When q_P is calculated using the corresponding values from the same experiment, HC cells of the wild-type and JU547 each display values of ~0.8, whereas Δ*glgC* is ~0.5, which is normally taken to indicate a more reduced PQ pool. It is important to note that the PSII quantum yields obtained using this formula underestimate the actual quantum yield because it assumes well-coupled light-harvesting antennae, which is not the case in cyanobacteria [42]. Therefore, rapid adjustments in antenna coupling cannot be excluded as the basis for relatively higher fluorescence yields during steady state fluorescence in Δ*glgC* that render an appearance of lower levels of photochemical quenching. However, the fact that PSII electron acceptors can quench this higher fluorescence supports the conclusion that acceptor side limitation is indeed the cause of higher PSII fluorescence, despite strong evidence that the PQ pool is oxidized.

4.3.8 NADPH fluorescence shows a highly reduced NADPH pool due to impaired glycogen synthesis.

Analysis of downstream PSI processes was performed by measuring NADPH fluorescence. Previous studies have shown this to be a reliable method for measuring NADPH levels *in vivo* despite potential complications arising from interfering NADH fluorescence [29, 43, 44]. Wild-type NADPH fluorescence displays characteristic peaks and phases analogous to Chl fluorescence (Fig. 4.10). Samples acclimated to darkness reach a steady-state minimum, N_0, where a minimum level of NADPH may be generated from the oxidative pentose phosphate pathway and other processes. Upon exposure to actinic illumination, fluorescence increases in a monophasic rise to a local peak, N_P. NADPH fluorescence also displays analogous peaks and phases at the P→S→M transitions seen in Chl fluorescence. However, very little decline is seen during the P→S transition. After approximately 30 seconds after the start of actinic illumination, NADPH fluorescence reaches a local maximum, N_M, and begins to decline. This decline has been associated with activation of the CBB cycle [29].

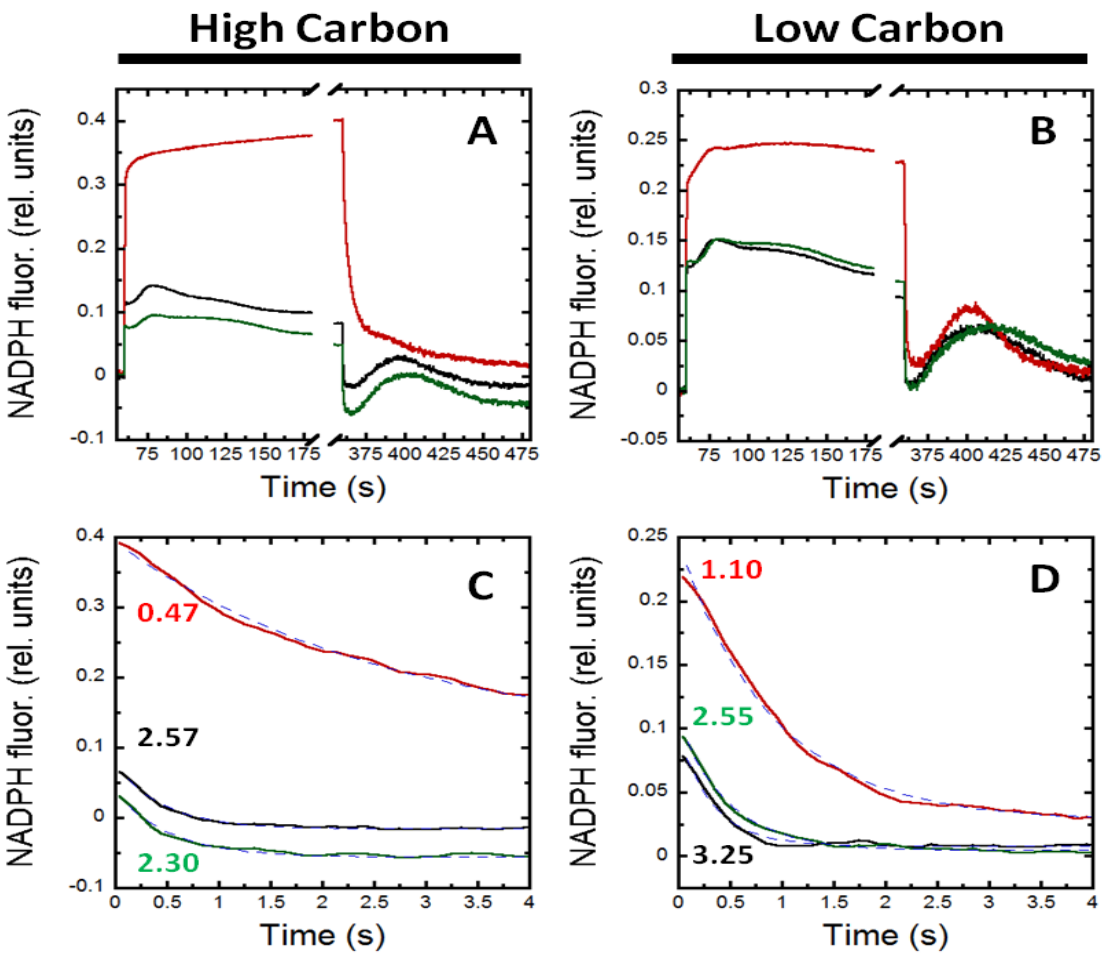

Figure 4.10. NADPH fluorescence kinetics during actinic illumination. Actinic illumination (53 µE m^{-2} s^{-1}) was activated at 60 seconds and terminated at 360 seconds. Black: WT, Red: Δ*glgC*, Green: JU547. Panels A & C: High carbon grown cultures. Panels B & D: Low carbon grown cultures. Panels C & D: Detail of post-illumination NADPH oxidation. Numerical values represent average reaction rate constants, k (turnovers s^{-1}) as determined from curve fits (blue dashed lines) of three biological replicates.

The amplitude and kinetic features of light induced NADPH fluorescence of the JU547 strain resembled the WT, although under HC conditions the amplitude in JU547 was routinely lower consistent with the enhanced flow of reductant towards the production of ethylene. This difference was mostly lost for LC JU547 cells, for reasons that are not clear, although presumably related to previously observed increases in catabolic metabolic pathways that occur upon adaptation of low C_i conditions [24-26]. In contrast, Δ*glgC* consistently displayed fluorescence values over two times greater than that of WT. Fluorescence continued to rise at a slow, constant

rate, until delayed activation of the CBB cycle. After this point, fluorescence fell, but only to initial N_P values, not towards WT or JU547 values. Therefore, under steady-state photosynthesis, Δ*glgC* likely contains a larger and/or highly reduced NADPH pool.

Following the termination of actinic illumination, NADPH fluorescence quickly declines. A large dark reduction event after approximately 30 seconds of darkness is seen and may be associated with oxidation of triose and pentose sugars [29] and approximately coincides with the 30 second post-illumination peak in Chl fluorescence assigned to the transfer of that reductant to the PQ pool [29]. For the first 7 seconds after actinic illumination, NADPH fluorescence declines monoexponentially, as seen in Fig.s 4.9C & 4.9D. After this time, the rise culminating in the 30 second N_R peak begins to be seen. Decay curves were fitted using exponential decay models, and decay constants and half times were found. In each strain, the decay in NADPH fluorescence occurs more quickly in cultures switched to low carbon gassing, likely due to induction of the CCM and its NADPH consuming complexes. The difference is most prominent in the Δ*glgC* transformant, where decay rates were over twice as fast when cultures were switched to air gassing.

4.3.9 Transition to low carbon availability induces the CCM of transformant strains

To assess whether proteins of the high affinity CCM were present and inducible in the transformant strains under these experimental conditions, immunoblot assays were performed using commercially available anti-SbtA antibody (Agrisera, Sweden), which is diagnostic of the high affinity CCM response. Cells in the HC and LC physiological states were obtained from the same cultures used for the above spectroscopic analyses. Because 2OG serves as a signaling cofactor for the repression of CCM-related genes [45], these transformants with altered metabolism around 2OG may display mis-regulated expression of CCM proteins. The Sbt operon is under transcriptional control of the DNA-binding CcmR protein, whose mechanism uses 2OG

as a co-repressor [45]. In WT cells, no detectable level of SbtA is observed in high carbon grown cultures, however, after switched to low carbon gassing, SbtA can be detected (Figure 4.10A).

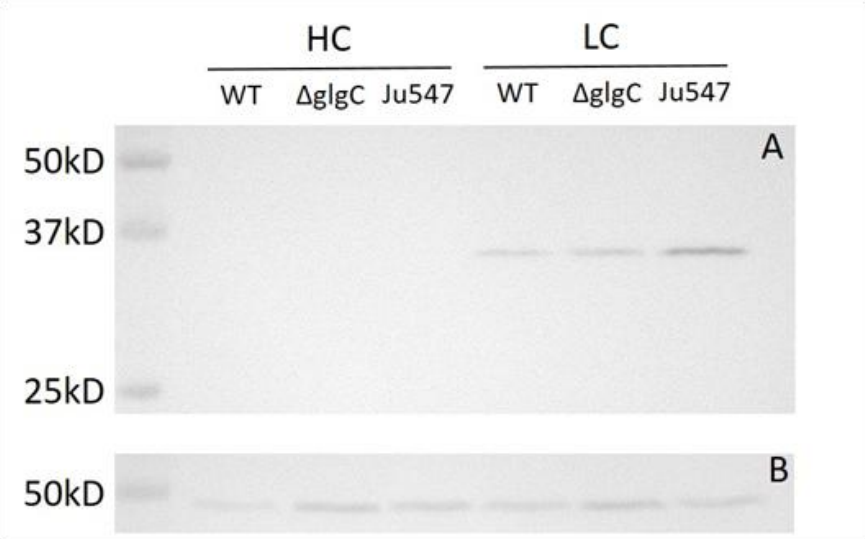

Figure 4.11. Immunoblots from samples of wild-type and transformant strains under different carbon regimes. Samples were loaded to 5 µg Chl on a 12% SDS-PAGE gel and transferred to a PVDF membrane. Panel A: Immunoblot probed with α-SbtA as a primary antibody showing induction of the CCM-related *sbtA* gene. Panel B: The same immunoblot membrane probed using α-PsbC as a loading control.

Similarly, transformant strains also show no detectable levels of SbtA when cultured under high carbon conditions. Low carbon culturing shows expression of SbtA in both transformants, with the JU547 transformant having a higher concentration of SbtA relative to WT. Since CcmR also regulates expression of the *ndhF3/D3/cupA* operon [46], it is likely that these genes follow similar patterns as well, but further analysis was not performed. Overall, it appears that the diversion of photosynthate in JU457 indeed results in increased demand for C_i as evidenced by the enhanced expression in LC JU457, yet the Δ*glgC* shows no differences in expression relative to the WT as hypothesized. Instead, it appears that the Δ*glgC* transformant retains near WT-like patterns of CCM gene expression with respect to changes in C_i conditions. In addition, experiments assaying the whole cell affinity characteristics of each of the strains in the HC and LC state were performed and indicated that wild-type and JU547 exhibited the expected increases in affinity (Supplemental Fig. S4.4), whereas the evaluation of Δ*glgC* was more problematic due to the low activities of oxygen evolution in this strain.

4.4 Discussion

The aim of this work was to analyze how biotechnologically significant alterations in cyanobacterial carbon metabolism affect photosynthetic performance. The photosynthetic characteristics and CCM properties were examined in the ethylene-producing strain (JU547), which partitions at least 10% of their fixed carbon toward the release of ethylene [20, 22]. It has been engineered to express the ethylene forming enzyme (EFE) from the organism *Pseudomonas syringae* [18, 20]. The ethylene-forming enzyme uses 2OG as a substrate for the synthesis of ethylene, a volatile compound, which escapes the medium as a gas. The JU547 strain therefore has an additional, engineered carbon and electron sink available. As an experimental contrast, the corresponding analysis was also performed on the well-studied Δ*glgC*, which is deficient in glycogen biosynthesis and thus no longer has a key sink for photosynthate [51]. The Δ*glgC* transformant was originally constructed to explore ways to enhance product yields by eliminating a potentially competing sink pathway. However, the Δ*glgC* strain also proved interesting since it excretes organic acids, including 2OG, upon nitrogen starvation [51, 52]. This latter observation is relevant to C_i nutrition since 2OG plays a role in the regulation of the genes of the high affinity CCM [53].

4.4.1 Predicted and unpredicted alterations in photosynthetic performance

The motivating hypothesis in this study was that strains with increased sink capacity, exemplified by the JU547, will exhibit increased demand for C_i and correlated effects on the characteristics of the photosynthetic mechanism such as enhanced electron transport capacity. Conversely, strains such as Δ*glgC*, will exhibit opposite effects due to decreased sink capacity. Some of the predictions were supported and consistent with the previously identified alterations in metabolism. For example, we observed increased rates of respiration and faster re-reduction of oxidized P700 in JU547 presumably due to the closure of the TCA cycle via provision of

succinate during the synthesis of ethylene with its consequent ability to reduce the electron transport chain [20, 22]. Succinate serves as an electron donor to the plastoquinone pool through the succinate dehydrogenase complex, which may serve as a major donor of electrons during respiration [19] and accounts for the predictable increase electron flow to $P700^+$. Likewise, the enhanced expression of the high affinity bicarbonate transporter was observed in JU547 is consistent with predictions for increased demand for C_i. On the other hand, the Δ*glgC* mutant proved more difficult to predict, with phenotypic characteristics that were strongly dependent upon whether or not the cells were subjected to Ci-limitation. While the hypothesized changes in high affinity CCM genes proved not to occur, there were unexpected features of electron transport that are revealing of the mechanisms by which the cyanobacterial photosynthetic apparatus adjusts to cope with stress.

4.4.2 Impaired glycogen metabolism has far-reaching effects even in the light and is affected by C_i availability

Perhaps one of the biggest puzzles is an apparent redox paradox concerning the states of the PQ pool *vis-a-vis* the rate of electron flow through PSI in in Δ*glgC.* Simply put, the high Chl fluorescence characteristics (Fig. 4.5) would normally be interpreted as reflecting a more reduced intersystem electron transport chain and yet all other evidence points to the opposite. The re-reduction of $P700^+$ due to CEF is very slow, but fast rates can be restored by the addition of glucose, which shows that 1.) catabolism of glucose efficiently provides reductant to the intersystem electron transport chain and 2.) the PQ pool in Δ*glgC* is actually in a comparatively oxidized condition (Figs. 4.6, 4.7 and 4.8). This is true even for samples under steady state actinic illumination so it is not simply due to the depletion of carbon skeletons in the dark in Δ*glgC* (Fig. 4.9A). Based upon the steady-state electron transport measurements of photosystem relative quantum yields, it appears that PSII is even more ‘closed’ than PSI and may actually limit electron flow through the electron transport chain, which would yield a more oxidized PQ pool.

Furthermore, besides steady-state linear electron flow, cyclic flow to the $P700^+$ is also retarded in the Δ*glgC* mutant as evidenced by the very slow rate at which $P700^+$ is re-reduced in the absence of electron input from PSII, which is alleviated by the addition of glucose (Fig. 4.8B). Moreover, growth under low C_i availability conditions also tends to alleviate this and many of the other observations suggesting that a shift in metabolic regulation towards a more catabolic configuration consistent with previous metabolomics studies of Ci-limitation [24-26].

*4.4.3 Evidence for induction of a relatively uncharacterized energy dissipation mechanism in Δ*glgC*

All the P700 re-reduction results point toward a more oxidized PQ pool in Δ*glgC.* And yet, by each measure of Chl fluorescence (Φ_{II}, q_P) or by simple inspection of the fluorescence induction traces (Fig. 4.5A, B), the fluorescence is higher in a manner usually interpreted to indicate a significantly more reduced condition of the PQ pool. It appears that the apparent diminished PSII photochemical quenching, q_P, observed in Δ*glgC* could be due to increases in fluorescence not actually associated with q_P i.e. not actually due to the return of excitons to the antenna system because of Q_A^-. Such a model could involve a rapidly reversible uncoupling of the phycobilisomes to accommodate the reduced electron flux capacity through the electron transport chain and with excitation energy dissipated as fluorescence to account for the higher level of fluorescence yield. However, the fact that the elevated level of fluorescence can be quenched by the addition of DCBQ and at the same time allow the high rates of O_2 evolution, indicates that this is not the case. Therefore, the diminished q_P very likely reflects an elevated Q_A^-/Q_A ratio accounting for the elevated fluorescence. In other words, we observed high levels of quenchable fluorescence most easily explained as closed reaction centers in the Q_A^- state. It is also important to note that this was not alleviated by the addition of uncouplers, similar to what was found for C_i limited *Synechococcus* cells [36]. Thus, we conclude that we have an elevated Q_A^-/Q_A ratio in Δ*glgC*, but it is somehow not communicating with the PQ pool. This implies that either Q_A^- is re-

oxidized via back-reaction with the donor side of PSII or there exists a mechanism for shunting the electrons elsewhere. The back-reaction alternative appears unlikely since this would produce a kinetic profile similar to DCMU treatment, but what is observed are complex kinetics not unlike the modulations associated with forward electron transfer into the PQ pool. Thus, the results are most consistent with the presence of an alternative forward pathway to oxidize Q_A^-. Furthermore, this alternative path is inferred to have a pool capacity and provides kinetic resistance to impede the oxidation of Q_A^- as this pool fills and is progressively depleted of oxidant. In some ways, this pool can be considered a photochemical quencher, much like the PQ pool, since its state also governs the oxidization Q_A^-, however, this is a dissipative pathway and does not contribute to anabolic photosynthetic processes. Because of its kinetic similarity, but different and apparently dissipative mechanism of oxidizing Q_A^-, we propose to call this component as q_{PD} to indicate its inferred dissipative photochemical character. Accordingly, photochemical quenching in cyanobacteria might best be considered as the sum of the productive (PQ pool reducing) and dissipative (unknown pool reducing) components or $q_{P,\ total}=q_P + q_{PD}$. The results are somewhat reminiscent of the fluorescence properties assigned to an unusual form of cyanobacterial q_N associated with C_i depletion, that like the unusual 'dissipative q_{PD}' proposed here, was difficult to distinguish from q_P [42].

It is tempting to attribute the deduced PSII electron dissipation mechanism, q_{PD}, to a path through the flavodiiron proteins, Flv2/4 [28, 54, 55]. This assumes that they can provide 'kinetic resistance' to the oxidation of Q_A^- due to a saturation of an (intermediate) acceptor pool, perhaps the finite pool of flavodiiron proteins themselves. The problem with that assignment is that the Flv2/4 proteins seem to accelerate the oxidation of Q_A^- [56]. Therefore they would not appear to explain the observed accumulation of Q_A^- because of the efficiency with which they oxidize it. Indeed, overexpression of the Flv2/4 proteins diminishes steady state variable fluorescence [28]. However, those measurements were performed under single turnover conditions where an

exhaustible oxidant pool is not a factor [56]. Because [Q_A^-] represents a quasi-steady state of formation and decay, the parameters q_P and q_{PD} depend upon the characteristics of the pool size/turnover rates of the Q_A^- oxidant governing decay as well as net rate of formation by PSII charge separation. Therefore, the path through the Flv2/4 protein is a distinct possibility given the reasonable assumption that the oxidation rate that it provides begins to slow as its pool is exhausted in much the same way the PQ pool is exhausted as it becomes progressively reduced. A model summarizing the proposed energy dissipating pathway that presumably leads to regulated shunting of excess electrons to O_2 is shown in Fig. 4.12. On the other hand, the present results are also consistent with any mechanism that involves an exhaustible pool of oxidant of Q_A^- with a finite recovery time and gives the appearance of a highly reduced PQ pool, yet more likely reflects another saturatable pool of alternative electron acceptor. However, neither the molecular mechanisms involved nor the regulatory signals eliciting their mobilization are understood. That there should be a disconnect, at least under certain conditions, between the redox state of Q_A^- and the redox state of the PQ pool could be surprising, but on the other hand, it is entirely in line with recent similar observation where high fluorescence was not connected with changes in redox state of the overall PQ pool in *Synechocystis* [57].

Finally, it is worth noting that the redox state of the NADPH pool *seemingly* behaves as expected for the two engineered strains: addition of a new sink for carbon and reductant in the form of ethylene production in JU547 produces a modest yet reproducible shift to a more oxidized condition of the NADPH pool under steady state illumination. In contrast, closing a sink in the form of glycogen synthesis in Δ*glgC* results in a much more reduced NADPH pool. This indicates, as expected, that glycogen synthesis from CO_2 fixation, with its concomitant consumption of NADPH, constitutes a major avenue of metabolic reductant consumption in the light. However, assuming that NADPH donates electrons to CEF, a highly reduced NADPH pool is expected to produce a more reduced PQ pool and a faster rate of $P700^+$ re-reduction. The

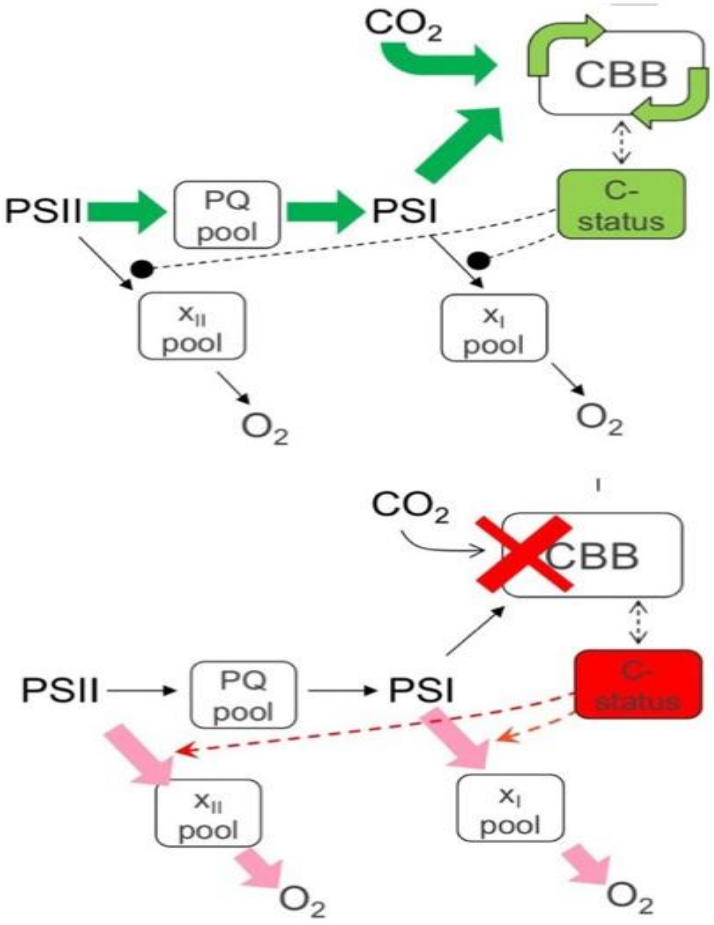

Figure 4.12. Schematic of the deduced regulatory mechanisms that appear to have evolved to maintain the PQ pool homeostasis. Electron input from PSII to the PQ pool is switched to a dissipative mode that shunts electrons to unknown acceptor pools, X_{II}, to avoid over-reduction of the PQ pool. A similar mechanism for PSI (involving pool, X_I) is proposed to balance the LEF through the entire chain, although evidence for that pool remains to be obtained. Based upon similarities to the characteristics of C_i –limited cyanobacterial cells at the compensation point, O_2 is proposed to be the ultimate electron acceptor of the electron dissipative pathway. The regulatory switch for this proposed mechanism is proposed to respond to C_i status, although any number of metabolites, besides C_i itself, could act as effectors as seen for the induction of the high affinity CCM [53].

opposite was observed regarding P700$^+$ re-reduction. The primary donor to the NDH-1 complexes is now believed to be Fd [58], yet there appear to be mechanism(s) allowing the oxidation of NADPH by NDH-1 complexes based on earlier results [39]. Thus, the present results with Δ*glgC* indicate that there exists a mechanism down-regulating CEF activity, and together with decreased electron flow from PSII into the PQ pool, results in preventing the PQ pool from being over-reduced. In the case of Δ*glgC*, this mechanism would appear to be responding to the changed metabolism of sugars that result in impaired start-up of the CBB pathways (Fig. 4.4), which was previously shown to be the result of depletion of CBB cycle intermediates when glycogen metabolism is impaired [23].

In summary, it is clear that the impact of mutations directed at altering metabolic flux can have both expected and unexpected consequences with respect to the operation of the overall

photosynthetic mechanism, and particularly, the activities of the electron transport chain. Even basic cell parameters important for performance evaluation, such as cellular Chl content, are sensitive to engineered alterations, although the mechanistic basis for these global cellular responses remains poorly understood. The findings with the already well-studied Δ*glgC* mutant were particularly striking, especially regarding its Chl fluorescence characteristics. The results were best interpreted to indicate the operation of a photoprotective mechanism that dissipates excess reductant from PSII. Overall, some initial predictions were verified, such as more oxidized pools of the redox carriers PQ and NADP and an enhanced expression of the high affinity CCM in JU547. However, some observations, notably in the Δ*glgC* mutant, could not be easily rationalized in the framework of simple enhanced or thwarted sink model.

4.5 Acknowledgements

We thank Prof. Aaron Kaplan for useful discussions on the unusual characteristics, fluorescence and otherwise, cyanobacteria under stress conditions. We also like to thank Prof. Dean Price for his generous advice on assaying whole cell inorganic carbon affinity. This work was supported by the grant no. DE-FG02-08ER15968 funded by the U.S. Department of Energy, Office of Science, Basic Energy Sciences at OSU (SCH, JA, NTM and RLB, physiological and spectroscopic measurements). Work at NREL was supported by the U.S. Department of Energy, Office of Science, Basic Energy Sciences (MC, JY and MLG, glycogen mutant studies), and by the U.S. Department of Energy, Office of Energy Efficiency and Renewable Energy, Bioenergy Technologies Office (JY, ethylene-producing mutants studies).

4.6 Supplemental materials

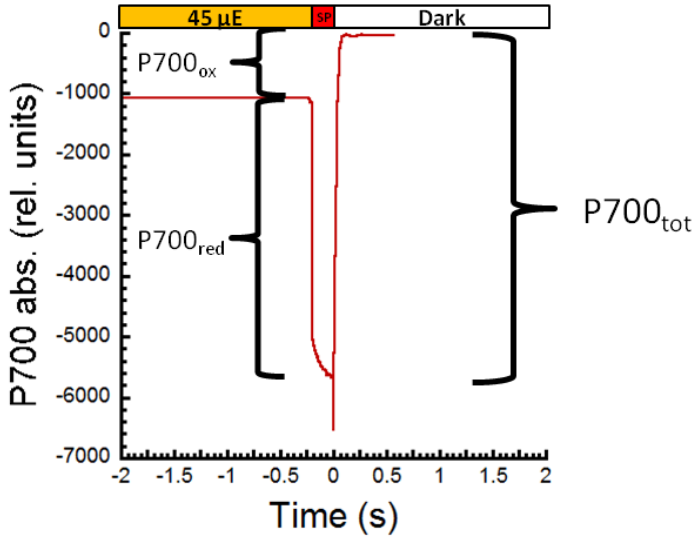

Supplemental Figure 4.1: P700 absorbance kinetics of an illuminated sample given a saturating pulse. Sample transient has been normalized to fully reduced P700 values. In order to determine relative quantities of oxidized and reduced P700 of illuminated samples, samples were subjected to the following assay. Samples were illuminated under actinic illumination (45 µE) for 10 minutes ($t < 0$). A 200 ms saturating pulse (2500 µE) was delivered in order to fully oxidize P700. All illumination was terminated and absorbance was tracked to fully reduced P700 levels in darkness. The absolute deflection value between the saturating pulse (fully oxidized) and darkness (fully reduced) values were taken as a measure of total P700 ($P700_{tot}$). The values of absorbance during actinic illumination, divided by the total deflection were taken as a relative measure of P700 oxidized during illumination ($P700_{ox}$).

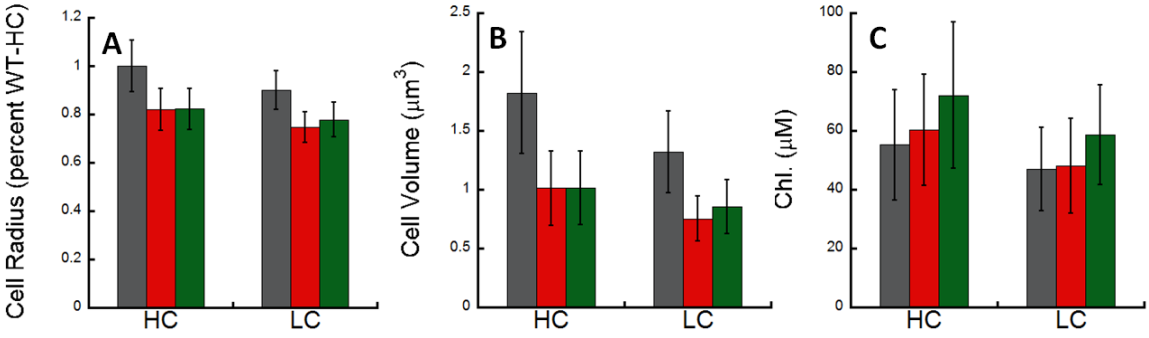

Supplemental Figure 4.2: Cell morphology and physiology measurements. Cells were visualized with a Nikon Eclipse Ni series differential interference contrast microscope. Black: WT, Red: Δ*glgC*, Green: JU547 Panel A: The relative area of cells under 100x magnification were obtained by using area measurements of manually selected cells using ImageJ software (NIH, Maryland, USA). Panel B: Cell volume estimates were made using the relative cell radius measurements and assuming a wild-type cell diameter of 1.5 µm [37]. Panel C: Using Chl determination measurements (Figure 2) the intracellular concentration of Chl was determined.

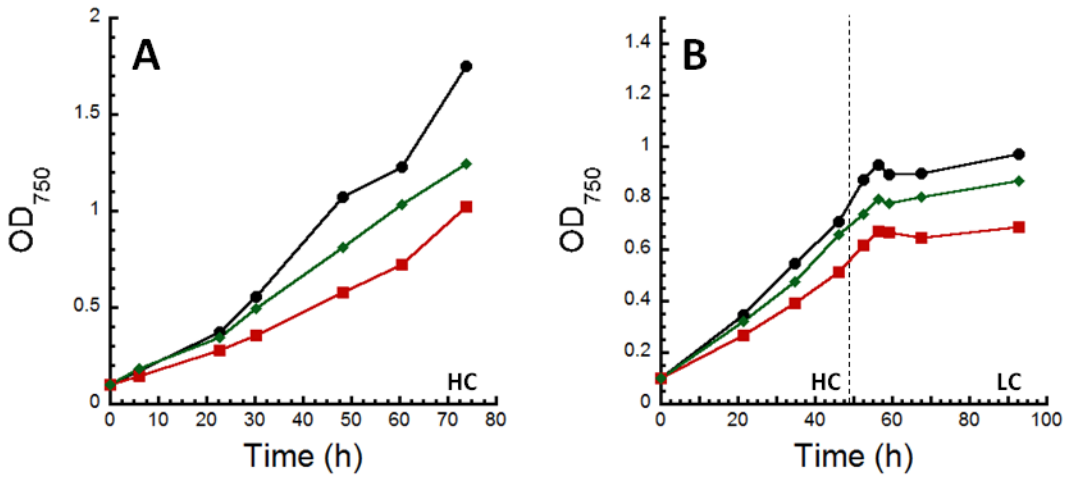

Supplemental Figure 4.3: Representative growth curves of wild-type and mutant strains in high and low carbon conditions. Black: WT, Red: Δ*glgC*, Green: JU547. Panel A: Growth of cultures obtained over three days of high carbon (3% CO_2 gassing) culturing. Panel B: Growth of cultures with 2 days of high carbon (3% CO_2) gassing, switched to low carbon (ambient air) at 48 hours.

In order to assay the affinity of each strain for inorganic carbon, oxygen evolution assays were performed on carbon depleted cell samples. Cell samples from HC and LC cultures were first harvested in low carbon BG11 medium. Samples were resuspended to a Chl concentration of 5 µg Chl · ml^{-1}. Samples were illuminated with saturating white light (~1500 µE) in order to consume residual inorganic carbon while oxygen evolution was monitored. Carbon depletion was established by cell cultures reaching the CO_2 compensation point, where oxygen evolution is equal to oxygen consumption. Inorganic carbon was added to cell samples and rates of oxygen evolution were fitted to the Michaelis-Menton kinetics equation. From this equation and values of oxygen evolution, the maximum rate of oxygen evolution, V_{max}, can be determined. However, the applicability of this equation is theoretically not well-supported because oxygen evolution is a

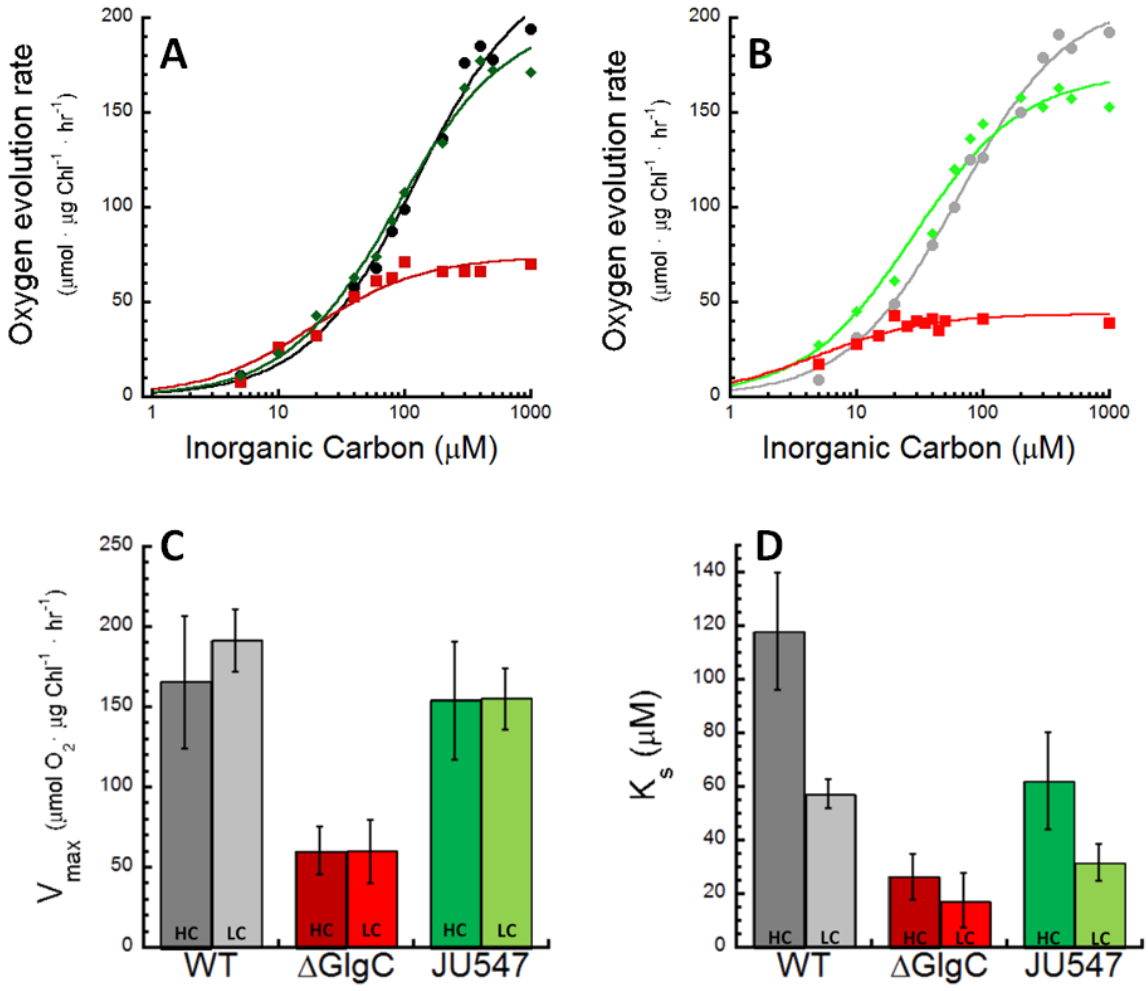

Supplemental Figure 4.4. Inorganic carbon affinity measurements for wild-type and transformant strains as measured by oxygen evolution using a Clark-type electrode. Black: WT; Red: GlgC; Green: JU547. Panels A & B: Representative traces from high carbon (A) and low carbon (B) grown cultures assayed for oxygen evolution as a measure of carbon affinity. Solid lines represent calculated curve fits using the Michaelis-Menton equation. Panels C & D: Values of maximum reaction rate (C) and inorganic carbon affinity (D) calculated from curve fit data. Error bars represent standard deviation from at least three replicates.

byproduct of a number of upstream processes (i.e. carbon transport, diffusion, PSII efficiency) and these are likely to distort the derived parameters, especially the affinity constant K_M [58]. Therefore, the affinity values are reported as the concentration of inorganic carbon in which this system performs at half maximum, K_s. Transition from HC to LC conditions increases the affinity of each strain for inorganic carbon (Supplementary Figure 4.4D). As seen in Figure 4.4, V_{max} is slightly lower than earlier reported values of oxygen evolution (Figure 4.3A). This is likely due to the longer assay duration causing adjustments in photosynthesis (e.g. state transitions and other

photoprotective mechanisms) to modulate electron transfer rate. Nevertheless, similar trends in oxygen evolution are seen, with WT and JU547 having similar rates, and an impairment seen in Δ*glgC*. Although the high-affinity CCM involves induction of carbon transporters with a lower flux component [59], no significant changes in V_{max} or K_m were observed for Δ*glgC* between HC and LC cultures under these conditions.

4.7 Chapter 4 references

1. Oliver, J.W. and S. Atsumi, *Metabolic design for cyanobacterial chemical synthesis.* Photosynth Res, 2014. **120**(3): p. 249-61.

2. Hays, S.G. and D.C. Ducat, *Engineering cyanobacteria as photosynthetic feedstock factories.* Photosynth Res, 2015. **123**(3): p. 285-95.

3. Angermayr, S.A., A. Gorchs Rovira, and K.J. Hellingwerf, *Metabolic engineering of cyanobacteria for the synthesis of commodity products.* Trends Biotechnol, 2015. **33**(6): p. 352-61.

4. Oliver, J.W. and S. Atsumi, *A carbon sink pathway increases carbon productivity in cyanobacteria.* Metab Eng, 2015. **29**: p. 106-12.

5. Nguyen, B.T. and B.E. Rittmann, *Predicting Dissolved Inorganic Carbon in Photoautotrophic Microalgae Culture via the Nitrogen Source.* Environ Sci Technol, 2015. **49**(16): p. 9826-31.

6. Ibelings, B.W. and S.C. Maberly, *Photoinhibition and the availability of inorganic carbon restrict photosynthesis by surface blooms of cyanobacteria.* Limnology and Oceanography, 1998. **43**(3): p. 408-419.

7. Verspagen, J.M., et al., *Rising CO2 levels will intensify phytoplankton blooms in eutrophic and hypertrophic lakes.* PLoS One, 2014. **9**(8): p. e104325.

8. Riebesell, U., et al., *Enhanced biological carbon consumption in a high CO2 ocean.* Nature, 2007. **450**(7169): p. 545-8.

9. Lea-Smith, D.J., et al., *Phycobilisome-Deficient Strains of Synechocystis sp. PCC 6803 Have Reduced Size and Require Carbon-Limiting Conditions to Exhibit Enhanced Productivity.* Plant Physiology, 2014. **165**(2): p. 705-714.

10. Kamennaya, N.A., et al., *Installing extra bicarbonate transporters in the cyanobacterium Synechocystis sp. PCC6803 enhances biomass production.* Metabolic Engineering, 2015. **29**: p. 76-85.

11. Burnap, R.L., M. Hagemann, and A. Kaplan, *Regulation of CO_2 concentrating mechanism in cyanobacteria.* Life (Basel), 2015. **5**(1): p. 348-71.

12. Fukuzawa, H., T. Ogawa, and A. Kaplan, *The uptake of CO_2 by cyanobacteria and microalgae*, in *Photosynthesis: Plastid Biology, Energy Conversion and Carbon Assimilation*, J.J. Eaton Rye, B.C. Tripathy, and T.D. Sharkey, Editors. 2012. p. 625-650.

13. Price, G.D., et al., *Advances in understanding the cyanobacterial CO_2-concentrating-mechanism (CCM): functional components, Ci transporters, diversity, genetic regulation and prospects for engineering into plants.* J. Exp. Bot., 2008. **59**(7): p. 1441-1461.

14. Yeates, T.O., et al., *Protein-based organelles in bacteria: carboxysomes and related microcompartments.* Nat Rev Microbiol, 2008. **6**(9): p. 681-91.

15. Kramer, D.M. and J.R. Evans, *The importance of energy balance in improving photosynthetic productivity.* Plant Physiol, 2011. **155**(1): p. 70-8.

16. Alric, J., J. Lavergne, and F. Rappaport, *Redox and ATP control of photosynthetic cyclic electron flow in Chlamydomonas reinhardtii (I) aerobic conditions.* Biochimica Et Biophysica Acta-Bioenergetics, 2010. **1797**(1): p. 44-51.

17. Carrieri, D., et al., *Photo-catalytic conversion of carbon dioxide to organic acids by a recombinant cyanobacterium incapable of glycogen storage.* Energy & Environmental Science, 2012. **5**(11): p. 9457-9461.

18. Ungerer, J., et al., *Sustained photosynthetic conversion of CO2 to ethylene in recombinant cyanobacterium Synechocystis 6803.* Energy & Environmental Science, 2012. **5**(10): p. 8998-9006.

19. Cooley, J.W. and W.F.J. Vermaas, *Succinate dehydrogenase and other respiratory pathways in thylakoid membranes of Synechocystis sp strain PCC 6803: Capacity comparisons and physiological function.* Journal of Bacteriology, 2001. **183**(14): p. 4251-4258.

20. Xiong, W., et al., *The plasticity of cyanobacterial metabolism supports direct CO2 conversion to ethylene.* Nature Plants, 2015. **1**: p. 15053.

21. Krishnan, A., et al., *Metabolic and photosynthetic consequences of blocking starch biosynthesis in the green alga Chlamydomonas reinhardtii sta6 mutant.* Plant Journal, 2015. **81**(6): p. 947-960.

22. Ungerer, J., et al., *Sustained photosynthetic conversion of CO2 to ethylene in recombinant cyanobacterium Synechocystis 6803.* Energy & Environmental Science, 2012. **5**(10): p. 8998-9006.

23. Shimakawa, G., et al., *Respiration accumulates Calvin cycle intermediates for the rapid start of photosynthesis in Synechocystis sp. PCC 6803.* Bioscience Biotechnology and Biochemistry, 2014. **78**(12): p. 1997-2007.

24. Orf, I., et al., *Integrated Analysis of Engineered Carbon Limitation in a Quadruple CO2/HCO3- Uptake Mutant of Synechocystis sp. PCC 6803.* Plant Physiol, 2015. **169**(3): p. 1787-806.

25. Schwarz, D., et al., *Effects of inorganic carbon limitation on the metabolome of the Synechocystis sp. PCC 6803 mutant defective in glnB encoding the central regulator PII of cyanobacterial C/N acclimation.* Metabolites, 2014. **4**(2): p. 232-47.

26. Hackenberg, C., et al., *Low-carbon acclimation in carboxysome-less and photorespiratory mutants of the cyanobacterium Synechocystis sp. strain PCC 6803.* Microbiology, 2012. **158**(Pt 2): p. 398-413.

27. Helman, Y., et al., *Genes encoding a-type flavoproteins are essential for photoreduction of O_2 in cyanobacteria.* Current Biology, 2003. **13**(3): p. 230-5.

28. Allahverdiyeva, Y., et al., *Flavodiiron proteins Flv1 and Flv3 enable cyanobacterial growth and photosynthesis under fluctuating light.* Proc Natl Acad Sci U S A, 2013. **110**(10): p. 4111-6.

29. Holland, S.C., A.D. Kappell, and R.L. Burnap, *Redox changes accompanying inorganic carbon limitation in Synechocystis sp. PCC 6803.* Biochim Biophys Acta, 2015. **1848**(3): p. 355-63.

30. Stirbet, A. and Govindjee, *On the relation between the Kautsky effect (chlorophyll a fluorescence induction) and Photosystem II: Basics and applications of the OJIP fluorescence transient.* Journal of Photochemistry and Photobiology B-Biology, 2011. **104**(1-2): p. 236-257.

31. Govindjee, *63 Years since Kautsky - Chlorophyll-a Fluorescence.* Australian Journal of Plant Physiology, 1995. **22**(2): p. 131-160.

32. Briantais, J.M., et al., *Quantitative Study of the Slow Decline of Chlorophyll Alpha-Fluorescence in Isolated-Chloroplasts.* Biochimica Et Biophysica Acta, 1979. **548**(1): p. 128-138.

33. Kana, R., et al., *The slow S to M fluorescence rise in cyanobacteria is due to a state 2 to state 1 transition.* Biochimica Et Biophysica Acta-Bioenergetics, 2012. **1817**(8): p. 1237-1247.

34. Campbell, D., et al., *Chlorophyll fluorescence analysis of cyanobacterial photosynthesis and acclimation.* Microbiology and Molecular Biology Reviews, 1998. **62**(3): p. 667–683.

35. Miller, A.G., G.S. Espie, and D.T. Canvin, *Chlorophyll-a fluorescence yield as a monitor of both active CO_2 and HCO_3^- transport by the cyanobacterium Synechococcus UTEX 625.* Plant Physiology, 1988. **86**(3): p. 655-658.

36. Badger, M. and U. Schreiber, *Effects of inorganic carbon accumulation on photosynthetic oxygen reduction and cyclic electron flow in the cyanobacterium Synechococcus PCC7942.* Photosynthesis Research, 1993. **37**(3): p. 177-191.

37. Battchikova, N., et al., *Identification of novel Ssl0352 protein (NdhS), essential for efficient operation of cyclic electron transport around photosystem I, in NADPH: plastoquinone oxidoreductase (NDH-1) complexes of Synechocystis sp. PCC 6803. (vol 286, pg 36992, 2011).* Journal of Biological Chemistry, 2012. **287**(11): p. 8660-8660.

38. Holland, S.C., A.D. Kappell, and R.L. Burnap, *Redox changes accompanying inorganic carbon limitation in Synechocystis sp PCC 6803.* Biochimica Et Biophysica Acta-Bioenergetics, 2015. **1847**(3): p. 355-363.

39. Mi, H., et al., *Thylakoid membrane-bound, NADPH-specific pyridine nucleotide dehydrogenase complex mediates cyclic electron transport in the cyanobacterium Synechocystis sp. PCC 6803.* Plant Cell Physiol., 1995. **36**: p. 661-668.

40. Bolychevtseva, Y.V., et al., *Photosystem activity and state transitions of the photosynthetic apparatus in cyanobacterium Synechocystis PCC 6803 mutants with different redox state of the plastoquinone pool.* Biochemistry (Mosc), 2015. **80**(1): p. 50-60.

41. Cooley, J.W. and W.F. Vermaas, *Succinate dehydrogenase and other respiratory pathways in thylakoid membranes of Synechocystis sp. strain PCC 6803: capacity comparisons and physiological function.* J Bacteriol, 2001. **183**(14): p. 4251-8.

42. Miller, A.G., G.S. Espie, and D. Bruce, *Characterization of the non-photochemical quenching of chlorophyll fluorescence that occurs during the active accumulation of inorganic carbon in the cyanobacterium Synechococcus PCC 7942.* Photosynthesis Research, 1996. **49**(3): p. 251-262.

43. Mi, H., C. Klughammer, and U. Schreiber, *Light-induced dynamic changes of NADPH fluorescence in Synechocystis PCC 6803 and its ndhB-defective mutant M55.* Plant Cell Physiol, 2000. **41**(10): p. 1129-35.

44. Kauny, J. and P. Setif, *NADPH fluorescence in the cyanobacterium Synechocystis sp PCC 6803: A versatile probe for in vivo measurements of rates, yields and pools.* Biochimica Et Biophysica Acta-Bioenergetics, 2014. **1837**(6): p. 792-801.

45. Daley, S.M.E., et al., *Regulation of the Cyanobacterial CO2-Concentrating Mechanism Involves Internal Sensing of NADP(+) and alpha-Ketogutarate Levels by Transcription Factor CcmR.* Plos One, 2012. **7**(7).

46. Figge, R.M., et al., *Characterization and analysis of an NAD(P)H dehydrogenase transcriptional regulator critical for the survival of cyanobacteria facing inorganic carbon starvation and osmotic stress.* Molecular Microbiology, 2001. **39**(2): p. 455-468.

47. Allen, M.M., *Simple conditions for growth of unicellular blue-green algae on plates.* Journal of Phycology, 1968. **4**(1): p. 1-4.

48. Wang, H.L., B.L. Postier, and R.L. Burnap, *Alterations in global patterns of gene expression in Synechocystis sp PCC 6803 in response to inorganic carbon limitation and the inactivation of ndhR, a LysR family regulator.* Journal of Biological Chemistry, 2004. **279**(7): p. 5739-5751.

49. Williams, J.G.K., *Construction of specific mutations in Photosystem II photosynthetic reaction center by genetic engineering methods in Synechocystis 6803.* Methods in Enzymology, 1988. **167**: p. 766-778.

50. Ritchie, R.J., *Consistent sets of spectrophotometric chlorophyll equations for acetone, methanol and ethanol solvents.* Photosynthesis Research, 2006. **89**(1): p. 27-41.

51. Carrieri, D., et al., *Photo-catalytic conversion of carbon dioxide to organic acids by a recombinant cyanobacterium incapable of glycogen storage.* Energy & Environmental Science, 2012. **5**(11): p. 9457-9461.

52. Miao, X., et al., *Changes in photosynthesis and pigmentation in an agp deletion mutant of the cyanobacterium Synechocystis sp.* Biotechnol Lett, 2003. **25**(5): p. 391-6.

53. Daley, S.M., et al., *Regulation of the cyanobacterial CO_2-concentrating mechanism involves internal sensing of $NADP^+$ and alpha-ketogutarate levels by transcription factor CcmR.* PLoS One, 2012. **7**(7): p. e41286.

54. Shimakawa, G., et al., *FLAVODIIRON2 and FLAVODIIRON4 proteins mediate an oxygen-dependent alternative electron flow in Synechocystis sp. PCC 6803 under CO2-limited conditions.* Plant Physiol, 2015. **167**(2): p. 472-80.

55. Allahverdiyeva, Y., et al., *Interplay between flavodiiron proteins and photorespiration in Synechocystis sp. PCC 6803.* J Biol Chem, 2011. **286**(27): p. 24007-14.

56. Bersanini, L., et al., *Flavodiiron Protein Flv2/Flv4-Related Photoprotective Mechanism Dissipates Excitation Pressure of PSII in Cooperation with Phycobilisomes in Cyanobacteria.* Plant Physiology, 2014. **164**(2): p. 805-818.

57. Schuurmans, R.M., et al., *The redox potential of the plastoquinone pool of the cyanobacterium Synechocystis species strain PCC 6803 is under strict homeostatic control.* Plant Physiol, 2014. **165**(1): p. 463-75.

58. Ma, W. and T. Ogawa, *Oxygenic photosynthesis-specific subunits of cyanobacterial NADPH dehydrogenases.* IUBMB Life, 2015.

CHAPTER V

Conclusions

The focus of this research was to analyze the redox physiology of *Synechocystis* under different regimes of carbon availability and carbon sink alterations. In the first set of experiments (Chapter 3), conditions were arranged to emulate gradual, natural consumption and depletion of inorganic carbon in the external medium. The following experiments (Chapter 4) analyzed the effects of alterations in internal metabolic pathways as well as external carbon availability. The first experiments helped create a foundation and framework of interpretation for understanding some of the observations seen in the later experiments.

The early experiments defined carbon-sensitive markers in chlorophyll and NADPH fluorescence. Well-characterized modulations of chlorophyll fluorescence (e.g. F_0, F_P, F_S, F_M) were found to have analogous features in NADPH fluorescence. Characterization of these features can provide additional insight when analyzing mutants of CBB cycle activity (F_M/N_M decline) or sugar metabolism (F_R/N_R peak).

A prominent rise in minimum chlorophyll fluorescence (F_0) was observed upon carbon depletion. The cause of this rise is unknown, but may be a result of glycogen breakdown and increased respiration. This rise was mirrored in steady-state fluorescence during illumination (F_T). This rise

is likely due to decreased electron flow into the CBB cycle and a resulting reduction of upstream electron carriers. This rise gradually declined, as photoprotective mechanisms were induced, such as flavodiiron proteins.

The research also added to the sparse set of experiments that analyze NADPH fluorescence in cyanobacteria. Importantly, it showed that changes in carbon-dependent NADPH consumption (predominantly due to the CBB cycle) are most prominent at least 30 seconds after illumination is initiated, the described N_M decline. Some previous studies [1] were tentatively assigning modulations in NADPH fluorescence to CBB activity in illuminations fewer than 10 seconds in duration. While the data for this paper was being analyzed and prepared for publication, another publication by Kauny and Sétif was published [2]. Using actinic illuminations that varied in their duration, these authors found that post-illumination NADPH consumption reached its maximum after approximately 32 seconds of illumination. This is consistent with our finding that CBB cycle activity initiates, or reaches it maximum rate, at this time.

In addition to the assigning of fluorescence transients, the fluorescence data reveals some clues to the redox poise of the total cellular NADP(H) pool during carbon depletion. This is an important question, as the availability of $NADP^+$ influences the DNA binding properties of NdhR, a transcriptional regulator of many CCM components [3]. First the steady state NADPH fluorescence of dark-adapted cells, N_0, increases throughout the 16 hour assay (Chapter 3, Figure 3). Unfortunately, this increase in fluorescence coincides with cell growth in the cuvette, and is likely a cause of a majority of increased fluorescence. It is seen however, that steady-state levels of NADPH during illumination (N_T and also N_T-N_0) are increased after carbon depletion. This arises from a lower consumption of NADPH in the CBB cycle, and may trigger de-repression of gene expression by NdhR. Unfortunately, the affinity of NdhR for $NADP^+$ is not well defined, and it is unknown what range of concentrations influence NdhR activity, and by what degree.

Attempts were made to biochemically analyze the total concentrations of $NADP^+$ and NADPH using biochemical assays. However, the signal response obtained from these assays (not shown) was not large enough to be certain of the reliability of the results, and was therefore abandoned. There are practical problems with sample harvesting that also arise. According to fluorescence data, nearly all light-induced fluorescence is consumed within 7 seconds of darkness, therefore sampling methods would have to take this into account. A brief review of non-fluorescence NADP(H) measurements shows that these measurements may be highly variable. Measurements of NADP(H) have reported ranges from 0% [4], 28% [5], 50% [6], and up to 75% [7] reduced, though dark/light and carbon availability was not clearly defined in all studies and may be different in each case.

In summary, transitioning from a carbon-replete to a carbon-limited environment caused a large reduction event in the PQ and NADPH pools. The later, gradual decline in steady-state chlorophyll fluorescence (F_T) was evidence of induced photoprotective mechanisms, and therefore the large over-reduction in the PQ pool may be obscured if sampling intervals are too far apart in later studies. For future studies in NADPH utilization, it is also necessary to ensure illumination durations are planned mindful of CCB activity.

In the second study, presented in Chapter 4, strains with internal perturbations in carbon metabolism were examined as external carbon availability was altered. The presence or absence of a carbon sink was found to have an effect on redox state of the photosynthetic electron transport chain. When a sink is closed (Δ*glgC* mutant) chlorophyll and NADPH fluorescence shows evidence of a highly reduced electron transport chain, conversely, integration of a new carbon sink results in more oxidized electron carriers. In the Δ*glgC* mutant, the switch to low-carbon conditions caused the PQ and NADPH pools to become more oxidized. While this effect is not fully understood, and may seem counterintuitive to the results presented in the previous study (Chapter 3), the transition to low-carbon conditions and oxidative sugar metabolism may be

providing an a pathway for electrons to be removed from the photosynthetic electron transport chain. Consistent with this model, respiration was seen to increase in the Δ*glgC* mutant in low carbon conditions. However, an alternate explanation of high chlorophyll fluorescence is discussed below, that alters the interpretation of redox state of the PQ pool.

Analysis of CEF in the carbon metabolism mutants showed that CEF was highly impaired in the Δ*glgC* mutant (Chapter 4, Figure 6). Interestingly, the standard method used to measure CEF, the rate of P700 rereduction in the presence of DCMU, is at odds with another measure of CEF: the presence and intensity of the F_N rise which is largely attributable to the activity of the NDH-1 complexes [8]. The Δ*glgC* mutant displays a highly prominent F_N rise (Chapter 4, Figure 5). The discrepancy in these two findings may warrant further investigation. It was observed that CEF in the JU547 mutant was increased in comparison to the wild-type strain, consistent with the prediction that succinate from the EFE reaction provides an additional route pathway of CEF.

Initial hypotheses about the Δ*glgC* mutant and JU547 mutants predicted that these strains would have alterations in the expression of the high-affinity transporters. In JU547, consumption of 2OG by the EFE was predicted to relieve repression of the *ndhR* regulon. Under high carbon growth conditions, repression of SbtA expression was still observed, however, an increase was observed under low carbon conditions (Chapter 4, Figure 11). No evidence of misregulation was observed in the Δ*glgC* mutant. Unfortunately, EFE activity and the 'energy-spilling' activity of the Δ*glgC* mutant under the conditions used here are unknown.

Analysis of the Δ*glgC* mutant also confirmed the finding by other authors that glycogen breakdown during darkness serves as a method of replenishing CBB cycle metabolites, and that the absence of glycogen breakdown results in a delay in CBB activation [9]. This can also be seen in the post-illumination F_R rise that we tentatively assigned to the oxidation of sugars created during illumination (Chapter 3, Figure 6). In high-carbon grown samples, when CBB induction is

delayed, the F_R rise is absent or negligible (Chapter 4, Figure 5). However, cultures switched to low-carbon conditions display an increase in chlorophyll fluorescence at this time. Since activation of the CBB cycle is no longer delayed under these conditions, CBB cycle sugars have accumulated and can be oxidized, likely through the pentose phosphate pathway. The Δ*glgC* mutant may be a good candidate strain to further confirm and study the assignment of F_R/N_R to sugar oxidation.

The most intriguing results obtained with the Δ*glgC* mutant regards the apparent disconnect between the chlorophyll fluorescence and $P700^+$ reduction rates. Canonically, high chlorophyll fluorescence values have been interpreted as high levels of reduced plastoquinone. That is, chlorophyll fluorescence is a direct measure of the redox poise of the plastoquinone pool. It logically follows that high levels of reduced PQ should lead to increased reduction rates for $P700^+$. However, the opposite effect was observed (Chapter 4; Figure 7). This points to the conclusion that the PQ pool in the Δ*glgC* mutant grown under high carbon conditions is actually more oxidized than chlorophyll fluorescence would indicate.

Schuurmans *et al.* have recently provided evidence that demonstrates a disparity in chlorophyll fluorescence and the biochemically analyzed redox state of the PQ pool [10]. In this study, the Cyt b_6f inhibitor, DBMIB caused a rapid increase in chlorophyll fluorescence, as expected if electron donation from PQH_2 to Cyt b_6f is inhibited. However, under high carbon growth conditions, the biochemically measured PQ pool was shown to only be approximately 20% reduced, equivalent to that of no-inhibitor control samples [1]. Further illustrating the disconnect between chlorophyll fluorescence and the redox state of the plastoquinone pool the authors show that during low carbon availability, high chlorophyll fluorescence was only slightly quenched by the addition of DCBQ, an electron acceptor biochemically shown to oxidize the PQ pool. Therefore it would appear that for wild-type *Synechocystis* cells grown in low carbon conditions,

high chlorophyll fluorescence may be due to a saturated pool of electron acceptor other than plastoquinone.

The investigation into the mechanistic cause of high chlorophyll fluorescence and corresponding low $P700^{+}$ reduction rates and low biochemically measured concentrations of reduced PQ is alluring. It could open investigation into novel mechanisms of photoprotection, redox stress protection, and cyclic or alternate electron flow pathways. If further evidence demonstrates the independence of chlorophyll fluorescence and the oxidation state of the PQ pool, then the current models of electron transport and redox regulation may need reexamination.

Chapter 5 references

1. Mi, H., C. Klughammer, and U. Schreiber, *Light-induced dynamic changes of NADPH fluorescence in Synechocystis PCC 6803 and its ndhB-defective mutant M55.* Plant Cell Physiol, 2000. **41**(10): p. 1129-35.

2. Kauny, J. and P. Setif, *NADPH fluorescence in the cyanobacterium Synechocystis sp PCC 6803: A versatile probe for in vivo measurements of rates, yields and pools.* Biochimica Et Biophysica Acta-Bioenergetics, 2014. **1837**(6): p. 792-801.

3. Daley, S.M.E., et al., *Regulation of the Cyanobacterial CO2-Concentrating Mechanism Involves Internal Sensing of NADP(+) and alpha-Ketogutarate Levels by Transcription Factor CcmR.* Plos One, 2012. **7**(7).

4. Osanai, T., et al., *Capillary electrophoresis-mass spectrometry reveals the distribution of carbon metabolites during nitrogen starvation in Synechocystis sp. PCC 6803.* Environ Microbiol, 2014. **16**(2): p. 512-24.

5. Korn, A., et al., *Ferredoxin:NADP+ oxidoreductase association with phycocyanin modulates its properties.* J Biol Chem, 2009. **284**(46): p. 31789-97.

6. Tamoi, M., et al., *The Calvin cycle in cyanobacteria is regulated by CP12 via the NAD(H)/NADP(H) ratio under light/dark conditions.* Plant J, 2005. **42**(4): p. 504-13.

7. Cooley, J.W. and W.F.J. Vermaas, *Succinate dehydrogenase and other respiratory pathways in thylakoid membranes of Synechocystis sp strain PCC 6803: Capacity comparisons and physiological function.* Journal of Bacteriology, 2001. **183**(14): p. 4251-4258.

8. Battchikova, N., et al., *Identification of novel Ssl0352 protein (NdhS), essential for efficient operation of cyclic electron transport around photosystem I, in NADPH: plastoquinone oxidoreductase (NDH-1) complexes of Synechocystis sp. PCC 6803. (vol 286, pg 36992, 2011).* Journal of Biological Chemistry, 2012. **287**(11): p. 8660-8660.

9. Shimakawa, G., et al., *Respiration accumulates Calvin cycle intermediates for the rapid start of photosynthesis in Synechocystis sp. PCC 6803.* Bioscience Biotechnology and Biochemistry, 2014. **78**(12): p. 1997-2007.

10. Schuurmans, R.M., et al., *The Redox Potential of the Plastoquinone Pool of the Cyanobacterium Synechocystis Species Strain PCC 6803 Is under Strict Homeostatic Control.* Plant Physiology, 2014. **165**(1): p. 463-475.

VITA

Steven Christopher Holland

Candidate for the Degree of

Doctor of Philosophy

Thesis: THE EFFECTS OF INORGANIC CARBON LIMITATION IN WILD-TYPE AND CARBON SINK MUTANTS OF THE CYANOBACTERIUM *SYNECHOCYSTIS* SP. PCC 6803.

Major Field: Microbiology and Molecular Genetics

Biographical:

Education:

Completed the requirements for the Doctor of Philosophy in Microbiology and Molecular Genetics at Oklahoma State University, Stillwater, Oklahoma in May, 2016.

Completed the requirements for the Bachelor of Science in Biology at University of South Alabama, Mobile, Alabama in 2006.

Experience:

Graduate Research Assistant in Laboratory of Dr. Robert L. Burnap, Microbiology and Molecular Genetics Department, Oklahoma State University 2009-2016

Peer Reviewed Publications

Holland SC, Kappell AD, and Burnap RL. "Redox changes accompanying inorganic carbon limitation in *Synechocystis* sp. PCC 6803." Biochimica et Biophysica Acta. 2015 Mar; 1848(3): 355-63.

Burnap RL, Namudiri R, Holland S. "Regulation of the carbon-concentrating mechanism in the cyanobacterium *Synechocystis* sp. PCC 6803 in response to changing light intensity and inorganic carbon availability." Photosynthesis Research. 2013 Nov; 118(1-2): 115-24.

Professional Memberships:

International Society of Photosynthesis Research (2013-2014)